

**University of Alberta**

**BAD-interacting proteins in breast cancer cells**

by

**Alison Claire Craik**

A thesis submitted to the Faculty of Graduate Studies and Research  
in partial fulfillment of the requirements for the degree of

**Master of Science**

**Department of Biochemistry**

©Alison Claire Craik

Fall 2012

Edmonton, Alberta

Permission is hereby granted to the University of Alberta Libraries to reproduce single copies of this thesis and to lend or sell such copies for private, scholarly or scientific research purposes only. Where the thesis is converted to, or otherwise made available in digital form, the University of Alberta will advise potential users of the thesis of these terms.

The author reserves all other publication and other rights in association with the copyright in the thesis and, except as herein before provided, neither the thesis nor any substantial portion thereof may be printed or otherwise reproduced in any material form whatsoever without the author's prior written permission.

For Jess, Karen, Lisa, Dean and Matt

## **Abstract**

Taxane chemotherapy is widely used in the treatment of breast cancer. Despite its widespread clinical use, the molecular mechanisms of paclitaxel induced apoptosis remain unclear. Our laboratory has identified an important role for the BH3-only protein, BAD, in the paclitaxel induced cell death pathway of breast cancer cells. Furthermore, BAD expression correlates with sensitivity to taxanes in vitro and in clinical studies. While BAD is a well characterized pro-apoptotic member of the BCL-2 family, our studies demonstrate a novel, non-apoptotic role for BAD in paclitaxel-induced cell death. Specifically, this work suggests a role for BAD in cell cycle progression or diminished apoptotic signaling, consistent with data from the laboratory documenting pro-growth activity of BAD. We screened for BAD interacting proteins to improve our understanding of BAD molecular dynamics and identify protein partners that may contribute to BAD pro-growth activity. BAD interactions with BCL-XL and 14-3-3 protein isoforms were examined.

## **Acknowledgements**

I would like to acknowledge the support and guidance of all the parties that helped make this thesis possible:

First, I thank my supervisor, Dr. Ing Swie Goping, for welcoming me into the laboratory to embark on this project. I am grateful for all the support, opportunities, encouragement and constructive criticism you have provided during this degree. I am also very grateful to my supervisory committee members, Dr. Richard Fahlman and Dr. Thomas Simmen for their feedback and support with this project.

I appreciate the work of all the collaborators, whose skill and expertise has helped further our understanding of BAD. Thank you to Dr. Richard Fahlman, Dr. Jack Moore and everyone else in the IBD facility for helping me with the mass spectrometry portion of this project. Thank you to our clinical collaborators: Dr. John Mackey, Dr. Sunita Ghosh, Dr. Sambasivarao Damaraju and Dr. Raymond Lai for their work on the BAD tissue microarray study. Thank you to Dr. Alan Underhill for compiling the gene expression microarray data. These clinical insights are motivating further study of BAD.

Elucidation of an important role for BAD in taxane-induced cell death required collaboration amongst many laboratory members, past and present. I gratefully acknowledge the work of Matt Czernick, former technician, who laid the foundation for future studies of BAD and taxane sensitivity. I also credit the work of Timothy Buckland, fellow graduate student, who furthered our knowledge of non-apoptotic BAD roles in breast cancer. I also thank Tim for use of the BAD-overexpressing cell lines. Additionally, I thank Richard Veldhoen for

his contributions to the BAD project. Finally, I am very grateful to Shanna Banman, laboratory technician, for sharing her expertise with confocal microscopy and for all of her hard technical work in the laboratory.

I would also like to thank Dr. Chris Bleackley and his laboratory members for being so generous and accommodating of our research group, particularly for sharing their equipment, space and reagents with us. I extend this gratitude to all members of the Departments of Biochemistry and Cell Biology who have been great colleagues, friends and collaborators. In particular, I would like to acknowledge Dr. Carolina Ilkow, Emily Lynes and Dr. Arun Raturi for helpful discussions and technical advice. I also thank the Department of Biochemistry administrative staff, including our Graduate Program Advisor, Kimberly Arndt, and Administrative Assistant, Sue Smith, for supporting me throughout my graduate program.

This project was made possible in part by a graduate studentship from the Alberta Cancer Foundation. I am also grateful to the Faculty of Graduate Studies & Research at the University of Alberta for the Queen Elizabeth II Graduate Scholarship funding. Further grant funds from the Canadian Breast Cancer Foundation also supported our laboratory's study of BAD.

Finally, these acknowledgements would not be complete without crediting the support of some truly amazing friends and responders, to whom this thesis is dedicated: Jessica van der Ahé, Karen Cheung, Lisa Oishi, Dean Smith and Matt Caindec. We have had so many adventures over the last few years, and I am blessed to be part of such a great team. You persevered with me, motivated and

inspired me, and went out of your way to help me. I will keep trying to thank you enough – so here's to the team that made this journey a whole lot of fun!

## TABLE OF CONTENTS

<b>Chapter 1: Introduction</b> .....	1
1.1 Apoptosis .....	2
1.2 Evasion of apoptosis in cancer.....	2
1.3 Molecular modulators of apoptosis: the BCL-2 family .....	3
1.4 Taxanes as chemotherapeutic agents .....	4
1.4.1 Paclitaxel.....	4
1.4.2 Docetaxel .....	7
1.5 Microtubule structure and dynamics.....	8
1.6 Taxanes promote microtubule stabilization and assembly .....	9
1.7 Characterization of the taxane binding site on microtubules.....	10
1.8 Mechanisms of taxane induced cell death .....	12
1.8.1 Apoptosis at low nanomolar paclitaxel concentrations .....	12
1.8.2 Role of BIM in paclitaxel induced apoptosis.....	13
1.9 Staurosporine induced apoptosis.....	16
1.10 Role of BAD in paclitaxel induced apoptosis.....	17
1.10.1 BAD expression correlates with taxane sensitivity in vitro	17
1.10.2 BAD expression correlates with taxane sensitivity in clinical studies .....	17
1.11 BAD (BCL-2 antagonist of cell death) .....	21
1.11.1 Identification and characterization.....	21
1.11.2 Physiological roles .....	21
1.11.3 BH3 domain .....	23
1.12 Thesis objective 1 .....	26
1.13 Non-apoptotic BAD functions .....	26
1.13.1 Novel pro-growth role for BAD in breast cancer cells .....	26
1.13.2 BAD proliferative capacity in breast cancer cells.....	27

1.13.3 Role of BCL-2 family members in cell cycle progression	28
1.14 Regulation of BAD activity	32
1.14.1 BAD phosphorylation	32
1.14.2 Lipid binding properties	35
1.15 BAD-interacting proteins	36
1.15.1 BAD:BCL-2, BCL-XL and BCL-W interactions	36
1.15.2 14-3-3 proteins	37
1.15.3 BAD:14-3-3 interactions	38
1.15.4 BAD:Glucokinase interaction	39
1.15.5 BAD:Phosphofructokinase-1 interaction	40
1.16 Hypothesized BAD:Hexokinase interactions	41
1.16.1 The Warburg Effect	41
1.16.2 Hexokinase involvement in the Warburg Effect and cancer promotion	42
1.16.3 Hexokinases: isoforms and functions	43
1.16.4 Hexokinases as potential BAD-interacting proteins	45
1.17 Thesis objective 2	45
<b>Chapter 2: Materials and Methods</b>	<b>48</b>
2.1 Cell lines	49
2.2 Propagation	49
2.3 Buffers and commonly used solutions	50
2.4 Antibodies	51
2.4.1 Primary antibodies	51
2.4.2 Secondary Antibodies	53
2.5 SDS-PAGE and western blotting	53
2.6 Drugs and treatment	54
2.6.1 Paclitaxel	54
2.6.2 Staurosporine	55

2.7 BAD coimmunoprecipitation study in MCF-7 cells.....	55
2.8 MCF-7 subcellular fractionation.....	56
2.9 BAD siRNA knock-down.....	57
2.10 DNA content analysis.....	57
2.11 Mitotic shake-off assay.....	58
2.12 Molecular subcloning.....	59
2.12.1 Plasmids.....	59
2.12.2 Primers.....	61
2.12.3 PCR amplification.....	61
2.12.4 Agarose gel electrophoresis.....	62
2.12.5 Gateway <sup>®</sup> Cloning.....	62
2.12.6 Bacterial Transformation.....	63
2.12.7 Restriction enzyme digests.....	63
2.12.8 Site-directed mutagenesis.....	64
2.13 Generation of stable cell lines.....	65
2.14 Screen for GST-BAD interacting proteins in MDA-MB-231 cells..	66
2.14.1 GST pull-down assay.....	66
2.14.2 Gel Staining.....	67
2.14.3 Mass Spectrometry.....	69
2.15 MDA-MB-231 subcellular fractionation.....	69
2.16 BAD coimmunoprecipitation.....	69
2.17 Immunofluorescence.....	70
2.18 Myc-BAD coimmunoprecipitation.....	71
2.19 Vimentin fractionation.....	72
2.20 In vitro transcription translation coupled-coimmunoprecipitation assays.....	72
2.20.1 BAD-Vimentin coimmunoprecipitation study.....	73

2.20.2 BAD-Hexokinase coimmunoprecipitation study with cross-linking .....	73
2.21 Screen for GST-BAD Serine 118A/D interacting proteins.....	74
2.21.1 GST pull-down assay in HEK 293T/17 cells.....	74
2.21.2 In gel trypsin digestion.....	75
2.21.3 Mass Spectrometry.....	76
2.22 GST-BAD transient transfections .....	76
2.23 Miscellaneous Procedures.....	76
2.23.1 Antibody cross-linking.....	76
<b>Chapter 3: Results</b> .....	<b>78</b>
3.1 BAD mediates paclitaxel cytotoxicity through a nonapoptotic pathway .....	79
3.1.1 BAD:BCL-XL interactions are diminished in paclitaxel-treated MCF-7 cells.....	79
3.1.2 BAD remains localized to the cytosol in paclitaxel-treated MCF-7 cells .....	81
3.1.3 Investigating BAD pro-proliferative function .....	83
3.1.4 BAD stimulates cell cycle progression in MCF-7 cells.....	84
3.1.5 The proliferative role of BAD confers paclitaxel sensitivity.....	85
3.2 Defining BAD interacting proteins.....	89
3.2.1 BAD:Hexokinase putative interaction study .....	90
3.2.2 GST-BAD pull-down assay as a screen for BAD- interacting proteins.....	101
3.2.3 GST-BAD localizes to membrane subfractions with endogenous BAD .....	103
3.2.4 The GST-BAD interactome in MDA-MB-231 cells .....	103
3.2.5 Pursuing vimentin as a putative BAD interacting partner .	107
3.2.6 Determination of vimentin solubility in the presence or absence of NaCl .....	114

3.2.7 BAD:vimentin coimmunoprecipitations in the absence of NaCl .....	116
3.2.8 Screening for GST-BAD S118A/D interacting proteins ...	119
3.3 Summary .....	122
<b>Chapter 4: Discussion &amp; Future Directions .....</b>	<b>125</b>
4.1 Role of BAD in paclitaxel induced cell death .....	126
4.1.1 BAD is involved in paclitaxel induced cell death through a novel, non-apoptotic pathway .....	126
4.1.2 BAD stimulates cell cycle progression .....	128
4.1.3 BAD is required for paclitaxel induced cell death in cycling cells but not in G2/M phase arrested cells .....	129
4.2 BAD interacting proteins study .....	130
4.2.1 Discussion of Hexokinases .....	130
4.2.2 Discussion of Vimentin.....	132
4.2.3 Discussion of NMHC II-A.....	133
4.3 BAD:BCL-XL interactions.....	134
4.4 BAD:14-3-3 interactions.....	135
4.5 Additional future directions .....	137
4.5.1 Paclitaxel-induced cell death .....	137
4.5.2 The role of BAD in cancer.....	137
4.6 Summary.....	139
<b>Chapter 5: References .....</b>	<b>140</b>

## LIST OF TABLES

<b>Table 1.1</b> BAD phosphorylation sites and kinases.....	33
<b>Table 2.1</b> Cell lines and propagation.....	49
<b>Table 2.2</b> Primary antibodies .....	51
<b>Table 2.3</b> Secondary Antibodies .....	53
<b>Table 2.4</b> Plasmid sources and applications.....	59
<b>Table 2.5</b> Primers used in cloning.....	61

## LIST OF FIGURES

<b>Figure 1.1</b> Orchestration of direct and indirect activation models of BAX and BAK leading to mitochondrial outer membrane permeabilization. ....	5
<b>Figure 1.2</b> Molecular structures of taxane drugs. ....	6
<b>Figure 1.3</b> BAD gene expression correlates with docetaxel sensitivity in breast cancer patients. ....	19
<b>Figure 1.4</b> BAD protein levels correlate with docetaxel sensitivity in breast cancer patients. ....	20
<b>Figure 1.5</b> BH3 domain sequence alignment. ....	25
<b>Figure 1.6</b> hBAD primary amino acid sequence annotated with phosphorylation sites and domains. ....	34
<b>Figure 3.1</b> Paclitaxel does not induce typical pro-apoptotic BAD activity. ....	80
<b>Figure 3.2</b> BAD stimulates cell cycle progression. ....	86
<b>Figure 3.3</b> BAD sensitizes MCF-7 cells to paclitaxel induced cell death via its proliferative role, and is not essential for death of M phase arrested cells. ....	87
<b>Figure 3.4</b> BAD does not detectably coimmunoprecipitate with HK I or HK II. ....	93
<b>Figure 3.5</b> Myc-BAD does not detectably coimmunoprecipitate with HK I-V5. ....	94
<b>Figure 3.6</b> Myc-BAD does not detectably coimmunoprecipitate with HK II-V5. ....	95
<b>Figure 3.7</b> BAD does not detectably coimmunoprecipitate with HK I-V5 or HK II-V5 in vitro. ....	97
<b>Figure 3.8</b> Formaldehyde cross-linking does not reveal an interaction between BAD and HK I-V5 or HK II-V5 in vitro. ....	99

<b>Figure 3.9</b> Formaldehyde cross-linking does not reveal an interaction between BAD and HK I-V5 or HK II-V5 in cells.....	100
<b>Figure 3.10</b> Validating GST-BAD pull-down assay in MDA-MB-231 cells. ....	102
<b>Figure 3.11</b> GST-BAD and endogenous BAD both localize to membrane fractions.....	104
<b>Figure 3.12</b> GST-BAD pull-down assay to isolate interacting proteins in MDA-MB-231 cells.....	105
<b>Figure 3.13</b> BAD interacting targets verified by coimmunoprecipitation in MDA-MB-231 cells and 231.BAD cells. ....	108
<b>Figure 3.14</b> Vimentin expression in breast cancer cell lines.....	109
<b>Figure 3.15</b> BAD localizes to membrane fractions and may be the site of interaction with multiple proteins. ....	111
<b>Figure 3.16</b> BAD localizes to mitochondria in MDA-MB-231 cells.....	112
<b>Figure 3.17</b> BAD and vimentin do not interact in vitro. ....	113
<b>Figure 3.18</b> Salt depletion increases solubility of vimentin in lysis buffer.....	115
<b>Figure 3.19</b> Myc-BAD does not coimmunoprecipitate detectably with Vimentin-V5 in cotransfected cells. ....	117
<b>Figure 3.20</b> Salt depletion does not enable detection of BAD:vimentin interactions.....	118
<b>Figure 3.21</b> GST-BAD Serine 118 mutants interact with multiple 14-3-3 isoforms.....	121
<b>Figure 3.22</b> BAD Serine 118 phosphorylation site mutants interact equivalently with 14-3-3 isoforms in HEK293T/17 cells.....	123

**Figure 3.23** BAD S118D interacts preferentially with 14-3-3 isoforms compared with BAD S118A in MDA-MB-231 cells. .... 124

## LIST OF SYMBOLS & ABBREVIATIONS

A (Ala)	Alanine
AIF	Apoptosis-inducing factor
ATP	Adenosine triphosphate
A1	BCL-2 related protein A1
BAD	BCL-2 antagonist of cell death
BAK	BCL-2-associated X protein
BAX	BCL-2 antagonist/killer protein
BCL-2	B-cell lymphoma 2
BCL-W	BCL-2 like protein 2
BCL-XL	BCL-2 like protein extra large
BCL-XS	BCL-2 like protein extra small
BH	BCL-2 homology domain
BID	BH3-interacting domain death agonist
BIK	BCL-2-interacting killer
BIM	BCL-2-interacting mediator of cell death
BMF	BCL-2 modifying factor
BNIP3	BCL-2/adenovirus E1B 19kDa interacting protein 3
BOK	BCL-2-related ovarian killer
BSA	Bovine serum albumin
BubR1	Bub1-related protein kinase
CaCl <sub>2</sub>	Calcium chloride
CaMKII	Calcium/Calmodulin-dependent protein kinase II
Cdk	Cyclin-dependent kinase
Chk1	Checkpoint kinase 1
CHAPS	3-[(3-Cholamidopropyl)dimethylammonio]-1-propanesulfonate
CK2	Casein kinase 2
coIP	coimmunoprecipitation
CX-1	Human colon adenocarcinoma cell line
ddH <sub>2</sub> O	Distilled, deionized water
DIABLO	Direct inhibitor of apoptosis-binding protein of low pI
DMEM	Dulbecco's Modified Eagle Medium
DMP	dimethyl pimelimidate
DMSO	Dimethyl sulfoxide
DNA	Deoxyribonucleic acid
dNTP	Deoxyribonucleoside triphosphate
DTT	Dithiothreitol
ECL	Enhanced chemiluminescence
EDTA	Ethylenediaminetetraacetic acid
E-site	Exchangeable site
EMT	Epithelial-mesenchymal transition
ER	Endoplasmic reticulum
E2F1	E2F transcription factor 1
E2F4	E2F transcription factor 4
FACS	Fluorescence activated cell sorting

FADH <sub>2</sub>	Flavin adenine dinucleotide, reduced form
FCS	Fetal calf serum
GAPDH	Glyceraldehyde 3-phosphate dehydrogenase
GDP	Guanosine 5'-diphosphate
GK	Glucokinase
GKRP	Glucokinase regulatory protein
GrA	Granzyme A
GST	Glutathione S-transferase
GTP	Guanosine 5'-triphosphate
G0 phase	Resting or quiescent state
G1 phase	Interphase – gap phase 1
G2 phase	Interphase – gap phase 2
G-6-P	Glucose 6-phosphate
hBAD	Human BAD
HBS	HEPES-buffered saline
HCl	Hydrochloric acid
HEK	Human embryonic kidney
HK	Hexokinase
HPLC	High performance liquid chromatography
HRK	Harakiri
HRP	Horseradish peroxidase
HtrA2/Omi	High temperature requirement protein A2
IAP	Inhibitor of apoptosis
IB	Immunoblot
IGF-1	Insulin-like growth factor 1
IgG	Immunoglobulin G
IL-3	Interleukin 3
IP	Immunoprecipitation
IVTT	In vitro transcription-translation
JNK	c-Jun N-terminal kinase
KCl	Potassium chloride
KH <sub>2</sub> PO <sub>4</sub>	Potassium phosphate monobasic
K <sub>m</sub>	Michaelis constant
LB	Lysogeny broth
LBD1	Lipid binding domain 1
LBD2	Lipid binding domain 2
LC-MS/MS	Liquid chromatography tandem mass spectrometry
LX-1	Human lung carcinoma cells
M phase	Mitotic phase
MAPs	Microtubule associated proteins
mBAD	Murine BAD
MCF-7	Michigan Cancer Foundation-7
MCL-1	Myeloid cell leukemia sequence-1
MDA-MB-231	M.D. Anderson-Metastatic Breast-231
MDA-MB-468	M.D. Anderson-Metastatic Breast-468
MEF	Mouse embryonic fibroblasts

MgCl <sub>2</sub>	Magnesium chloride
Mirk	Minibrain-related kinase
mRNA	Messenger RNA
MTT	Methylthiazole tetrazolium assay
MX-1	Human mammary carcinoma cells
MycER	Myc-estrogen receptor fusion protein
MYH9	Cellular myosin heavy chain 9
NaCl	Sodium chloride
NADH	Nicotinamide adenine dinucleotide, reduced form
NADPH	Nicotinamide adenine dinucleotide phosphate, reduced form
Na <sub>2</sub> HPO <sub>4</sub> ·7H <sub>2</sub> O	Sodium phosphate dibasic heptahydrate
NIH 3T3	Mouse embryonic fibroblasts
NMHC	Non-muscle myosin heavy chain
NMR	Nuclear magnetic resonance
NP-40	IGEPAL <sup>®</sup> CA-630
N.S.	Non-specific
NSCLC	Non-small cell lung cancer
N-site	Non-exchangeable site
Pac	Paclitaxel
PAGE	Polyacrylamide gel electrophoresis
PAK	p21-activated kinase
PBS	Phosphate-buffered saline
PFK	Phosphofructokinase
PIM	Provirus integration site for Moloney murine leukemia virus 1
PKA	cAMP-dependent protein kinase
PP1	Protein phosphatase 1
PP1c	Protein phosphatase 1 catalytic subunit
PP2A	Protein phosphatase 2A
PUMA	p53-upregulated modulator of apoptosis
PVDF	polyvinylidene fluoride
p70RSK	p70 ribosomal S6 kinase
p90RSK	p90 ribosomal S6 kinase
RNA	Ribonucleic acid
RNase	Ribonuclease
ROS	Reactive oxygen species
RPMI	Roswell Park Memorial Institute medium
S (Ser)	Serine
S phase	Interphase - synthesis phase
SAHB	Stabilized alpha-helix of BCL-2 family BH3 domain
SDS	Sodium dodecyl sulfate
siRNA	small interfering RNA
SMAC	Second mitochondria-derived activator of caspases
STS	Staurosporine
S118A	Serine 118 to Alanine mutation
S118D	Serine 118 to Aspartate mutation
tBID	truncated BH3-interacting domain

TBS-T	Tris-buffered saline Tween 20
TMRE	Tetramethylrhodamine ethyl ester
Tom20	Translocase of outer mitochondrial membranes 20 kDa
VDAC	Voltage-dependent anion channel
V5	Epitope tag
WAVE-1	Wiskott-Aldrich syndrome protein family member 1
wt	Wild type
$\Delta\psi$	Mitochondrial depolarization
$\Delta$	Deleted

## **Chapter 1: Introduction**

## **1.1 Apoptosis**

Apoptosis, commonly referred to as programmed cell death, is an evolutionarily conserved process amongst metazoa that leads to ordered dismantling of the cell. The term 'apoptosis' was first used by Kerr et al. in 1972 (1) to describe the morphological characteristics associated with this form of cell death. Namely, apoptosis is accompanied by chromatin condensation, nuclear fragmentation, cytoplasmic shrinkage, membrane blebbing and rounding-up of the cell (2). Cell components are fragmented into membrane-bound apoptotic bodies and rapidly engulfed by phagocytic cells (1).

Apoptotic cell death is an important homeostatic mechanism for the development and maintenance of healthy tissues. Physiological deletion of cells is important in such processes as embryological development, including embryoid cavitation (3) and death of the inner cell mass (4), digit formation (5,6), post-lactational involution of the mammary gland (7) and removal of damaged or abnormal cells. The latter is particularly important for tissue integrity and avoiding the cancerous phenotype.

## **1.2 Evasion of apoptosis in cancer**

The transformation of normal cells to cancerous cells of unrestrained cellular proliferative and invasive capabilities involves a multi-step process of genetic changes (8). Amongst the commonly acquired characteristics of cancer cells, including sustained growth signaling and proliferative capacity, cancer cells often acquire the ability to evade apoptosis (9). This has been described as one of

the key hallmark features of cancer cells (9). In the presence of genetic damage that would cause normal cells to undergo apoptosis or senescence, cancer cells continue to proliferate and sustain genetic damage that can enhance the proliferative and invasive phenotype.

### **1.3 Molecular modulators of apoptosis: the BCL-2 family**

The apoptotic pathway is an intrinsic cell death pathway modulated by the BCL-2 family of proteins. This protein family includes: pro-apoptotic BH3 only proteins (BID, BIM, BAD, BIK, PUMA, NOXA, BMF, HRK, BNIP3); multidomain pro-apoptotic proteins (BAX, BAK, BOK); and anti-apoptotic proteins (BCL-2, BCL-XL, BCL-W, A1, MCL-1) (reviewed in (10)). The BH3 only proteins can be further subdivided into direct activators of BAX and BAK (BIM, tBID and PUMA) and indirect activators or sensitizers of BAX and BAK (BAD, NOXA, BIK, BMF) (11). In the direct activation model of apoptosis, BH3 only proteins must be activated to directly engage and activate BAX and BAK through their BH3 domain. First, sensitizer BH3 only proteins are activated in response to an apoptotic stimulus and bind anti-apoptotic BCL-2 family members. This derepresses direct activator BH3-only proteins that can directly engage BAX and BAK (12). In the indirect activation model, BAX and BAK are primed in healthy cells and need to be repressed by anti-apoptotic proteins to prevent cell death. BH3-only proteins are required not to directly engage Bax and BAK, but to derepress BAX and BAK by inhibiting their anti-apoptotic protein binding partners (12). There is ongoing controversy as to the relevance of each model of

BAX/BAK activation, and indeed, both models may be partially correct (reviewed in (11)) (**Figure 1.1**).

Following activation, BAX and BAK oligomerize at the outer mitochondrial membrane causing release of pro-apoptotic factors from the intermembrane space (cytochrome c, AIF, SMAC/DIABLO, HtrA2/Omi and endonuclease G) (13). AIF and endonuclease G are involved with DNA fragmentation (13). SMAC/DIABLO and HtrA2/Omi inhibit IAPs to derepress caspase activation (13). Cytochrome c assembles with Apaf-1 to form the apoptosome that initiates activation of the caspase cascade that ultimately results in cellular demolition (14).

## **1.4 Taxanes as chemotherapeutic agents**

### **1.4.1 Paclitaxel**

Taxol<sup>®</sup> (trademark of Bristol-Myers Squibb), also known as Paclitaxel, was originally isolated from the bark of the Pacific yew tree, *Taxus brevifolia*, as part of the National Cancer Institute directed Cancer Chemotherapy National Service Centre screening program for natural products with cytotoxic activity (15). The molecular structure of paclitaxel is shown in **Figure 1.2 A**. With its initial publication, paclitaxel was found to possess anti-tumor activity against murine leukemias, lung tumors and carcinosarcoma models (15). Studies on cells isolated from ascites fluid of paclitaxel treated mice bearing P388 leukemia provided the first evidence that paclitaxel possessed the antimitotic activity

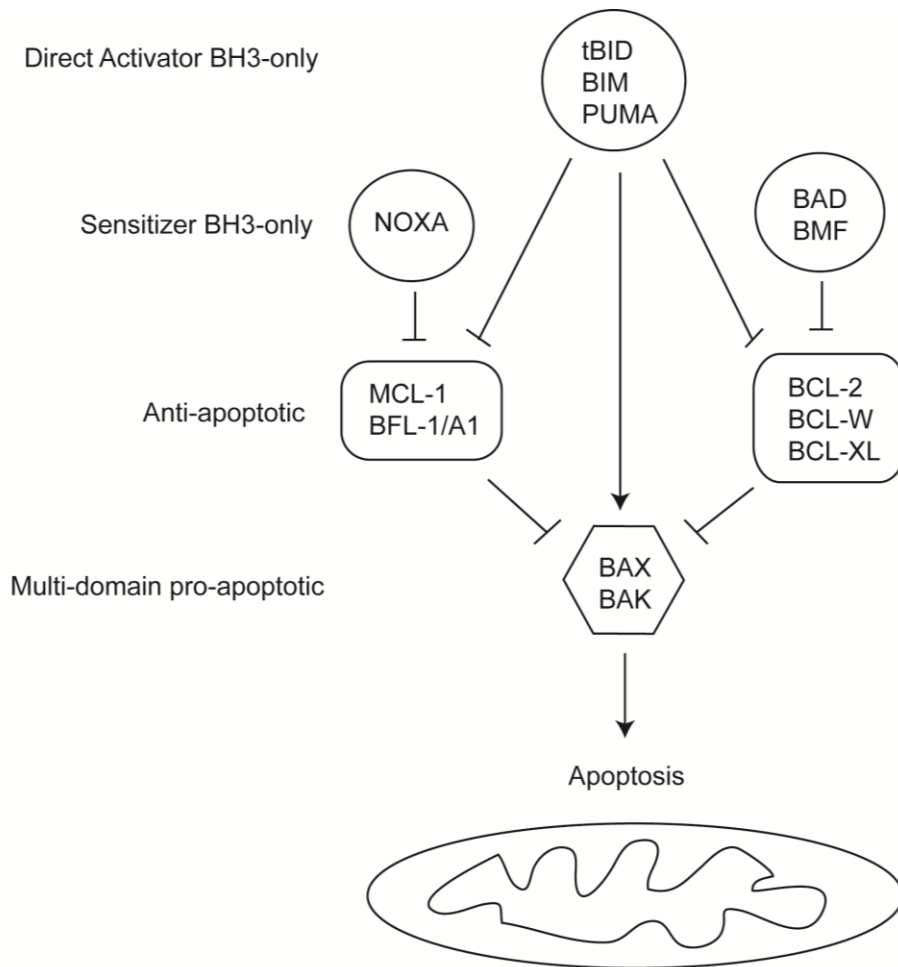


**Figure 1.1 Orchestration of direct and indirect activation models of BAX and BAK leading to mitochondrial outer membrane permeabilization.** In the direct activation model, sensitizer BH3-only proteins are activated by an apoptotic stimulus and inhibit anti-apoptotic proteins. This releases direct activator BH3-only proteins (tBID, BIM, PUMA) that are required to directly engage and activate BAX and BAK. In the indirect activation model, BAX and BAK are primed for cell death but held in check by anti-apoptotic proteins. BH3-only proteins are activated to neutralize anti-apoptotic BCL-2 family binding partners and release BAX and BAK primed for activation. BAD is an indirect activator of BAX and BAK that targets anti-apoptotic proteins BCL-2, BCL-W and BCL-XL. Image adapted from (16).

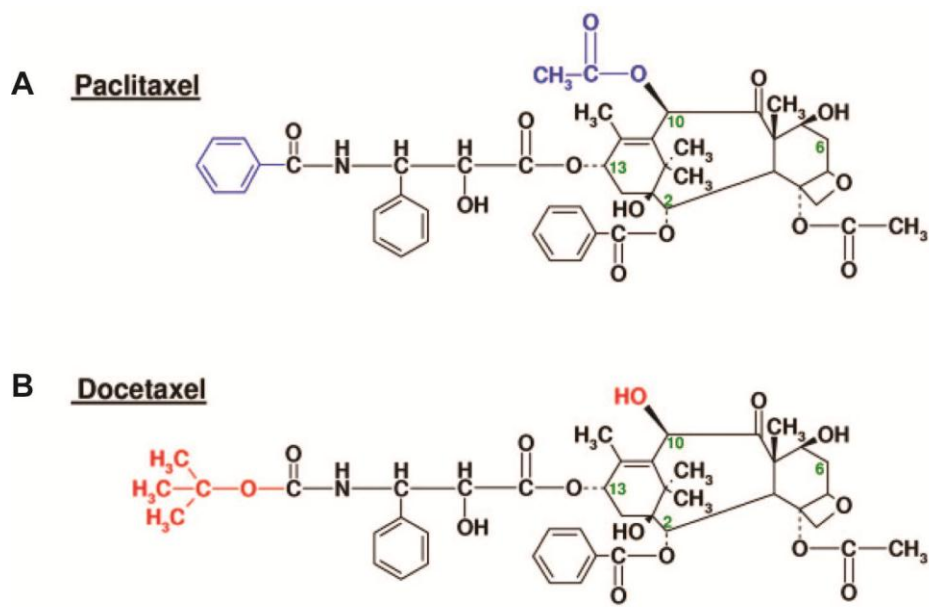


**Figure 1.2 Molecular structures of taxane drugs.**

(A) Paclitaxel and (B) Docetaxel are shown with differing substituents. Docetaxel is a semisynthetic analog of paclitaxel prepared from 10-deacetyl baccatin III. Adapted from Anderson, A et al (17).

characteristic of the vinca alkaloids, although it was a less efficient mitotic spindle poison (18). In vitro studies later identified a novel mechanism of action for paclitaxel as a microtubule stabilizing and polymerizing agent (19) that led to cell cycle arrest at G2/M phase (20). Paclitaxel was the first microtubule polymerizing agent to be introduced with anti-neoplastic effects. Up until its discovery, microtubule depolymerizing agents colchicine and vinca alkaloids were commonly used (reviewed in (21)).

Clinical interest in paclitaxel was generated by its success in screens of human tumors xenografted into mice including MX-1 mammary tumor, CX-1 colon tumor and LX-1 lung tumor as well as against murine B16 melanoma (reviewed in (21)). Furthermore, paclitaxel was also effective against solid human tumors of primary breast, endometrium, lung, ovary, tongue and brain tumors implanted into mice (22).

Paclitaxel was first approved by the US Food and Drug Administration in 1992 for the treatment of refractory ovarian cancer. Paclitaxel has since been widely used in the treatment of breast, ovarian and lung cancers.

#### **1.4.2 Docetaxel**

Progress in clinical trials of paclitaxel was hindered by its limited availability from natural resources and the high cost and low-yielding extraction process from the bark of the Pacific yew tree. Docetaxel was prepared as a semi synthetic taxol analogue by the Institut de Chimie des Substances Naturelles with the Centre National de la Recherche Scientifique in France using a noncytotoxic

compound, 10-deacetyl baccatin III, extracted from the leaves of the European yew tree, *Taxus baccata L.* (23,24). The molecular structure of docetaxel is shown in **Figure 1.2 B**. Like paclitaxel, docetaxel induces tubulin assembly in vitro in the absence of GTP, induces microtubule bundle formation, and inhibits cell division (25). At equal drug concentrations, docetaxel is a slightly more potent promoter of tubulin polymerization and more potent inhibitor of proliferation of murine leukemia and macrophage-like cell lines (25). Docetaxel has been approved by the US Food and Drug Administration for the treatment of head and neck cancer, gastric cancer, breast cancer and prostate cancer.

### **1.5 Microtubule structure and dynamics**

Microtubules are an important cytoskeletal component of eukaryotic cells (26), composed of alternating 50 kDa  $\alpha$  and  $\beta$  tubulin subunits. Microtubules are assembled by the head-to-tail polymerization of  $\alpha/\beta$  tubulin heterodimers to form long, linear, polarized protofilaments (27,28). Protofilaments assemble laterally to form a hollow tube of 25 nm diameter (29). It is generally thought that in vivo, 13 such protofilaments assemble to form a microtubule. In vitro, the number of protofilaments can vary significantly, from 11-15 (30,31).

Each soluble  $\alpha/\beta$  tubulin heterodimer is bound by two molecules of guanine nucleotide: one GTP is irreversibly bound at a non-exchangeable site of the  $\alpha$ -subunit (N-site) and one GTP is reversibly bound at the exchangeable site of the  $\beta$ -subunit (E-site) (reviewed in (32)). As microtubules polymerize, a conformational change of the incorporated subunits promotes hydrolysis of GTP

bound at the E-site of the  $\beta$ -subunit to non-exchangeable GDP (33), which remains bound in the polymerized microtubule. Notably, while GTP hydrolysis at the  $\beta$  subunit is dependent on tubulin polymerization, these two processes are kinetically uncoupled (34); GTP hydrolysis occurs subsequent to polymerization (35). Therefore at steady state, a GTP rich cap forms at the + ends of microtubules (35). In vivo, the loss or presence of the GTP cap allows for microtubule catastrophe or rescue (36,37). In this way the rate of GTP hydrolysis helps modulate microtubule dynamic instability and microtubule length (38).

Microtubule dynamics are critical for appropriate cell division at mitosis. The dynamic instability of spindle microtubules, anchored at the centrosome at their – ends, probe the cytoplasm through a ‘search and capture’ mechanism for the presence of condensed chromosomes (39). Bipolar attachment of paired kinetochores to opposite spindle poles must occur to bypass the spindle assembly checkpoint and allow for anaphase progression (40). By interfering with microtubule dynamics, mitotic spindle poisons can serve as effective chemotherapeutics to arrest cell division (41). Spindle poisons such as paclitaxel lead to prolonged activation of the spindle assembly checkpoint (40,41), which has been associated with apoptotic cell death directly following mitotic arrest or following mitotic slippage (42).

### **1.6 Taxanes promote microtubule stabilization and assembly**

Taxanes induce mitotic arrest in cells by stabilizing microtubules or causing microtubule bundling (20). Paclitaxel was first shown to promote in vitro

assembly of purified tubulin into microtubules with altered equilibrium and kinetic parameters that reduced the lag time and the critical concentration of soluble tubulin required for microtubule polymerization (19). Microtubules polymerized in the presence of paclitaxel are uniquely resistant to depolymerization by dilution, low temperature (4°C) or 4 mM CaCl<sub>2</sub> (19). The microtubule assembly process in the presence of paclitaxel can also take place in the absence of typical microtubule assembly factors such as GTP and microtubule associated proteins (43). Both paclitaxel and docetaxel induce maximal tubulin polymerization at 1:1 molar ratios of drug and  $\alpha\beta$  tubulin heterodimer, suggesting uniform stoichiometric binding of the drug along the microtubule (44). A competition assay by Diaz et al showed that docetaxel had 1.9 times the affinity of paclitaxel for common binding sites on microtubules (44). Furthermore, docetaxel was also a more potent inducer of tubulin polymerization than paclitaxel that had a 2.1 fold larger equilibrium constant (44).

### **1.7 Characterization of the taxane binding site on microtubules**

Paclitaxel binds to the globular domain of  $\beta$ -tubulin in a hydrophobic pocket opposite the GTPase domain on the inner luminal surface of microtubules (reviewed in (45)). Taxane binding occurs with 1:1 stoichiometry of bound drug to  $\alpha\beta$  tubulin heterodimer of polymerized microtubules, but does not bind to monomeric soluble tubulin (44,46).

The paclitaxel binding site was initially identified on  $\beta$ -tubulin using [<sup>3</sup>H] taxol and photoaffinity labeling of purified microtubule protein (47). Photoaffinity

labeling studies using taxol analogues mapped the  $\beta$ -tubulin binding site (48-50). Three contact points were proposed by these authors at amino acids 1-31, 217-233 and amino acid arginine 282, which is also important for adjacent protofilament interactions (50). Furthermore, there was good agreement in the paclitaxel binding model proposed by Rao et al in photoaffinity labeling studies and the proposed location of the taxol binding site in reconstructed 3-dimensional models of electron crystallography studies of zinc induced  $\alpha\beta$  tubulin sheets (46,51,52).

While the above studies characterized a high affinity binding site for taxanes on the luminal surface of microtubules, kinetic data was irreconcilable with models proposing simple diffusion of taxanes through fenestrations of the microtubule wall to reach the luminal binding site (53,54). Binding of taxol to microtubules was extremely rapid, reversible, and could disrupt protofilament number (55). The rapid binding kinetics of fluorescent taxoid derivatives required an alternative model of taxane-microtubule binding where docking could occur at a more easily accessible site, most likely on the exterior of the microtubule (53). Further kinetics studies provided evidence for a microtubule external ligand binding site. Diaz et al found that fluorescent taxol derivatives undergo diffusion controlled association with microtubules, and association kinetics were greatly impeded by microtubule associated proteins (MAPs) on the surface of microtubules (56). While it is still not clear how taxanes molecules bound at low affinity sites on the exterior of microtubules are internalized to the luminal face, currently accepted models suggest a mechanism of penetration of microtubule stabilizing agents through pre-formed pores in the microtubule wall (54,57,58).

## **1.8 Mechanisms of taxane induced cell death**

### **1.8.1 Apoptosis at low nanomolar paclitaxel concentrations**

The molecular effects of paclitaxel vary considerably with the concentration and time of application of the drug (59). Breast cancer cells treated with titrated doses of paclitaxel, from 5 nM to 25  $\mu$ M, revealed a biphasic dose-response curve with distinct death mechanisms (60). At low nanomolar concentrations, 5-50 nM, paclitaxel induced mitotic arrest, inhibited S phase progression and induced apoptotic cell death (60). However, increasing the paclitaxel concentration from 1.25  $\mu$ M to 25  $\mu$ M reduced apoptotic cell death and increased necrotic cell death (60). Furthermore, micromolar drug concentrations induced microtubule bundling which was not observable at the lower concentration range (60).

We used low nanomolar concentration paclitaxel (25 nM) in our experiments to induce breast cancer cell apoptosis at a clinically relevant dose, in agreement with previous work (61,62). This leads to stabilization of mitotic spindle microtubules (63,64) and activation of the spindle assembly checkpoint. However, in some cancer cells, weakened checkpoints may allow for aberrant mitosis to proceed without cytokinesis, also termed mitotic slippage (65,66).

Altogether, these studies support a mechanism for paclitaxel induced mitotic arrest followed by apoptosis in cells treated with low nanomolar concentrations of paclitaxel. However, the molecular mechanisms of paclitaxel induced cell death of breast cancer cells remains unknown. Our laboratory initially used multiple parameters to measure paclitaxel-induced apoptosis,

including loss of mitochondrial membrane potential using the fluorescent dye tetramethylrhodamine ethyl ester perchlorate (TMRE) (Invitrogen, cat. T669), phosphatidylserine externalization with Annexin V staining and caspase activation using a fluorescent CaspACE<sup>™</sup> FITC-VAD-FMK stain (Promega, cat. G7461). TMRE is a cationic dye taken up by mitochondria with  $\Delta\Psi_m$ . CaspACE<sup>™</sup> FITC-VAD-FMK irreversibly binds active caspases. These stains were monitored in previous work by FACS analysis (data not shown). These experiments verified an apoptotic phenotype of breast cancer cells treated with 25 nM concentration paclitaxel. In the experiments presented in this thesis, cell death was monitored using TMRE stain and FACS analysis (67).

### **1.8.2 Role of BIM in paclitaxel induced apoptosis**

The BH3-only protein, BIM, is a direct activator of BAX and BAK (68,69) but is also capable of interacting with anti-apoptotic BCL-2 family members including BCL-2, BCL-XL, MCL-1 and A1 (70,71). Studies have implicated a critical role for BIM in paclitaxel-induced apoptosis of non-small cell lung cancer cell lines (72), prostate cancer cell lines (72), neuroblastoma cells (73) and murine thymocytes (74). In a panel of non-small cell lung cancer cell lines, Li R et al first assessed protein expression levels of BCL-2 family members, and noted a correlation between increased BIM expression and enhanced sensitivity to paclitaxel induced apoptosis (72). This correlation was also found in a panel of breast and prostate cancer cells in the same study (72). Transient or stable depletion of BIM provided protection from paclitaxel cytotoxicity (72).

Inversely, BIM overexpression in a resistant NSCLC cell line conferred sensitivity to paclitaxel (72). In neuroblastoma cells, downregulation of BIM also provides protection from paclitaxel induced cell death (73). Overall, these studies provide a quantitative link between BIM protein expression and paclitaxel induced apoptosis.

Using a similar approach, our laboratory correlated protein expression levels with paclitaxel sensitivity in a panel of breast cancer cell lines (67). We found that higher BIM and BAD protein expression in cell lysate correlated with paclitaxel sensitivity, with the greatest expression in SKBR-3, MCF-7 and MDA-MB-468 cells. Surprisingly, however, BIM depletion prior to paclitaxel treatment does not afford protection of these cells from paclitaxel induced apoptosis (75). In MCF-7 cells, BIM provided very minor protection from apoptosis compared to the dramatic protection offered by BAD depletion (67). We also pursued the relevance of BIM expression by analyzing gene expression profiles of docetaxel-treated primary breast cancer patients (data set compiled by (76)). Surprisingly, increased BIM expression in primary tumors correlated with docetaxel resistance (**Figure 1.3**). Overall, we concluded that BIM did not play a prevalent role in paclitaxel induced death of breast cancer cells.

Despite these findings, the role of BIM remains controversial. Our results contradict previous reports that determine a proapoptotic function for BIM in the context of paclitaxel treatment of MCF-7 cells (77,78). Sunter et al. reported FoxO3a induction of BIM expression in MCF-7 cells with paclitaxel treatment that correlates with apoptosis (78). Additionally, BIM depletion experiments in

MCF-7 cells conferred significant protection from paclitaxel induced apoptosis in multiple studies (77,78). A molecular model for the dynamics of BIM in taxane treated cells has been proposed, where an unknown upstream activation signal triggers BMF or PUMA to displace BIM from anti-apoptotic binding partners BCL-2 or BCL-XL respectively (77). This relieves a pool of free BIM that correlates with the activation of BAX and BAK (77). These authors, however, did not observe an upregulation of BIM expression in MCF-7 cells and is therefore inconsistent with the study of Sunters et al (77,78).

It is difficult to qualify these polar arguments that either enforce or refute the role of BIM as a major molecular player in the paclitaxel-induced apoptotic cell death pathway. Drug concentrations used in these studies were of similar range: 25 nM (75), 10 nM (78) and 100 nM (77), which are low doses that have been shown to induce the apoptotic cell phenotype. Our laboratory's study quantified the apoptotic phenotype of MCF-7 cells by loss of TMRE fluorescence, whereas Kutuk et al and Sunters et al quantified Annexin V positivity. It seems unlikely that we can account for discrepancy between these studies based on apoptotic readouts and a lack of functional caspase 3 in this cell line (79,80) since other work has shown that reinstatement of stable caspase-3 expression in MCF-7 cells saw no change in BAX induced apoptotic readouts by Annexin V staining (81). However, it is possible that genetic differences between individual MCF-7 cell lines may account for some of the discrepancy. Indeed, significant genetic (82), karyotypic and biological differences (83) have been revealed in MCF-7 cell

lines obtained from different sources, which may in part be attributed to inherent genomic instability during in vitro culture of these cells (84).

### **1.9 Staurosporine induced apoptosis**

Staurosporine is a microbial alkaloid isolated from *Streptomyces staurosporeus* (85) that has potent inhibitory activity against protein kinases with poor selectivity (86-88). Staurosporine has an ATP-competitive mode of action which may account for its wide-spectrum inhibition of both tyrosine and serine/threonine kinases (89,90). Staurosporine treatment induces apoptosis by both caspase-dependent and independent mechanisms (91-93). In caspase 3 deficient MCF-7 cells, apoptosis may proceed with activation of alternative caspases (94-96). Interestingly, the apoptotic phenotype is greatly enhanced in MCF-7 cells stably expressing caspase 3 by activation of extrinsic apoptotic pathway components, including caspase 8 and BID (95,97). However, both MCF-7 cells and caspase 3-expressing MCF-7 cells demonstrate staurosporine induced cytochrome c release (97). Altogether, these studies suggest that MCF-7 cells treated with staurosporine die as a result of mitochondrial dysfunction through caspase dependent or independent mechanisms. Additionally, dephosphorylation of BAD has previously been documented in HeLa cells treated with staurosporine, which corresponds with BAD activation (98). We used staurosporine treatment in our experiments to induce pro-apoptotic BAD activity and mitochondrial apoptosis in MCF-7 cells.

## **1.10 Role of BAD in paclitaxel induced apoptosis**

### **1.10.1 BAD expression correlates with taxane sensitivity in vitro**

Given the unknown mechanisms of paclitaxel induced apoptosis of breast cancer cells, our laboratory was interested in deciphering which BCL-2 family members were critical for the cell death process. We screened a panel of five breast cancer cell lines for sensitivity to paclitaxel and correlated apoptotic cell death with protein expression levels of BCL-2 family members in untreated cells (67). We observed that the expression levels of BH3-only BIM and BAD correlated with taxane sensitivity. Previous investigations in our laboratory using BIM depletion studies indicated that Bim protein levels were not critical for paclitaxel induced cell death of breast cancer cell lines (75). We therefore decided to focus our efforts on determining the role of BAD in paclitaxel cytotoxicity with the experiments in this thesis.

### **1.10.2 BAD expression correlates with taxane sensitivity in clinical studies**

Our laboratory sought to validate an in vitro correlation of BAD expression and paclitaxel sensitivity with in vivo data. Our clinical studies revealed a correlation between elevated BAD expression at the mRNA and protein level and sensitivity to taxanes in clinical studies (67). First, we compiled a gene expression microarray using expression data from 24 primary breast tumor biopsies that was published by Chang et al. (76). After sample collection in this study, patients received 4 cycles of neoadjuvant docetaxel treatment (76). Patient tumors were stratified as docetaxel sensitive or resistant based on residual tumor

volume of less or greater than 25% after chemotherapy (76). Our analysis of this gene expression data demonstrates a positive correlation of increased BIK, BAD and BAX expression with docetaxel sensitivity (**Figure 1.3**).

In our second clinical study, we sought an assessment of BAD protein levels and taxane sensitivity (67). Our clinical collaborators performed BAD immunohistochemistry staining on 180 formalin-fixed primary breast tumor specimens from patients who had been treated with adjuvant docetaxel chemotherapy. BAD staining was scored semi-quantitatively by a breast cancer pathologist and stratified into either high or low protein expression levels. Results were plotted on a Kaplan Meier survival curve (**Figure 1.4**). This study demonstrated that high BAD protein levels ( $>0.57$ ) were prognostic for improved disease-free and overall survival of breast cancer patients treated with docetaxel.

Altogether, the results of clinical studies were supportive of our in vitro data: BAD confers sensitivity to taxanes. These promising findings rationalized further investigation of the mechanisms of BAD function in breast cancer cells in response to paclitaxel treatment.

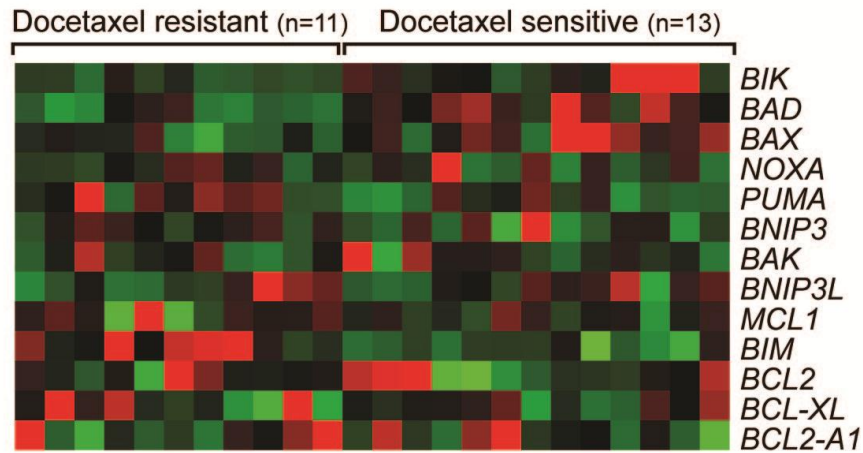


**Figure 1.3 BAD gene expression correlates with docetaxel sensitivity in breast cancer patients.**

Gene expression data obtained from (76) was analyzed for the expression of BCL-2 family proteins. This study analyzed gene expression data from primary breast tumors from 24 patients receiving neoadjuvant docetaxel chemotherapy. Red signals indicate higher gene expression levels; green signals indicate lower gene expression levels. Image adapted from (67).

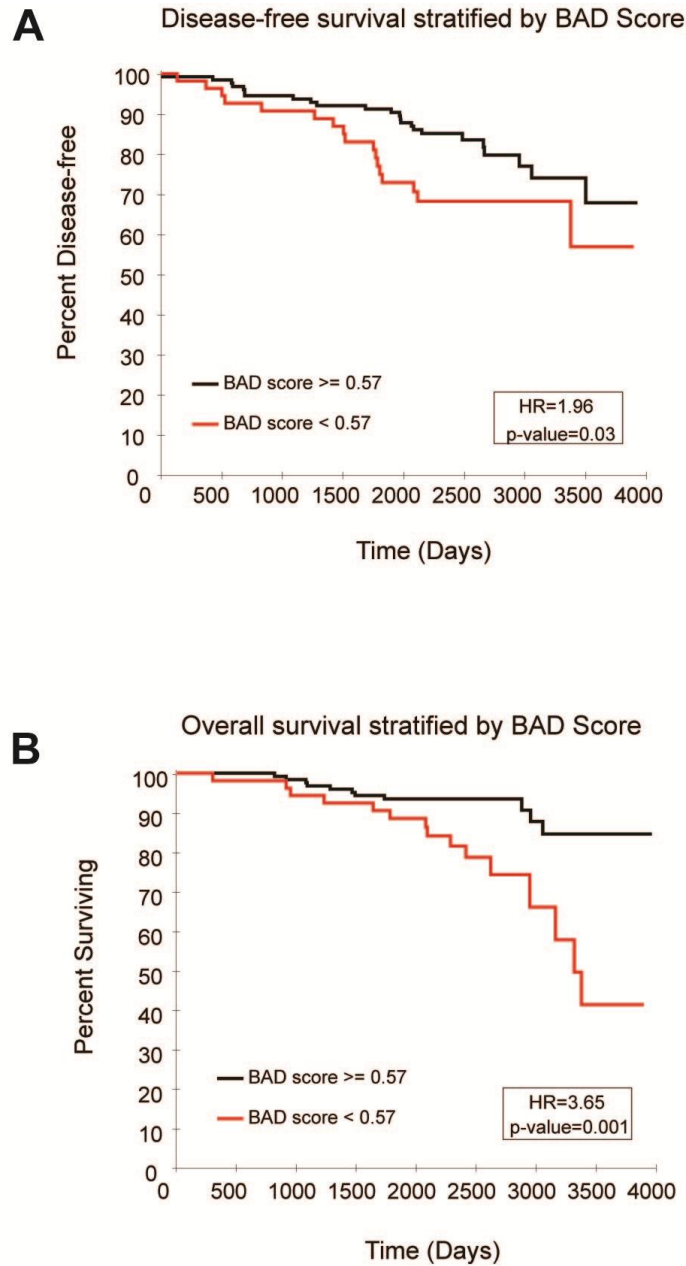


**Figure 1.4 BAD protein levels correlate with docetaxel sensitivity in breast cancer patients.**

BAD immunohistochemistry was performed on breast tumor samples from 180 primary breast cancer patients receiving adjuvant docetaxel chemotherapy. Kaplan-Meier curves show that BAD expression is prognostic for disease-free survival (A) and overall survival (B). Image adapted from (67).

## **1.11 BAD (BCL-2 antagonist of cell death)**

### **1.11.1 Identification and characterization**

BAD was first isolated as a BCL-2 interacting protein using a yeast two-hybrid screen and  $\lambda$  expression cloning (99). The primary sequence of murine BAD bears only highly conserved amino acids within the BH1 and BH2 domains and contains a highly conserved BH3 domain that confers its pro-death activity (100) and classifies the protein as a BH3-only member of the BCL-2 family. The BH3 domain in human BAD was independently mapped and encompasses amino acids 108-123 (101). The BH3 domain forms an amphipathic  $\alpha$ -helix that engages the hydrophobic groove of an anti-apoptotic protein to exert the pro-death phenotype (102,103). In response to an apoptotic stimulus, BAD pro-apoptotic activity is activated by dephosphorylation. When the hBAD BH3 domain is dephosphorylated, BAD can engage BCL-XL, migrate to the mitochondria and induce apoptosis (reviewed in (104)) (see also **section 1.15.1**).

### **1.11.2 Physiological roles**

BAD is an important apoptotic sensitizer with tumor suppressor activity in lymphocytes and lymphocytic precursors. BAD knock-out mice are developmentally normal with only mild abnormalities in B-cells bearing modestly reduced proliferation rates and significantly reduced production of IgG with LPS stimulation (105). With aging, however, additional phenotypes become evident including reduced survival of the *BAD*  $-/-$  mice compared to *BAD* WT mice. It was found that *BAD*  $-/-$  mice have increased mortality with incidence of diffuse

large B cell lymphoma (105). *BAD*  $-/-$  mice also develop lymphomas of the B and T cell lineages at higher rates than wild type counterparts when challenged with sublethal doses of  $\gamma$ -irradiation (105). Overall, studies of the BAD deficient mouse model suggest an important tumor suppressor function for BAD in the lymphoid system.

While there are no defects in T cell development in BAD deficient mice (105), an important role for BAD has nonetheless been elucidated in thymocytes (106). BAD expression is upregulated in thymocytes undergoing apoptosis in response to dexamethasone or  $\gamma$ -irradiation (106). Furthermore, transgenic mice that harbor T cell-specific overexpression of BAD have reduced numbers of T cells and enhanced T cell sensitivity to apoptotic stimuli. Overall, these studies suggest a critical tumor suppressor role for BAD in B-cells and an important physiological role for BAD in regulating T cell homeostasis and apoptosis.

BAD protein is widely expressed in human tissues, with highest expression levels in the testes, breast, spleen and tonsil (107).

Immunohistochemistry analysis for BAD revealed cytosolic localization as well as localization with discrete organelles in columnar epithelium of breast tissue (107). Physiologically, BAD expression is upregulated in mammary epithelial cells during lactation and involution (108,109), a remodeling of mammary glands to a pre-pregnancy like state characterized by extensive apoptosis (reviewed in (110)). Metcalfe et al suggest that BAD and BAK elevation primes epithelial cells for apoptosis when the levels of anti-apoptotic BCL-W decline during involution

(109). Thus, BAD may have a pro-apoptotic function in vivo in eliminating unneeded mammary epithelial cells.

### 1.11.3 BH3 domain

The BH3 domain was initially characterized in BAK, including amino acids 67-94, as a domain that was necessary and sufficient for inducing cell death activity and for binding BCL-XL (111). Chittenden et al also identified a homologous amino acid sequence in BAX, and found that the pro-death function of this domain was conserved. The BH3 domain in hBAD was first elucidated in binding assays using BAX and BAK BH3 peptides to compete a BAD:BCL-XL interaction (101). Peptides of the predicted hBAD BH3 sequence were also able to compete BAD:BCL-XL and BAX:BCL-XL interactions, indicating the critical role for the BH3 domain in establishing these interactions (101).

NMR structural studies indicated that the BAK BH3 peptide forms an amphipathic alpha helix that interacts with BCL-XL through hydrophobic and electrostatic interactions, dependent on conserved residues within the BH3 domain (102). **Figure 1.5** demonstrates an alignment of BH3 domains from a selection of both pro-apoptotic and anti-apoptotic BCL-2 family members (112). Important hydrophobic side chains of BAK residues that interact with the BCL-XL hydrophobic cleft include Val<sup>74</sup>, Leu<sup>78</sup>, Ile<sup>81</sup> and Ile<sup>85</sup> (102). Alanine substitutions at any of these sites dramatically reduces binding affinity with BCL-XL. Important electrostatic interactions were formed with charged BAK residues, Arg<sup>76</sup>, Asp<sup>83</sup>, and Asp<sup>84</sup>, which are stabilized by oppositely charged residues

within the BH3 binding pocket of BCL-XL (102). **Figure 1.5** illustrates the conservation of some of these critical residues in other BCL-2 family members. Notably, Leu<sup>78</sup> and Asp<sup>83</sup> at BH3 domain core residues 1 and 6 are highly conserved in both pro- and anti-apoptotic BCL-2 family subsets. However, Ile<sup>81</sup> at core residue 4 is conserved only in some pro-apoptotic members and is substituted by alanine in anti-apoptotic members (112). It may be that the positions of key amino acid residues with either charged or hydrophobic side chains may dictate the hierarchical binding between BH3 domain pro-apoptotic proteins and their cognate anti-apoptotic binding partners.



## **1.12 Thesis objective 1 – To investigate mechanisms of BAD mediated paclitaxel sensitivity of breast cancer cells**

Overall, previous studies suggested an important role for BAD in paclitaxel mediated cell death of breast cancer cells in vitro. BAD expression also correlated with positive clinical outcomes of breast cancer patients treated with taxanes. In cell based assays, BAD siRNA-mediated depletion led to significant reductions in apoptosis of breast cancer cells MCF-7, SKBR-3 and MDA-MB-468 (67). Given the well characterized pro-apoptotic role for BAD, we hypothesized that paclitaxel would induce pro-apoptotic BAD dependent cell death characterized by i) enhanced interactions of BAD with anti-apoptotic BCL-2 family members, and ii) translocation of BAD from the cytosol to the mitochondria. Therefore, our first objective in this project was to investigate the role of BAD in the paclitaxel induced cell death pathway in MCF-7 cells by looking for biochemical indications of proapoptotic BAD activity. This work is described in **Chapter 3.1**.

## **1.13 Non-apoptotic BAD functions**

### **1.13.1 Novel pro-growth role for BAD in breast cancer cells**

Ongoing studies in the laboratory demonstrated a novel, nonapoptotic role for BAD in breast cancer cells. BAD depletion studies in MCF-7 and SKBR-3 cells led to reduced cell numbers in proliferation assays (67). Additionally, MDA-MB-231 cells that stably expressed BAD reached higher cell numbers (~1.5 fold higher) than MDA-MB-231 vector control stable cell line and parental controls in

proliferation assays (113). The BAD pro-growth characteristic was also consistent with in vivo studies. Mouse tumor xenografts using 231.BAD stable cells grew to significantly larger tumor volumes than 231.vector controls cells, at least four-fold larger (113). Furthermore, the in vitro and in vivo studies suggested an important role for BAD Serine 118 in modulating the overall phosphorylation state of BAD, and in turn, the pro-growth effects of BAD. To our knowledge, this is the first report of BAD-modulated pro-growth activity that has been linked to the Serine 118 site, although the mechanisms of pro-growth activity modulated by BAD or BAD S118D remains unknown.

### **1.13.2 BAD proliferative capacity in breast cancer cells**

The role of BAD in breast cancer cells in relation to cell proliferation remains controversial. For example, our work suggests that BAD contributes to proliferation of MCF-7 cells ((67) and **Figure 3.2**), while an independent group published that BAD inhibited proliferation of this cell line (114). Specifically, work by Fernando et al determined that BAD localizes to the nucleus of MCF-7 cells and complexes with AP1 and c-Jun at the promoter of the cyclin D1 gene to repress its transcription. Cyclin D1 expression is important for G1/S transition as part of the cyclin D1/cdk4 complex (115). BAD mediated repression of cyclin D1 transcription prohibits S phase progression and reduces proliferation of MCF-7 cells (114). On the contrary, we have observed cytosolic staining patterns for BAD in MCF-7 cells without nuclear staining (data not shown) and have shown that BAD siRNA knock-down reduces cell numbers in proliferation assays (67).

Clearly, more work is required to clarify the effect of BAD on the cell cycle regulation of MCF-7 breast cancer cells. Additionally, our study did not determine whether increased cell counts of MCF-7 cells in proliferation assays was due to accelerated cell cycle progression or diminished cell death (67).

### **1.13.3 Role of BCL-2 family members in cell cycle progression**

Several BCL-2 family members have been demonstrated to regulate cell cycle progression in addition to apoptosis. Bax $\alpha$  overexpression in T cells correlates with reduced cdk inhibitor p27 levels and leads to enhanced S phase entry in cycling cells (116). BCL-2 and BCL-XL are anti-proliferative by prolonging G0 and delaying cell cycle entry in response to serum stimulation or Myc expression in NIH3T3 cells and Rat1MycER fibroblasts (117). Under these conditions, levels of the cdk inhibitor p27 are elevated which inhibits cyclinE/cdk2 and cyclinD/cdk4/6 and contributes to BCL-XL and BCL-2 mediated delay of cell cycle progression (117). The role for p27 in cell cycle delay is essential because BCL-2 and BCL-XL did not delay S phase entry in p27<sup>-/-</sup> MEFs in response to serum deprivation and re-stimulation (117), and this essential role for p27 has been elsewhere documented (118). An independent study in fibroblasts also found an essential role for elevated p130 in BCL-2-retarded cell cycle entry (118), where p130 purportedly interacts with E2F4 to repress E2F1 expression critical for G0 exit (118).

Follow-up studies elucidated an important role for Bax and Bak in sustaining the BCL-2/BCL-XL mediated G0 quiescent state (119). In wt cells, it is

thought that BCL-2 and BCL-XL induce G0 arrest through activation of G0 kinase Mirk, that phosphorylates p27 and stabilizes it (119). BAX and BAK normally repress p27 levels and their presence is required for BCL-2 and BCL-XL modulation of cell cycle arrest (119). *BAX/BAK* *-/-* cells already have high levels of p27 and exhibit cell cycle arrest that cannot be further exacerbated by BCL-2 or BCL-XL (119). Therefore, the effects of BCL-2 family members on control of cell cycle progression, arrest and reentry, are interdependent.

Notably, BAD can overcome cell cycle delay induced by BCL-2 and BCL-XL (120,121). Fibroblasts that overexpress BAD and BCL-XL fail to cell cycle arrest in growth arrest conditions due to low serum or confluence (121). Moreover, this study suggested that BAD:BCL-XL heterodimers could induce aberrant cell cycle progression and overcome the G0/G1 checkpoint in growth arrest conditions (121). We postulated that a similar pro-proliferative mechanism of action may exist for BAD in breast cancer cells, where BAD:BCL-XL heterodimerization meets a critical threshold that may allow for unrestrained cellular proliferation, similar to effects observed in fibroblasts (121).

Alternatively, BAD may promote proliferation via novel protein interactions. Our studies to try and identify these BAD interacting proteins are described in **Chapter 3.2.**

Other studies implicate a role for phosphorylated BAD in cellular proliferation and/or transformation. For instance, mBAD-transfected primary cells, chicken embryo fibroblasts, are capable of anchorage-independent growth in serum rich conditions in a manner dependent on S136 phosphorylation (122).

mBAD transfected cells with S136 phosphorylation also reach higher saturation densities in focus forming assays without significant differences in cell cycle profiles from S136A BAD mutants (122). These studies suggest that phosphorylated BAD promotes transformation of primary cells without measurable effects on cell cycle progression. In prostate cancer cells, BAD overexpression and knock-down studies have elucidated a pro-proliferative function for BAD (123). In vitro this was determined as increased numbers of BAD-expressing prostate cancer cells compared to controls in proliferation assays (123). In vivo, BAD-expressing prostate cancer cells also showed increased tumor growth when xenografted into mice (123). While this work also supports a pro-proliferative or pro-growth role for BAD in prostate cancer cells, these authors did not attempt to assess cell cycle profiles of BAD expressing cells versus controls. Nor did they assess relative levels of cellular death in the proliferation assays, although the authors did claim the proliferation results were consistent with MTT assays. Overall, this evidence suggests that BAD may confer growth advantages to cells in a phosphorylated, anti-apoptotic state and may explain the upregulation of BAD observed in prostate cancer cells (123,124).

Pro-growth BAD functions have been linked not only to the aforementioned phosphorylation site mBAD S136, but also to another C-terminal phosphorylation site, mBAD S170. Phosphorylation at S170 attenuates apoptosis and modulates cell cycle progression by shortening cellular doubling time and promoting progression through S phase in a hematopoietic progenitor cell line (125). Notably, cell synchronization experiments found that BAD S170A cells

had a significantly prolonged S phase and were significantly delayed in G2 onset compared to BAD S170D or BAD expressing cells (125). Furthermore, the activity of CaMKII- $\gamma$ , the kinase responsible for S170 phosphorylation, was elevated in S phase, indicating an important role for BAD phosphorylation modulation in cell cycle progression (125). This phosphorylation site is conserved in human BAD at S134, and was independently found to promote proliferation in human tumor cell lines in response to active B-RAF (126).

Collectively, these studies suggest that control of BAD phosphorylation at the C-terminus is critical in dictating either the apoptotic or pro-growth mediated BAD phenotype. However, it is not clear from these studies how phosphorylated BAD mechanistically mediates transformation or proliferation. In addition, it is unclear what dictates the cell type specific differences that lead to either increased death or increased proliferation with cellular transfection of BAD. For example, in breast cancer cells we have observed increased cell numbers in proliferation assays in cells that overexpress BAD (113). However, BAD transfected HeLa cells or HEK293 cells show reduced cell numbers in a proliferation assay indicative of death (126). Overall, it is important to more clearly define how upstream kinase activity modulates BAD function, how BAD affects cell cycle dynamics at G0/G1 and G1/S boundaries in cancer cells, and how BAD perpetuates pro-growth effects above control levels in vitro and in vivo.

## **1.14 Regulation of BAD activity**

### **1.14.1 BAD phosphorylation**

BAD is an apoptotic sentinel that is highly regulated by phosphorylation in response to trophic factors. Survival signaling pathways from factors such as IL-3 or IGF-1, lead to activation of BAD Serine 75, 99 and 118 kinases and inhibition of BAD pro-apoptotic function (104). There are currently nine phosphorylation sites that have been characterized in human BAD (**Table 1.1, Figure 1.6**). Phosphorylation of BAD at Serine 75, 99 and 118 is anti-apoptotic by inhibiting binding with BCL-XL and promoting cytosolic sequestration with 14-3-3 proteins. It is likely that phosphorylation at Serine 124 and 134 is also anti-apoptotic in nature since Serine to Alanine mutations at these sites promote serum-induced apoptosis in HeLa cells above that induced by wild type BAD (126). The effect of the Serine 25, 32 and 34 sites on cell survival are less clear (126) and have not been studied in detail.

Studies with mBAD suggest that phosphorylation of critical sites is a tiered process. Phosphorylation of the predominant 14-3-3 binding site, mBAD Serine 136, is an apical event that precedes Serine 155 phosphorylation (127). It is thought that phosphorylation at Serine 112/136 that promotes 14-3-3 binding may result in conformational changes in BAD that increase accessibility of survival kinases to the Serine 155 site in the BH3 domain (104,127).

**Table 1.1 BAD phosphorylation sites and kinases**

Phosphorylation site		Kinases	References
Human	Murine		
Serine 25	---	---	(128)
Serine 32/34	---	---	(128)
---	Serine 111	PAK	(129)
Serine 75	Serine 112	PIM, PAK, PKA, p90RSK, RAF	(128,130-136)
Serine 91	Serine 128	Cdc2, JNK	(126,137,138)
Serine 97	---	---	(128)
Serine 99	Serine 136	PIM, PAK, p70S6K, AKT, RAF	(128,130,131,139,140)
Serine 118	Serine 155	Chk1, PIM, PKA, RAF	(128,130,136,141-143)
Serine 124	---	---	(128)
Serine 134	Serine 170	PAK, B-RAF, Chk1, PIM, CaMKII- $\gamma$	(125,126,128,130,141, 144)
---	Threonine 117	CK2	(145)
---	Threonine 201	JNK	(146,147)

--- not identified

25 32 34 75  
 1 MFQIPEFEPSEQEDSSSAERGLGPFAPAGDGFSPAGDGKHHRRQAPGLLWDASHQQEQPTSSSHHGGAGAVEIRSRHSYPA<sup>14-3-3 site</sup>GTEDDE 84  
 91 97 99  
 85 GMGEEFSPFRGRSRSAPPNLWAAQRYGRELRRMSDEFVDSFKKGLPRPKSAGTATQMRQSSWTRVFQSWWDRNLGRGSSAPSQ 168  
 14-3-3 site BH3 domain LBD1 LBD2

**Figure 1.6 hBAD primary amino acid sequence annotated with phosphorylation sites and domains.**  
 BH3 domain (amino acids 108-123) in blue, LBD1 (amino acids 120-131) in light green, LBD2 (amino acids 131-168) in dark green, 14-3-3 binding sites in orange. BAD phosphorylation sites at Serine 25, 32/34, 75, 91, 97, 99, 99, 118, 124 and 134, indicated in red, underlined. Image adapted from Polzien et al (126).

BAD phosphorylation status is also regulated by phosphatases: PP1 (148), PP2A (149,150) and calcineurin (151). It has been suggested that BAD dephosphorylation is also a tiered process, since PP2A mediated dephosphorylation of mBAD pSer112 is an apical event that precedes dephosphorylation of pSer136 (150).

Overall, BAD phosphorylation status at key sites is important for regulation of BAD apoptotic activity. Phosphorylation at Serine 75, 99 and 118 of hBAD promotes 14-3-3 binding and inhibits apoptotic activity. Dephosphorylation at Serine 118 is important in allowing hBAD to engage its anti-apoptotic binding partner, BCL-XL, to induce apoptosis (152).

#### **1.14.2 Lipid binding properties**

The C-terminal 47 amino acids of hBAD are critical for interaction with membranes (153). This primary sequence possesses two distinct lipid binding properties: association with cholesterol rich lipids mediated by LBD1 and association with negatively charged lipids mediated by LBD2 (153). LBD1 comprises hBAD amino acids 120-131 and includes part of the BH3 domain (153). LBD2 is comprised of hBAD amino acids 131-168 (153) (**Figure 1.6**). An intact FKK motif embedded with LBD1 is important for efficient binding of BAD to both cholesterol-rich and acidic membranes (153). Interestingly, Hekman et al found that wt BAD could promote the binding of BCL-XL to liposomes while a BAD mutant lacking LBD2 could not (153). This indicates that BAD may act as a receptor that helps translocate BCL-XL to the mitochondrial membrane. Binding

of BAD to membranes is independent of its phosphorylation state, although phosphorylated BAD can be readily extracted by 14-3-3 proteins from mitochondrial liposomes, and may be redistributed to cholesterol-rich membranes (153).

## **1.15 BAD-interacting proteins**

### **1.15.1 BAD:BCL-2, BCL-XL and BCL-W interactions**

BAD promotes cell death by specifically engaging a subset of anti-apoptotic BCL-2 family members: BCL-2, BCL-XL and BCL-W (99,101,154). Neutralization of these anti-apoptotic proteins can relieve inhibition of both BAX/BAK and direct activators of BAX and BAK to promote apoptosis. BAD does not engage other anti-apoptotic proteins (A1 or MCL-1) or BAX or BAK (155).

Interactions with anti-apoptotic proteins are modulated by the BAD BH3 domain, an amphipathic helix that is thought to engage a hydrophobic pocket within a cognate binding partner (101,153) by means of hydrophobic and electrostatic interactions (reviewed in (157)). Mutations of highly conserved residues within the hydrophobic groove of the anti-apoptotic protein or mutations within the BH3 domain of a pro-apoptotic protein diminish binding affinity (102,156).

The major anti-apoptotic BAD binding partner in the MCF-7 cell line is BCL-XL (67). BCL-XL exists in the cytosol as soluble homodimers, where the hydrophobic transmembrane domains are thought to lie buried within the

hydrophobic cleft of the cognate dimer (158). Binding of the BAD BH3 domain is thought to displace the C-terminus of BCL-XL, exposing the transmembrane domain and promoting translocation of the heterodimer to the mitochondrial membrane (158). BAD:BCL-XL membrane translocation also requires LBD2 of BAD (153).

### **1.15.2 14-3-3 proteins**

14-3-3 proteins are a family of phosphoserine/threonine binding proteins that are ubiquitously expressed in all eukaryotic cells (159,160). Seven human isoforms of the 14-3-3 protein family have been documented:  $\alpha/\beta$ ,  $\gamma$ ,  $\epsilon$ ,  $\zeta/\delta$ ,  $\eta$ ,  $\sigma$  and  $\tau$  (also denoted  $\theta$ ), so-named by their reversed-phase HPLC elution profiles (161,162). In cells, 14-3-3 proteins exist as homo or heterodimers (163) where the N-terminal domain is used for dimerization (164). The propensity of different 14-3-3 isoforms to form homo or heterodimers varies; for example, human 14-3-3 $\sigma$  primarily homodimerizes (165) while 14-3-3 $\epsilon$  primarily heterodimerizes (166). Each monomer within the 14-3-3 dimer forms a conserved amphipathic ligand-binding cleft, which allows the dimer to bind two phosphoserine/threonine sites on the same substrate or serve as an adaptor to bridge two different substrates (167,168). As 14-3-3 proteins lack inherent enzymatic activity, their diverse functions largely result from modulation of their protein targets involved in signal transduction pathways. 14-3-3 binding can either mask critical protein sequences or structures, induce conformational changes in the protein target, or serve to scaffold target proteins in close proximity (reviewed in (169)). In this way, 14-3-3

proteins exert wide-spectrum effects on the control of cell cycle progression, cellular growth signaling and apoptosis (reviewed in (170)).

### **1.15.3 BAD:14-3-3 interactions**

Using phosphoserine-oriented peptide library screening methods, two 14-3-3 consensus binding motifs have been established: RSXpSXP (mode I) and RXY/FXpSXP (mode II) (171). The majority of 14-3-3 targets contain one or more of these consensus motifs, whereby basic residues of the amphipathic 14-3-3 binding cleft interact with the phosphopeptide (172). However, 14-3-3 proteins can also interact with targets in a phosphorylation-independent manner (173-175) or in a phosphorylation-dependent manner atypical of the consensus motifs (176). Two 14-3-3 binding sites were originally identified in murine BAD at Serine 112 and Serine 136 (152) embedded within RXRXXSXP sites. Zha et al compared these sites to two overlapping 14-3-3 consensus sites previously identified in RAF1: RSXpSXP and RXRXXpS sites. Serine 136 abides by a typical 14-3-3 consensus motif, RSXpSXP (actual sequence RSRpSAP), while Serine 112 differs at the -2 position of this motif (RHSpSYP) (152) and is therefore an atypical site. Further reports suggest that Serine 136 may be the primary 14-3-3 binding site that is most responsive to survival signaling and is sufficient for 14-3-3 binding (177). These murine 14-3-3 binding sites are conserved in hBAD at Serine 75 and Serine 99 (**Figure 1.6**).

Functionally, survival signaling that leads to BAD phosphorylation abrogates binding to BCL-XL and promotes binding to 14-3-3 proteins (152).

This leads to cytosolic sequestration of BAD and an inhibition of BAD pro-apoptotic function (152). Accordingly, BAD:14-3-3 complexes are widely considered non-functional complexes that serve to sequester inactive BAD. All seven 14-3-3 isoforms have previously been shown to bind to BAD and inhibit BAD mediated apoptosis (178,179). However, the 14-3-3 isoforms are thought to differ with respect to their affinity for BAD. Hekman et al demonstrated that 14-3-3 $\zeta$ ,  $\eta$  and  $\tau$  are most efficient at extracting BAD from mitochondrial liposomes, while 14-3-3  $\sigma$ ,  $\beta$ ,  $\gamma$  and  $\epsilon$  have either greatly reduced or no measurable ability to extract BAD (153). Additionally, association-dissociation studies with purified proteins in the absence of membranes found an 11-fold higher affinity of 14-3-3 $\zeta$  for BAD than 14-3-3 $\gamma$  (153).

In our study we wanted to quantify the extent of the binding of different 14-3-3 isoforms to BAD wt and BAD S118D in breast cancer cells to further characterize relevant BAD binding partners. These results are described in **Chapter 3.2.8**.

#### **1.15.4 BAD:Glucokinase interaction**

BAD and glucokinase interact in a mitochondrial complex with WAVE-1, PP1c and PKA in mouse liver and pancreatic cells (180,181). BAD is essential for assembly of this complex and for regulating glucokinase activity, since BAD depleted hepatocytes have reduced glucokinase activity, O<sub>2</sub> consumption and ATP production (180). The presence of BAD is also important for glucose homeostasis, since *BAD*<sup>-/-</sup> mice have impaired blood glucose clearance after a

glucose tolerance test (180). In response to glucose, mitochondrial mBAD in hepatocytes is phosphorylated at Serine 112 (180). This phosphorylation event is critical for stimulation of GK and also correlates with BAD conferred protection from apoptosis in response to glucose deprivation (180). In pancreatic islets, phosphorylation of mBAD Serine 155 is critical for glucose stimulated insulin secretion (181). The BH3 domain alone is sufficient for stimulating insulin release, since BAD BH3 SAHB peptides restore glucose stimulated insulin secretion of *BAD*<sup>-/-</sup> beta cells to wild type levels (181). A phosphomimetic BAD BH3 SAHB peptide enhances insulin release above that of wt BAD SAHB peptide at higher glucose concentrations. Furthermore, these authors found that glucokinase was a direct target of the BAD BH3 domain in pancreatic  $\beta$  cells (181).

#### **1.15.5 BAD:Phosphofruktokinase-1 interaction**

Studies in the hematopoietic cell line FL5.12 showed that JNK phosphorylates mBAD at Threonine 201 in response to IL-3 to inactivate BAD pro-apoptotic function and reduce binding to BCL-XL (182). However, JNK1 is also required for IL-3 stimulated or serum stimulated glycolysis, and Deng et al queried whether BAD was involved in the JNK1 mediated glycolytic pathway (147). A novel BAD:PFK-1 interaction was identified by coimmunoprecipitation studies from FL5.12 cells and verified in vitro using purified GST-BAD (147). While the BAD:PFK1 interaction is independent of BAD phosphorylation by JNK1, this phosphorylation event at the Threonine 201 site is required for BAD

stimulation of PFK-1 glycolytic activity (147). PFK-1 catalyzes the conversion of fructose-6-phosphate to fructose-1,6-bisphosphate, a critical committed step in the glycolytic pathway. While mBAD Thr 201 is not conserved in hBAD, this study does provide an interesting link between mBAD and stimulation of glycolysis.

## **1.16 Hypothesized BAD:Hexokinase interactions**

### **1.16.1 The Warburg Effect**

Normal tissues derive most of their cellular ATP from mitochondrial oxidative phosphorylation in the presence of oxygen. Glucose taken up by cells is metabolized to pyruvate in glycolysis; pyruvate then enters the citric acid cycle to produce reducing equivalents, NADH and FADH<sub>2</sub> which form the substrates of oxidative phosphorylation to produce ATP in the presence of oxygen. Under hypoxic conditions, cells anaerobically convert glucose to lactic acid as a temporary means of sustaining ATP production. Otto Warburg first noted the abnormal metabolism of tumor cells in the 1920s that contradicted the Pasteur Effect. Tumor cells demonstrated enhanced glycolysis and lactate production in the presence of oxygen (183). It was found that tumor cells could obtain up to 50% of their ATP requirements by converting glucose to lactate (184). This aerobic glycolytic phenotype of cancer cells later became known as the Warburg Effect (185).

### **1.16.2 Hexokinase involvement in the Warburg Effect and cancer promotion**

Cancer cells with high glycolytic rates have elevated levels of mitochondria-associated hexokinase activity (186) compared with normal tissues. At the mitochondria, hexokinases have preferred access to a mitochondrial pool of ATP which may accelerate G-6-P production (187) in the absence of oxygen, therefore conferring metabolic advantages to tumor cells. Aerobic glycolysis is clearly less efficient than oxidative phosphorylation, with 2 ATP vs 36 ATP generated respectively from the metabolism of one molecule of glucose (188). However, the likely advantages of the Warburg Effect are that increased G-6-P production may act as a precursor to nucleic acid synthesis via the pentose phosphate pathway and can be used to generate NADPH for lipid biosynthesis (188,189). Glycolytic intermediates also provide precursors for amino acid biosynthesis. Altogether, increased production of macromolecules necessary for proliferation may allow for accelerated tumor growth. Lactic acid produced by tumor cells also acidifies the microenvironment to protect against immune system attacks and better allow for tumor cell growth and invasion (189).

In cancer cells, HKII is the hexokinase isoform widely overexpressed (190,191), although HK I overexpression has also documented to a smaller extent (192,193). In addition to enhanced glycolysis, hexokinase overexpression also protects against apoptosis by binding to VDAC (194-196). It remains unclear how modulation of VDAC protects against apoptosis (196), although one hypothesized mechanism is that HK favors closure of the permeability transition pore (197).

### **1.16.3 Hexokinases: isoforms and functions**

We hypothesized that the pro-proliferative phenotype of BAD overexpressing breast cancer cells required metabolic changes conducive to accelerated growth. We speculated that BAD initiated a metabolic pathway through interaction with hexokinase isoforms, in a manner analogous to its interaction with glucokinase, to exert its pro-growth effect.

There are four mammalian hexokinase isoforms: HK I, II, III and IV that each catalyze the conversion of glucose to glucose-6-phosphate. These isoforms differ somewhat in their tissue specific expression and subcellular localization in normal tissues. HK I is ubiquitously expressed in all cell types, but is especially prevalent in the brain (198). HKI localizes to the outer mitochondrial membrane (199) where it is heavily involved with promoting glycolytic metabolism. HK I associates with mitochondria by integrating into the mitochondrial outer membrane (199) using its N-terminal hydrophobic sequence (200,201) and through association with VDAC (194).

HK II is predominantly expressed in insulin-sensitive tissues including skeletal muscle, cardiac muscle and adipose tissue (202) where it represents the dominant hexokinase activity (203). Unlike HK I, HK II localizes to both mitochondrial and cytosolic compartments (198). At the mitochondria, HK II also interacts with VDAC (204) and competes for mitochondrial binding (205) but with lower affinity than HK I (206). HK II dynamically translocates between subcellular compartments. In response to glucose, HK II association with the mitochondria increases where it directs glucose towards the glycolytic pathway

(207). In response to G-6-P accumulation, HK II translocates to the cytosol where it promotes G-6-P directed glycogen synthesis or lipid synthesis (207).

HK III is mainly expressed in lung, liver and kidney (202,208). HK III lacks the N-terminal hydrophobic sequence that allows HK I and II to associate with mitochondria (198). Accordingly, HK III localizes to the cytosol and has been found to loosely associate with the nuclear periphery (209). HK III expression is regulated by hypoxia, and protects against oxidative stress-induced cell death (208). All three HK isoforms have reportedly reduced ROS levels in H<sub>2</sub>O<sub>2</sub>-stressed cells and retained mitochondrial membrane potential (208,210).

HK IV (also known as glucokinase) differs from HK I-III in terms of glucose affinity, product inhibition and molecular weight. HK I-III are all 100 kDa low Km, high glucose affinity isoforms that are product inhibited by G-6-P (198). By contrast, HK IV is a 50 kDa isoform with low glucose affinity and is insensitive to G-6-P inhibition. HK IV is expressed in the liver and pancreas (211) as well as in glucosensing neurons of the hypothalamus (212). Glucokinase resides in the nuclear and cytoplasmic compartments, and is typically sequestered in the nucleus with GKRP (213). While this isoform lacks the N-terminal hydrophobic sequence that allows HK I and II to bind membranes, GK and GKRP have also been reported in hepatocyte mitochondrial fractions (214). In pancreatic  $\beta$  cells GK localizes to insulin granules and mitochondria (215). These cells lack GKRP, but GK is found to fractionate with another binding partner PFK2, which may act as a scaffold (215).

#### **1.16.4 Hexokinases as potential BAD-interacting proteins**

Hexokinase activity has been reported as widely upregulated in primary and metastatic breast tumors compared with normal breast tissue or benign tumors (216,217). Specifically HK I, II and III upregulated activity has been documented in malignant human breast tumors compared to non-pathological breast tissue using NADPH fluorescence assays and tetrazolium dye reduction methods (218), although there is one report that documents similar levels of HK II expression by immunostaining in both normal breast tissue and primary untreated breast tumor (219). Overall, given the prevalence of upregulated hexokinase activity in human cancers including breast cancer, and that glucokinase is not expressed in breast tissue, we decided to investigate whether BAD pro-growth activity was mediated through modulation of HK I or II. We therefore tested for BAD:HK I/II protein interactions. These experiments are described in **Chapter 3.2.1**.

#### **1.17 Thesis objective 2 – To investigate the mechanisms of BAD pro-growth activity in breast cancer cells by studying BAD protein interacting partners**

Ongoing studies in our laboratory continued to reveal evidence for a pro-growth BAD function both in vitro and in vivo (113). However, the molecular mechanisms of BAD mediated proliferation/pro-growth activity in breast cancer cells remains unknown. We hypothesized that this pro-growth BAD function was mediated by a novel pathway involving BAD protein-interacting partners. Previously, yeast two-hybrid assays have been used to identify BAD interactions with BCL-XL, BCL-2 and 14-3-3 isoforms (99,220). We decided to undertake

unbiased protein-interaction screens using GST-tagged BAD to define BAD-interacting proteins in MDA-MB-231 breast cancer cells, where much of the BAD pro-growth characterization was performed (113). The purpose of this study was to gain insight into molecular interactions of BAD in breast cancer cells that may dictate mechanisms of BAD pro-growth activity. The goals of the protein interaction study were three-fold:

- i) To identify any novel BAD:protein interactions in breast cancer cells
- ii) To further document BAD interactions with known BAD-binding partners, BCL-XL and 14-3-3 isoforms.
- iii) To investigate BAD interactions with hypothesized binding partners, Hexokinase I and II.

However, during the development of this work, further characterization of BAD pro-growth activity was performed. Unlike studies in non-transformed cells that demonstrated a role for BAD:BCL-XL heterodimers in cell cycle progression, our laboratory found that BAD stimulated growth in breast cancer cells did not correlate with increased BAD:BCL-XL binding (113). Instead, BAD S118A and BAD S118D mutants differed inversely in their propensity to stimulate growth activity. BAD S118D showed enhanced cell numbers in proliferation assays and significantly enhanced tumor growth in mouse xenograft studies with less BCL-XL binding compared to BAD S118A. Analysis of the phosphorylation state of the BAD S118D stably-expressed protein revealed hyperphosphorylation on multiple sites compared with BAD S118A mutant (113). Interestingly, some previous studies have shown that BAD phosphorylation state

influences its binding partners in a yeast two hybrid assay. For example, wild type BAD interacts with BCL-XL, BCL-2 and 14-3-3 isoforms (99,220) while underphosphorylated BAD mutated at one or both 14-3-3 binding sites interacts indiscriminately with anti-apoptotic proteins (BCL-2, BCL-W, BCL-XL, BFL-1/A1, MCL-1) (221) and with P11, a neurite extension factor that could also attenuate BAD apoptotic activity (220). We hypothesized that there might also be a different protein interactome for hyperphosphorylated BAD S118D compared to wild type BAD or BAD S118A. In particular, we hypothesized that BAD S118D would have an increased propensity for binding to 14-3-3 isoforms due to its hyperphosphorylated state. Therefore we undertook additional protein interaction screens using GST-BAD S118D and GST-BAD S118A with two specific aims:

- i) To determine any unique binding partners for BAD S118D and BAD S118A in MDA-MB-231 breast cancer cells
- ii) To quantify the extent of 14-3-3 binding to BAD S118D and BAD S118A.

Overall, these studies were designed to further our understanding of the novel, non-apoptotic BAD mechanisms of activity in breast cancer cells by pinpointing important protein molecular players.

## **Chapter 2: Materials and Methods**

## 2.1 Cell lines

**Table 2.1 Cell lines and propagation**

Cell line	Designation	Provider	Propagation
MCF-7	MCF-7	MD Anderson Cancer Centre	RPMI 1640 + 10% FCS
SKBR-3	SKBR-3	MD Anderson Cancer Centre	RPMI 1640 + 10% FCS
MDA-MB-231	MDA-MB-231	MD Anderson Cancer Centre	RPMI 1640 + 10% FCS
HEK293T/17	HEK293T/17	ATCC (cat CRL-11268)	DMEM 11965 + 10% FCS
BAD-overexpressing MDA-MB-231 stable cell line	231.BAD	Generated by Goping lab (113)	RPMI 1640 +1 mg/mL Geneticin® (Invitrogen) + 10% FCS
BAD S118D-overexpressing MDA-MB-231 cell line	231.BAD S118D	Generated by Goping lab (113)	RPMI 1640 +1 mg/mL Geneticin® (Invitrogen) + 10% FCS
GST-BAD overexpressing MDA-MB-231 stable cell line	231.GST-BAD	Generated by Goping lab (113)	RPMI 1640 +1 mg/mL Geneticin® (Invitrogen) + 10% FCS
GST-overexpressing MDA-MB-231 stable cell line	231.GST	Generated in this work	RPMI 1640 +1 mg/mL Geneticin® (Invitrogen) + 10% FCS

## 2.2 Propagation

Cell lines were propagated in RPMI 1640 (Invitrogen) or DMEM 11965 (Invitrogen) with 10% FCS (Sigma-Aldrich). Cells were passaged using 0.05% Trypsin-EDTA (Invitrogen) and split at approximately 1:5 or 1:10 ratios. Cells were grown in T-75 flasks maintained in a humidified tissue culture incubator at 37°C with 5% CO<sub>2</sub>.

### **2.3 Buffers and commonly used solutions**

**1% CHAPS lysis buffer.** 1% CHAPS, 150 mM NaCl, 50 mM Tris pH 7.4, 2 mM EDTA pH 8.0 supplemented with 1x Complete EDTA free protease inhibitor (Roche ).

**1% CHAPS GST-pull down buffer.** 1% CHAPS (w/v), 150 mM NaCl, 50 mM Tris pH7.4, 2 mM EDTA pH8.0, 2 mM DTT.

**Glutathione elution buffer.** 10 mM reduced glutathione (Sigma), 50 mM Tris-HCl pH8, 10 mM NaCl, 0.1% Triton X-100.

**2X laemmli buffer.** 0.1 M Tris-HCl pH 6.8, 16% Glycerol, 3% sodium dodecyl sulfate (SDS), 8%  $\beta$ -mercaptoethanol, 0.004% bromophenol blue.

**6X laemmli buffer.** 375 mM Tris-HCl pH 6.8, 9% SDS, 50% glycerol, 9%  $\beta$ -mercaptoethanol, 0.03% bromophenol blue.

**0.2% NP-40 IVTT buffer.** 0.2% NP-40, 142.5 mM KCl, 5 mM MgCl<sub>2</sub>, 1 mM EGTA, 20 mM Hepes pH 7.5 supplemented with 1x complete protease inhibitor (Roche, cat. 11873580001).

**1% NP-40 lysis buffer.** 1% NP-40, 150 mM NaCl, 50 mM Tris pH 7.4, 2 mM EDTA pH 8.0, 1x complete protease inhibitor (Roche, cat. 11873580001).

**10X PBS.** 27 mM KCl, 15 mM KH<sub>2</sub>PO<sub>4</sub>, 1380 mM NaCl, 81 mM Na<sub>2</sub>HPO<sub>4</sub>·7H<sub>2</sub>O pH 7.4.

**Propidium iodide stain.** 0.1% Triton X-100, 2 mg/mL RNase and 20 ug/mL propidium iodide (Invitrogen) in PBS.

**SDS-PAGE running buffer.** 3.5 mM SDS, 25 mM Tris, 192 mM Glycine

**1x TAE buffer.** 40 mM Tris-acetate, 1 mM EDTA.

**10X TBS.** 20 mM Tris, 137 mM NaCl pH 7.6 with HCl.

**1x TBS-T.** 2 mM Tris, 13.7 mM NaCl, 0.1% Tween-20.

**1xTE buffer.** 10 mM Tris pH 7.5, 1 mM EDTA pH 8.0.

**Western blot transfer buffer.** 192 mM glycine, 25 mM Tris, 20% methanol.

**Western blot transfer buffer – low methanol.** 192 mM glycine, 25 mM Tris, 0.05% (w/v) SDS, 16% methanol.

## 2.4 Antibodies

### 2.4.1 Primary antibodies

**Table 2.2 Primary antibodies**

Antibody	Source (Catalogue #)	Incubation conditions	Application
anti-BAD	Sigma-Aldrich (B0684)	1:1000 5% milk/TBS-T	Western blot
		1:400 0.2% gelatin/PBS	Immunofluorescence
anti-BCL-2	Cell Signaling (2872)	1:1000 5% BSA/TBS-T	Western blot
anti-BCL-W	Cell Signaling (2724)	1:1000 5% BSA/TBS-T	Western blot
anti-BCL-XL	Sigma-Aldrich (B9429)	1:1000 5% milk/TBST	Western blot
anti-BubR1	BD Biosciences (612502)	---	Immunoprecipitation
anti-Calnexin	Cell Signaling (2433P)	---	Immunoprecipitation
anti-Cytochrome c	BD Biosciences (556432)	1:200 0.2% gelatin/PBS	Immunofluorescence
anti-14-3-3 $\zeta$	Santa Cruz (sc-1019)	1:1000 5% milk/TBS-T	Western blot
Anti-14-3-3 $\beta/\alpha$	Cell Signaling (9636)	1:1000 5% BSA/TBS-T	Western blot
Anti-14-3-3 $\gamma$	Cell Signaling (9637)	1:1000 5% BSA/TBS-T	Western blot
Anti-14-3-3 $\epsilon$	Cell Signaling (9635)	1:1000 5% BSA/TBS-T	Western blot
Anti-14-3-3 $\zeta/\delta$	Cell Signaling	1:1000	Western blot

	(9639)	5% BSA/TBS-T	
Anti-14-3-3 $\eta$	Cell Signaling (9640)	1:1000 5% BSA/TBS-T	Western blot
Anti-14-3-3 $\tau$	Cell Signaling (9638)	1:1000 5% BSA/TBS-T	Western blot
anti-GAPDH	Sigma-Aldrich (G8795)	1:5000 5% milk/TBS-T	Western blot
anti-Granzyme A	Santa Cruz (sc11434)	---	Immunoprecipitation
anti-GST	Sigma-Aldrich (G7781)	1:1000 5% milk/TBS-T	Western blot
anti-Hexokinase I	Cell Signaling (C35C4)	1:1000 5% BSA/TBS-T	Western blot
anti-Hexokinase II	Cell Signaling (C64G5)	1:1000 5% BSA/TBS-T	Western blot
anti-Tom20	Generated by Dr. Goping (Shore lab)	1:2000 5% milk/TBS-T	Western blot
anti- $\alpha$ -Tubulin	Sigma-Aldrich (T5168)	1:8000 5% milk/TBS-T	Western blot
anti-Lamin A/C	Immuquest (IQ187)	1:500 5% milk/TBS-T	Western blot
anti-Myc	Dr. Hobman (Cell Biology)	1:1000 5% milk/TBS-T	Western blot
		1:300 0.2% Gelatin/PBS	Immunofluorescence
anti-MYH9	Sigma-Aldrich (SAB2101542)	1:1000 5% milk/TBS-T	Western blot
anti-Vimentin	Sigma-Aldrich (V8012)	1:6000 0.2% gelatin/PBS	Immunofluorescence
anti-Vimentin	Neomarkers (MS-129-P1)	1:1000 5% milk/TBS-T	Western blot
anti-V5	Sigma-Aldrich (V8012)	1:1000 5% milk/TBS-T	Western blot

## 2.4.2 Secondary Antibodies

**Table 2.3 Secondary Antibodies**

Antibody	Source (Catalogue #)	Incubation conditions	Application
Goat anti-Rabbit HRP	Bio-Rad (170-6515)	1:3000 5% milk/TBS-T	Western blot
		1:3000 5% BSA/TBS-T	Western blot
Goat anti-Mouse HRP	Bio-Rad (170-6516)	1:3000 in 5% milk/TBST	Western blot
		1:3000 in 5% BSA/TBST	Western blot
Alexa-Fluor 555 donkey anti-mouse IgG	Invitrogen (A-31570)	1:200 0.2% gelatin/PBS	Immunofluorescence
Alexa-Fluor 488 donkey anti-rabbit IgG	Invitrogen (A-21206)	1:200 0.2% gelatin/PBS	Immunofluorescence
Alexa-Fluor 555 Anti-rabbit IgG	Invitrogen (A-31572)	1:200 0.2% gelatin/PBS	Immunofluorescence
Alexa-Fluor 488 Anti-mouse IgG	Invitrogen (A-21202)	1:200 0.2% gelatin/PBS	Immunofluorescence

## 2.5 SDS-PAGE and western blotting

Polypeptides were separated by sodium dodecyl sulfate polyacrylamide gel electrophoresis (222,223) and detected by western blot analysis (224,225). Gels were prepared with 10% or 14% polyacrylamide separating gel and 4% polyacrylamide stacking gel. Protein samples were loaded onto gels and electrophoresed in SDS-PAGE running buffer at 170 V for 1 hour or until the dye front reached the bottom of the separating gel. Proteins were transferred to polyvinylidene fluoride (PVDF) membrane for 1 hour at 400 mA, or overnight at 15 V at 4°C in western blot transfer buffer. Membranes were blocked in 5%

(w/v) skim milk powder in 1X TBS-T or 5% BSA in 1x TBS-T. Primary antibodies were diluted in the respective blocking agent (**Table 2.2**) and incubated with the membrane for 1 hour at room temperature or overnight at 4°C on a rocking platform. Membranes were rinsed 3x10 minutes with 1x TBS-T prior to addition of secondary antibody. Species-specific secondary antibodies conjugated with horseradish peroxidase (**Table 2.3**) were diluted 1:3000 in the respective blocking agent and incubated with membranes for 1 hour at room temperature. Membranes were rinsed 3x10 minutes with 1x TBS-T. Protein detection was accomplished by exposing membranes to enhanced chemiluminescent reagents. Membranes were either exposed to ECL (GE Healthcare RPN2106) or ECL plus (GE Healthcare RPN2132). Western blots were developed on Amersham Hyperfilm ECL (cat. 28-9068-38) or HyBlot CL Autoradiography film (cat. E3018) in a dark room and then processed by a Kodak X-OMAT 2000 Processor.

## **2.6 Drugs and treatment**

### **2.6.1 Paclitaxel**

Paclitaxel (Sigma-Aldrich, cat. T-1912) was prepared as 10 mM stocks in anhydrous dimethyl sulfoxide (DMSO) for long term storage in the -86°C freezer. For use, 10 mM stocks were diluted in anhydrous DMSO to a stock concentration of 1 mM. Paclitaxel was diluted in RPMI 1640 media to a final working concentration of 25 nM immediately prior to use. MCF-7 cells and SKBR-3 cells were treated with paclitaxel for 48 hours, or as otherwise specified.

## 2.6.2 Staurosporine

Staurosporine (Sigma-Aldrich, cat. S4400) was prepared as 2 mM stocks in anhydrous DMSO and stored frozen at -20°C. Staurosporine stocks were thawed and diluted in RPMI1640 media to a final working concentration of 2.5 µM immediately prior to use. MCF-7 and SKBR-3 cells were treated with staurosporine for 4 hours.

## 2.7 BAD coimmunoprecipitation study in MCF-7 cells

$2.6 \times 10^6$  MCF-7 cells were plated in each of four 10-cm dishes. Two dishes of cells were treated with 25 nM paclitaxel for 48 hours, one dish of cells was treated with 2.5 µM staurosporine for 4 hours and one dish was left untreated. Fresh media was replaced on untreated dishes at the time of drug application. Treatments were terminated at the time of cell harvesting. All media was collected to retain floating or loosely attached apoptotic cells, and the remaining adherent cells were removed from the dish with trypsin. Cells were quantified by diluting an aliquot of cell suspension with an equal volume of 0.1% eosin/PBS and counting on a haemocytometer.  $6 \times 10^6$  cells of each treatment were collected by centrifugation at 500xg for 5 minutes at room temperature. Cells were lysed in 1% CHAPS lysis buffer with EDTA-free protease inhibitor (Roche, cat. 11873580001) at a concentration of  $10 \times 10^6$  per mL for 10 minutes on ice. Lysates were cleared by centrifugation at 10,000xg for 5 minutes at 4°C to remove membrane debris. 100 µL of input samples were boiled with 20 µL of 6x laemml buffer and stored at -20°C. BAD immunoprecipitation was performed by adding

1  $\mu\text{g}$  of anti-BAD antibody to 100  $\mu\text{L}$  of cell lysate followed by overnight incubation at 4°C. The following day, Protein A Sepharose™ CL-4B beads (GE Healthcare, cat. 17-0780-01) were equilibrated three times in 1% CHAPS lysis buffer. 20  $\mu\text{L}$  of 50% bead slurry was added to each sample and incubated for 1 hour at 4°C. Protein A Sepharose™ beads were subsequently pelleted by centrifugation at 500xg for 5 minutes at 4°C and rinsed three times in lysis buffer. Finally, beads were resuspended in 60  $\mu\text{L}$  of 1x laemmli buffer and boiled. Protein samples were resolved by SDS-PAGE and western blot with 30% IP input.

## **2.8 MCF-7 subcellular fractionation**

2.6x10<sup>6</sup> MCF-7 cells were plated in each of four 10-cm dishes and treated with 25 nM paclitaxel for 48 hours or 2.5  $\mu\text{M}$  staurosporine for 4 hours. 5x10<sup>6</sup> cells of each treatment were pelleted by centrifugation and washed twice with cold PBS. Subcellular fractionations were subsequently performed using the Qproteome® Cell Compartment Kit (Qiagen, cat. 37502). Fractionations were performed as outlined by the manufacturer's protocol using the provided extraction buffers. Briefly, extraction Buffer CE1 was used to isolate the cytosolic fraction; Buffer CE2 was used to isolate the membrane fraction; Buffer CE3 was used to isolate the nuclear fraction and Buffer CE4 was used to isolate the cytoskeletal fraction. Proteins were precipitated from each buffer fraction by adding 4 volumes of -20°C acetone and incubating overnight at -20°C. The next day, samples were centrifuged at 12,000xg for 10 minutes at 4°C. Pellets were dried then redissolved in 80  $\mu\text{L}$  ddH<sub>2</sub>O and boiled with 16  $\mu\text{L}$  of 6x laemmli

buffer. Equal proportions of each fraction were resolved by SDS-PAGE and analyzed by western blot.

## **2.9 BAD siRNA knock-down**

RNA interference was used to knock-down gene expression in cultured cells (226). Experimentally validated BAD siRNA (Hs\_Bad\_3 FlexiTube<sup>®</sup> siRNA cat. SI00299348) and AllStars Negative Control siRNA (Qiagen, cat. 1027281) were purchased from Qiagen. siRNA was resuspended with sterile RNase-free water provided by the manufacturer to a stock concentration of 10  $\mu$ M, and stored at -20°C. BAD siRNA knock-downs were performed in a 24-well format. MCF-7 cells were plated at 50,000 cells per well of a 24-well dish. 0.5  $\mu$ L of 10  $\mu$ M siRNA stock was added to 100  $\mu$ L of Opti-MEM Reduced Serum Medium (Invitrogen, cat. 31985) and incubated for 5 minutes. 3  $\mu$ L of HiPerFect<sup>®</sup> transfection reagent (Qiagen, cat. 301705) was added and incubated for 15 minutes at room temperature to allow transfection complexes to form. 400  $\mu$ L of fresh media was replaced in each well. 100  $\mu$ L of transfection complexes were added drop-wise to dilute the siRNA to a final working concentration of 10 nM. Cells were subsequently incubated with the transfection reagent for 24 hours.

## **2.10 DNA content analysis**

DNA content analysis of cell populations was performed using propidium iodide staining procedures (227). MCF-7 cells were seeded at 50,000 cells per well in 24-well dishes. Cells were treated with BAD siRNA or negative control siRNA as previously described. 24 hours post-transfection, cells were either

treated with 25 nM paclitaxel or left untreated. Fresh RPMI media was replaced on drug-free cells. Cells were harvested at 6, 12 and 24 hours of paclitaxel treatment. All media was collected and pooled with trypsinized adherent cells. Cell pellets were washed once with PBS, then resuspended in 200  $\mu$ L ice-cold 70% ethanol and transferred to a 96-well V-bottom polypropylene dish. Samples were fixed overnight at -20°C. The next day, the 96-well plate was centrifuged at 500xg for 5 minutes in an eppendorf Centrifuge Model 5810 R. Fixed cells were washed once with PBS, then resuspended in 200  $\mu$ L of freshly prepared propidium iodide stain and incubated at 37°C for 15 minutes. Samples were analyzed by flow cytometry on a FACScan instrument (BD) or on a FACSCalibur instrument (BD) in the FL-2 channel. Results were analyzed using CellQuest Pro software (BD Biosciences).

### **2.11 Mitotic shake-off assay**

MCF-7 cells were plated at 160,000 cells per well of a 12-well tissue culture dish. The next day, cells were treated with BAD siRNA and negative control siRNA using twice the volumes of reagents described for a knock-down in 24-well format. The day after transfection, cells were treated with 25 nM paclitaxel or left untreated. At 39 hours of paclitaxel treatment, the dish was knocked to lift rounded mitotic cells. Media containing the mitotic cells was transferred to a separate sterile well and media containing 25 nM paclitaxel was replaced on adherent cells. At 48 hours of paclitaxel treatment, all cells were harvested and washed once with PBS. Cells were then resuspended in 100  $\mu$ L of

100 nM tetramethylrhodamine, ethyl ester (TMRE) (Invitrogen, cat. T669) to measure mitochondrial membrane potential (228,229). Cells were stained at 37°C for 15 minutes then rinsed with 100 µL of PBS. Cell pellets were isolated by centrifugation and resuspended in a final volume of 200 µL PBS before transferring to 5 mL polystyrene tubes. Samples were analyzed by flow cytometry in the FL-2 channel.

## 2.12 Molecular subcloning

### 2.12.1 Plasmids

**Table 2.4 Plasmid sources and applications**

Plasmid construct	Notes	Source	Application
pDEST <sup>TM</sup> 27	Empty vector	Invitrogen (cat.11812-013)	Gateway <sup>®</sup> cloning of GST-BAD construct
GST-pDEST27	GST control vector	Goping lab	Generation of stable cell lines in MDA-MB-231 cells
BAD-pDEST27	N-terminal GST tagged BAD	Goping lab	Generation of stable cell lines in MDA-MB-231 cells
pEBG	GST backbone vector	Dr. Hobman (Dept. Cell Biology)	GST control for pull-down in HEK293T/17 cells
BAD-pEBG	N-terminal GST-tagged BAD	Goping lab	GST-BAD pull down in HEK293T/17 cells
BAD S118A-pEBG	N-terminal GST-tagged BAD mutant	generated in this work	GST-BAD pull down in HEK293T/17 cells
BAD S118D-pEBG	N-terminal GST-tagged BAD mutant	generated in this work	GST-BAD pull down in HEK293T/17 cells
pcDNA <sup>TM</sup> 3.2/V5-DEST	Vector alone	Invitrogen (cat.12489-019)	Gateway <sup>®</sup> cloning of BAD and vimentin constructs
BAD-pcDNA3.2/V5-DEST	untagged BAD	generated in this work	In vitro transcription-translation reactions

<b>Vimentin-</b> pcDNA3.2/V5- DEST	untagged Vimentin	generated in this work	In vitro transcription- translation reactions
<b>Myc-BAD-</b> pcDNA3.2 V5/DEST	N-terminal Myc tag	generated in this work	Cotransfection and coimmunoprecipitation
<b>Vimentin-V5-</b> pcDNA3.2/ V5- DEST	C-terminal V5 tag	generated in this work	Cotransfection and coimmunoprecipitation
<b>mEmerald-</b> <b>Vimentin</b>	Fluorescently tagged	Gift from Dr. Michael Davidson (Florida State University)	Template for vimentin PCR
<b>Hexokinase I-V5-</b> pcDNA3.2/V5- DEST	C-terminal V5 tag	Goping lab (Erin Austen)	Cotransfection and coimmunoprecipitation
<b>Hexokinase II-</b> <b>V5-pcDNA3.2/</b> V5-DEST	C-terminal V5 tag	Goping lab (Erin Austen)	Cotransfection and coimmunoprecipitation

### 2.12.2 Primers

**Table 2.5 Primers used in cloning**

Plasmid construct	Forward primer	Reverse primer	Application
<b>BAD S118A-</b> pEBG	5'-CGA GCT CCG GAG GAT <u>GGC</u> <u>TGA</u> CGA GTT TGT GGA C-3'	5'-GTC CAC AAA CTC GTC AGC CAT CCT CCG GAG CTC G-3'	BAD S118 site- directed mutagenesis
<b>BAD S118D-</b> pEBG	5'-CGA GCT CCG GAG GAT <u>GGA</u> <u>TGA</u> CGA GTT TGT GGA C-3'	5'-GTC CAC AAA CTC GTC ATC CAT CCT CCG GAG CTC G-3'	BAD S118 site- directed mutagenesis
<b>BAD-</b> pcDNA3.2/V5- DEST	5'-CAC <u>CAT</u> GTT CCA GAT CCC AGA GTT TGA GCC-3'	5'- <u>TCA</u> CTG GGA GGG GGC GGA- 3'	Gateway <sup>®</sup> cloning of BAD
<b>Vimentin-</b> pcDNA3.2/V5- DEST	5'-CAC <u>CAT</u> GTC CAC CAG GTC CGT GTC-3'	5'- <u>TTA</u> TTC AAG GTC ATC GTG ATG CTG-3'	Gateway <sup>®</sup> cloning of Vimentin
<b>Myc-BAD-</b> pcDNA3.2/V5- DEST	5'-CAC <u>CAT</u> <i>GGA</i> <i>GCA</i> AAA <i>GCT</i> <i>CAT</i> <i>TTC</i> <i>TGA</i> <i>AGA</i> <i>GGA</i> <i>CTT</i> <i>GTT</i> CCA GAT CCC AGA G-3'	5'- <u>TCA</u> CTG GGA GGG GGC GGA GCT TCC CCT G-3'	Gateway <sup>®</sup> cloning of Myc-tagged BAD
<b>Vimentin-V5-</b> pcDNA3.2/V5- DEST	5'-CAC <u>CAT</u> GTC CAC CAG GTC CGT GTC-3'	5'-TTC AAG GTC ATC GTG ATG CTG AGA-3'	Gateway <sup>®</sup> cloning of V5- tagged vimentin

Italics denote the myc-tag sequence

### 2.12.3 PCR amplification

BAD and Vimentin cDNA sequences were PCR amplified Phusion<sup>®</sup> High Fidelity DNA Polymerase kit (Fermentas, cat. F-530). Reactions contained: 4.0  $\mu$ L 5x Phusion<sup>®</sup> Buffer, 0.4  $\mu$ L of 10 mM dNTPs, 1.0  $\mu$ L of 10  $\mu$ M forward primer, 1.0  $\mu$ L of 10  $\mu$ M reverse primer, 1.0  $\mu$ L of 10 ng/ $\mu$ L plasmid template, 0.2  $\mu$ L of 2U/ $\mu$ L Phusion<sup>®</sup> DNA Polymerase enzyme, and 12.4  $\mu$ L ddH<sub>2</sub>O for a final volume of 20  $\mu$ L. Plasmids used as DNA templates include BAD-pENTR/D-TOPO and mEmerald-Vimentin. PCR amplifications were performed as follows:

1. 98°C for 30 seconds for initial denaturation
2. (98°C for 10 seconds denaturation, X°C for 30 seconds annealing, 72°C 40 seconds extension) x 30 cycles  
X = 58°C for full length vimentin amplification  
X = 61°C for vimentin $\Delta$ TAA amplification  
X = 67°C for BAD amplification
3. 72°C for 10 minutes extension

#### **2.12.4 Agarose gel electrophoresis**

PCR amplified products were separated on 0.8% agarose gels prepared in 1XTAE buffer supplemented with 0.5  $\mu$ g/mL ethidium bromide to detect DNA. DNA bands were excised using a clean razor blade, and extracted using a GeneJET™ Gel Extraction Kit (Fermentas, cat. K0691). 10  $\mu$ L of gel-extracted DNA was run on 0.8% agarose gels for DNA quantification against GeneRuler™ 1kb DNA Ladder Plus (Fermentas).

#### **2.12.5 Gateway® Cloning**

Blunt-end PCR products were cloned using Gateway® Cloning Technology (Invitrogen). Entry cloning was performed with the pENTR™/D-TOPO® directional TOPO cloning kit (Invitrogen, cat. K2400-20) and a 1:1 molar ratio of PCR product:entry vector. Destination vectors pcDNA™ 3.2/V5-DEST and pDEST™27 were purchased from Invitrogen. Destination vector cloning was

performed using The Gateway<sup>®</sup> LR Clonase<sup>®</sup> II Enzyme mix (Invitrogen, cat. 11791-020) with 75 ng of entry vector and destination vector.

### **2.12.6 Bacterial Transformation**

2  $\mu$ L of cloning reaction (above) was added to 50  $\mu$ L of subcloning efficiency DH5 $\alpha$  (Invitrogen cat. 18265-017). The mixture was stirred with a pipette tip and incubated on ice for 20 minutes. The bacteria were then heat-shocked at 42°C for 30 seconds then replaced on ice. 250  $\mu$ L of S.O.C. media was added and the bacteria were incubated for 1 hour at 37°C in a shaking incubator at 200 rpm. 50-100  $\mu$ L of the transformation reaction was then plated LB agar plates containing appropriate antibiotic. Entry clones were plated on 30  $\mu$ g/mL Kanamycin LB agar plates and destination vector clones were plated on 100  $\mu$ g/mL Ampicillin LB agar plates.

### **2.12.7 Restriction enzyme digests**

Entry clones were screened for the presence of insert by restriction enzyme digestion. BAD entry clones were digested with PvuII restriction enzyme. Restriction digests were set up by mixing 0.5  $\mu$ g DNA, 2.0  $\mu$ L of 10xNEB2 buffer (New England Biolabs), 0.5  $\mu$ L of 10U/ $\mu$ L PvuII (New England Biolabs) and ddH<sub>2</sub>O to 25  $\mu$ L. Vimentin entry clones were restricted with HincII enzyme and reactions were prepared using 10xReact 4 buffer (Invitrogen). Restriction digests were performed at 37°C for 1 hour. DNA fragments were separated by agarose gel electrophoresis and compared with predicted fragment

sizes calculated using Vector NTI Advance<sup>®</sup> 10 software (Invitrogen). Entry vectors were verified by DNA sequencing using M13 forward or M13 reverse primer. Destination vector clones were sequenced with T7 primer. 150-225 ng plasmids were submitted with 0.53  $\mu$ M sequencing primer to The Applied Genomics Centre at the University of Alberta for sequencing.

### **2.12.8 Site-directed mutagenesis**

BAD S118A and S118D mutations were created in the BAD/pEBG vector using QuikChange<sup>®</sup> Lightning Site-Directed Mutagenesis Kit (Stratagene, cat. 210518) and Phusion<sup>®</sup> DNA Polymerase (Fermentas). Reactions were prepared with 2.5  $\mu$ L of 10x reaction buffer, 25-50 ng DNA template, 62.5 ng forward primer, 62.5 ng reverse primer, 0.5  $\mu$ L of 10 mM dNTP mix, 0.75  $\mu$ L of QuikSolution reagent and 0.5  $\mu$ L of Phusion<sup>®</sup> High Fidelity DNA Polymerase (Fermentas). Thermal cycling was performed as follows:

1. 98°C for 2 minutes for denaturation
2. (95°C for 20 seconds, 60°C for 10 seconds, 68°C for 3.5 minutes) x 18 cycles
3. 68°C for 5 minutes for extension

1  $\mu$ L DpnI enzyme provided in the kit was added to each amplification reaction, and incubated for 5 minutes at 37°C prior to transformation of DH5 $\alpha$ .

### 2.13 Generation of stable cell lines

To generate the GST-stably expressing MDA-MB-231 cell line (231.GST), 50,000 MDA-MB-231 cells were plated per well of a 24-well dish. pDEST<sup>TM</sup>27 control vector was transfected using Lipofectamine<sup>TM</sup> 2000 (Invitrogen, cat. 11668-027) according to the manufacturer's protocol. Briefly, 0.8 µg of plasmid DNA was diluted in 50 µL Optim-MEM Reduced Serum Medium and mixed. 2 µL of Lipofectamine<sup>TM</sup> 2000 was diluted in a separate tube containing 50 µL Optim-MEM. The two mixtures were incubated separately for 5 minutes; then diluted DNA and diluted Lipofectamine<sup>TM</sup> were mixed and incubated for 20 minutes at room temperature. 100 µL of transfection complexes were then added dropwise to the cells.

After 2 days of growth in culture media, transfected cells were trypsinized and plated in 10 cm dishes in RPMI1640 media supplemented with 1 mg/mL Geneticin<sup>®</sup> (Invitrogen). Transfected cells were positively selected in this media and grew to form colonies. 20 sizeable colonies were trypsinized with 2 µL trypsin and transferred to a 96-well plate into 100 µL of RPMI with 1 mg/mL Geneticin<sup>®</sup> media. Clones that continued to grow in the 96-well plate were trypsinized and reseeded in a 24-well plate, and then a 6-well plate. Finally, the clones were transferred to T-25 flasks. The G418 resistant clones were screened for GST expression by western blotting. Cell lysates were prepared by pelleting  $\sim 1 \times 10^6$  cells and boiling in 100 µL 1x laemmli buffer. Clones that were positive for GST expression were frozen at  $2 \times 10^6$  to  $4 \times 10^6$  cells in 1.5 mL of RPMI1640

media with 10% FCS (v/v) and 10% DMSO (v/v) in cryovials. Vials were cooled to -86°C then transferred to liquid nitrogen for long term storage.

## **2.14 Screen for GST-BAD interacting proteins in MDA-MB-231 cells**

### **2.14.1 GST pull-down assay**

BAD was expressed as a fusion protein with an N-terminal GST tag for glutathione sepharose pull-down as a method of detecting interacting proteins. Large-scale pull-downs for protein identification were performed by harvesting 50 confluent 150 mm dishes of each of 231.GST and 231.GST-Bad cells.  $1.6 \times 10^9$  cells were counted and centrifuged at 500xg for 5 minutes. Cell pellets were washed three times with PBS then stored at -86°C. For the GST pull-down assay, cell pellets were thawed on ice then lysed at  $10 \times 10^6$  cells per mL in freshly prepared 1% CHAPS GST pull-down lysis buffer with freshly added DTT and protease inhibitor. Cells were lysed at 4°C with gentle agitation for 45 minutes. Insoluble material was pelleted by centrifugation at 13,000xg for 5 minutes at 4°C. 200 µL of Glutathione Sepharose™ 4B beads (GE Healthcare, cat. 17-0756-01) were prepared by rinsing once in 0.1% Triton X-100 in PBS, then rinsing three times in 1% CHAPS lysis buffer. 100 µL beads were incubated with each of the 231.GST and 231.GST-BAD cell lysates overnight at 4°C with gentle agitation. The next day, the beads were washed three times with 1% CHAPS lysis buffer. Finally, the beads were eluted twice sequentially with 210 µL of freshly prepared glutathione elution buffer. Eluate was boiled with 42 µL of 6x laemmli buffer and stored at -86°C before loading on SDS-PAGE gels. Samples were

electrophoresed on two 1.5 mm 14% polyacrylamide gels until the dye front reached the bottom of the gel. One gel was colloidal coomassie-stained, while the other gel was silver-stained.

### **2.14.2 Gel Staining**

All reagents used in the preparation of SDS-PAGE gels and staining procedures were prepared using newly purchased reagents and clean HPLC grade submicron filtered water (Fisher Scientific, CAS 7732-18-5). Glass plates and containers were rinsed 30% methanol and clean ddH<sub>2</sub>O prior to use. Containers were covered and nitrile gloves were worn throughout to reduce keratin contamination.

#### **2.14.2.1 Colloidal Coomassie Staining**

Blue-silver staining protocol was obtained from Dr. Fahlman (Dept of Biochemistry, University of Alberta) and was based on the staining protocol of Neuhoff et al., modified by Candiano et al (230,231). This staining protocol modifies the Neuhoff colloidal coomassie staining protocol by increasing the concentration of Coomassie Brilliant Blue G-250 and phosphoric acid (231). First, samples were run by SDS-PAGE then the separating gel was fixed in 50% ethanol and 2% phosphoric acid for 2 hours. The gel was washed 2x20 minutes in ddH<sub>2</sub>O then stained overnight with Colloidal Coomassie G-250 stain: 0.12% (w/v) Coomassie Brilliant Blue G-250 (ThermoFisher Scientific), 10%

phosphoric acid (v/v), 10% ammonium sulfate (w/v) and 20% methanol (v/v) (231). The next day the gel was rinsed with ddH<sub>2</sub>O.

Visible protein bands were excised with a clean razor blade. For each band excised from the GST-BAD pull-down lane, an adjacent band was excised from the GST control pull-down lane. Each excised band was diced into approximately 2mm<sup>3</sup> cubes and transferred to 100 µL of ddH<sub>2</sub>O in a 96-well plate. The sample plate was covered and stored at -86°C prior to submission for mass spectrometry.

#### **2.14.2.2 Silver Staining**

Silver staining was performed as outlined by the Short Silver Nitrate staining protocol of Chevallet et al (232). The protocol is reproduced here in brief. All solutions were prepared fresh immediately prior to use. The SDS-PAGE separating gel was fixed in 30% (v/v) ethanol and 10% (v/v) acetic acid for 30 minutes. The gel was rinsed 2x10 minutes in 20% (v/v) ethanol, then 2x10 minutes in ddH<sub>2</sub>O. After rinsing, the gel was sensitized by soaking in 0.02% (w/v) sodium thiosulfate for one minute. The gel was then rinsed 2x1 minute in ddH<sub>2</sub>O. The gel was impregnated with 12 mM silver nitrate for 20 minutes, rinsed in ddH<sub>2</sub>O for 10 seconds then developed until no new protein bands appeared, ~30 minutes. Developer solution was prepared with 3% (w/v) potassium carbonate and addition of 250 µL formalin and 125 µL of 10% (w/v) sodium thiosulfate per litre. After developing, the gel was transferred to stop solution containing 4% (w/v) Tris and 2% (v/v) acetic acid for 30 minutes. Finally the gel was rinsed 2x30 minutes in ddH<sub>2</sub>O. The entire GST-BAD and GST pull-

down lanes were excised as individual bands, cut into 2 mm<sup>3</sup> cubes and transferred to individual wells of a 96-well plate for mass spectrometry, as previously indicated.

### **2.14.3 Mass Spectrometry**

Samples were analyzed by liquid chromatography-tandem mass spectrometry (LC-MS/MS) using an LCQ Deca XP ion trap mass spectrometer in collaboration with Dr. Richard Fahlman and Dr. Jack Moore at the Institute for Biomolecular Design (IBD), University of Alberta. Protein identification was performed using the Mascot search engine (Matrix Science).

### **2.15 MDA-MB-231 subcellular fractionation**

Subcellular fractionations of MDA-MB-231, 231.GST-BAD, 231.GST and 231.BAD cells were performed using the Qproteome<sup>®</sup> Cell Compartment Kit (Qiagen, cat. 37502) as previously described. Cells were grown to confluency in 10 cm dishes prior to harvesting. Equal proportions of non-precipitated fractions were analyzed by western blotting.

### **2.16 BAD coimmunoprecipitation**

For BAD coimmunoprecipitation experiments, MDA-MB-231 cells and 231.BAD cells were harvested at confluency and counted with a haemocytometer. Cells were pelleted by centrifugation at 500xg for 5 minutes at room temperature. Cell pellets were rinsed once with PBS and resuspended at 10x10<sup>6</sup> cells/mL in 1%

CHAPS lysis buffer as indicated, supplemented with Complete protease inhibitor cocktail, EDTA-free (Roche, cat. 11 873 580 001). BAD coimmunoprecipitations testing for interactions with vimentin were performed with sodium chloride-free 1% NP-40 lysis buffer. Cells were lysed on ice for 15 minutes then centrifuged at 10,000xg for 5 minutes at 4°C to pellet insoluble material. Approximately 400 µL of soluble lysate was incubated with 1 µg of rabbit anti-BAD IgG for BAD coimmunoprecipitation. Negative control immunoprecipitation reactions were performed with 0.5 µg of rabbit anti-Granzyme A or equivalent volumes of rabbit anti-Calnexin or mouse-anti BubR1 antibodies. Incubations were performed overnight at 4°C with gentle mixing to allow immune complexes to form. The next day, Protein A Sepharose™ beads (GE Healthcare) were equilibrated 3x5 minutes with lysis buffer. 40 µL of 50% slurry beads were added to each IP to recover immune complexes. Beads were rinsed 3x5 minutes with lysis buffer, boiled in 50 µL 1x laemmli buffer and analyzed by western blotting. For detection of NMHC II-A/MYH9, a 220 kDa protein, samples were resolved by electrophoresis on 8% polyacrylamide gels at 100 V for 3-4 hour then transferred to PVDF membrane in 16% methanol Western blot transfer buffer, overnight at 30V at 4°C. The next day, the voltage was increased to 90V for 1 hour.

## **2.17 Immunofluorescence**

Cells were grown on ethanol-sterilized, 12 mm #1.5 glass coverslips (Electron Microscopy Sciences, cat. 72230-01) in 24-well dishes. To visualize mitochondria, cells were stained live with 200 nM MitoTracker® Red CMXRos

(Invitrogen, cat. M-7512) at 37°C for 15 minutes. Cells were fixed with 4% formaldehyde/PBS for 15 minutes and permeabilized with freshly prepared 0.1% Triton X-100/PBS for 2 minutes. Cells were rinsed 4 times over 5 minutes with PBS then blocked with 0.2% gelatin/PBS for 1 hour at room temperature. Primary antibody was diluted in 0.2% gelatin/PBS (**Table 2.2**) and incubated overnight at 4°C. The next day, coverslips were washed four times over 5 minutes with PBS prior to application of secondary antibody. Species-specific Alexa-Fluor conjugated secondary antibodies (Invitrogen) (**Table 2.3**) were diluted 1:200 in blocking agent and incubated 1 hour in the dark at room temperature. Coverslips were rinsed four times with PBS then mounted in mounting media (Dako, cat. S3023). Fluorescent images were acquired on a Leica TCS SP5 laser scanning confocal microscope (Leica Microsystems). Images were acquired using Argon and HeNe543 lasers and a 100X magnification objective lens (numerical aperture 1.44). Images were viewed using Leica Microsystems LAS AF Lite software (Leica Application Suite, Advanced Fluorescence Lite 2.3.5 build 5379).

### **2.18 Myc-BAD coimmunoprecipitation**

MDA-MB-231 cells were cotransfected with 15 µg total Myc-BAD and Vimentin-V5-pcDNA3.2/V5-DEST vectors at 1:2 molar ratios using *TransIT*<sup>®</sup>-LT1 Transfection Reagent (Mirus, cat. MIR 2300). Cells were harvested and lysed at 4°C in sodium chloride-free 1% NP-40 lysis buffer supplemented with 1x complete protease inhibitor and 1x PhosSTOP<sup>®</sup> phosphatase inhibitor (Roche, cat.

04906837001). 30  $\mu$ L of Myc and V5-antibody cross-linked Protein A Sepharose beads were added to 250  $\mu$ L of lysate and incubated overnight at 4°C. After washing the beads, immunoprecipitated proteins were eluted with 50  $\mu$ L of 0.1 M Glycine pH 2.5. Beads were pelleted at 500xg, then the eluate was pipetted into a separate microfuge tube for neutralization with 5  $\mu$ L of 1M Tris pH 9.5. Finally, the eluate was boiled with 11  $\mu$ L of 6x laemmli buffer.

### **2.19 Vimentin fractionation**

The solubility of vimentin was compared in 1% NP-40 lysis buffers that either contained 150 mM NaCl or no NaCl (+/- salt). MDA-MB-231 cells were lysed in 1% NP-40 lysis buffer (+/- NaCl) supplemented with protease and phosphatase inhibitor at  $10 \times 10^6$  cells/mL. All subsequent steps were performed at 4°C. The lysate was centrifuged at 500xg for 5 minutes, and the supernatant was recentrifuged at 10,000xg for 5 minutes then 16,000xg for 5 minutes. 500xg and 16,000xg pellets were resuspended in 100  $\mu$ L 1x laemmli buffer and boiled for SDS-PAGE. 500xg, 10,000xg and 16,000xg soluble fractions were boiled with 6x laemmli buffer. Equal proportions of each fraction (1/10<sup>th</sup> input) were analyzed for vimentin content by western blotting.

### **2.20 In vitro transcription translation coupled-coimmunoprecipitation assays**

In vitro transcription-translation (IVTT) coupled reactions were performed using the TNT<sup>®</sup> T7 Coupled Reticulocyte Lysate System kit (Promega, cat. L4610) according to the manufacturer's protocol.

### **2.20.1 BAD-Vimentin coimmunoprecipitation study**

BAD and vimentin proteins were synthesized by IVTT reactions using BAD/pcDNA3.2 V5-DEST, Vimentin/pcDNA3.2 V5-DEST and pcDNA3.2 V5-DEST (empty vector) were used as plasmid templates. 50  $\mu$ L reactions were set up (or scaled accordingly) at 4°C containing: 25.0  $\mu$ L of rabbit reticulocyte lysate, 2.0  $\mu$ L TNT reaction buffer, 1.0  $\mu$ L T7 RNA Polymerase, 1.0  $\mu$ L amino acid mixture minus methionine (1 mM), 2.0  $\mu$ L methionine (1 mM) (Promega, cat. L118A), 1.0  $\mu$ L RNasin<sup>®</sup> Ribonuclease Inhibitor (40 U/ $\mu$ L) (Promega, cat. N211A), 1.0  $\mu$ g of plasmid template and made up to final volume with nuclease-free ddH<sub>2</sub>O. Reactions were incubated at 30°C for 90 minutes for protein synthesis.

Coimmunoprecipitation was performed at room temperature. First 10  $\mu$ L of each IVTT reaction to 50  $\mu$ L of 0.2% NP-40 IVTT buffer (233). Mixtures were incubated for 1 hour with gentle agitation prior to addition of antibody. The mixture was incubated with 1  $\mu$ L of antibody for 1 hour then immune complexes were recovered with Protein A Sepharose<sup>™</sup> beads. Beads were washed four times in IVTT buffer and boiled in 2x laemmli buffer to recover proteins.

### **2.20.2 BAD-Hexokinase coimmunoprecipitation study with cross-linking**

BAD and Hexokinase I and II were synthesized in 50  $\mu$ L IVTT reactions employing BAD/pcDNA 3.2 V5-DEST, Hexokinase I/pcDNA 3.2 V5-DEST and Hexokinase II/pcDNA 3.2 V5-DEST as plasmid templates for protein synthesis. 50  $\mu$ L IVTT reactions were set up as above, except 0.5  $\mu$ L of amino acid mixture

minus leucine (1 mM) and 0.5  $\mu$ L of amino acid mixture minus methionine (1 mM) were mixed. All subsequent steps were performed at room temperature. Following protein synthesis 10  $\mu$ L of each of two IVTT reactions was added to 50  $\mu$ L of detergent-free buffer IVTT buffer. The samples were incubated for 1 hour prior to protein cross-linking. Protein cross-linking was performed with 1% formaldehyde for 10 minutes at room temperature. Cross-linking was quenched with 0.25 M glycine for 5 minutes. Coimmunoprecipitations were performed by adding 1  $\mu$ L of antibody to each sample with one hour incubation followed by one hour incubation with 20  $\mu$ L protein A sepharose beads. Finally, immune complexes were recovered and protein cross-links were reversed by boiling the beads for 20 minutes in 1x laemmli buffer. Immunblotting for BAD and Hexokinases was performed with 14% and 10% SDS-PAGE gels respectively.

## **2.21 Screen for GST-BAD Serine 118A/D interacting proteins**

### **2.21.1 GST pull-down assay in HEK 293T/17 cells**

HEK293T/17 cells were seeded at  $2 \times 10^6$  cells in 10-cm dishes. 48 hours after seeding, cells were transfected with pEBG, BAD/pEBG, BAD S118A/pEBG or BAD S118D/pEBG using calcium phosphate transfection method (234). 15  $\mu$ g of plasmid DNA was diluted in sterile water to a total volume of 450  $\mu$ L. 50  $\mu$ L of 2.5 M  $\text{CaCl}_2$  was added and the mixture was vortexed. 500  $\mu$ L of 2x HBS pH 7.3 was added to the mixture while vortexing. The transfection mixture was immediately added dropwise to the cells. 24 hours post-transfection, the cells were harvested and lysed in 1% CHAPS GST pull-down buffer with freshly

added DTT and protease inhibitor. GST-pull downs were performed as previously described.

### **2.21.2 In gel trypsin digestion**

Samples were electrophoresed on 1.5 mm 14% polyacrylamide gels until the dye front had just run into the separating gel. The gel was then stained with colloidal coomassie G-250. A single band was excised from each of the non-transfected, GST, GST-BAD, GST-BAD S118A or GST-BAD S118D lanes. The protocol for in gel trypsin digestion was obtained from Dr. Richard Fahlman (Dept of Biochemistry, University of Alberta) and is reproduced here in brief. Each band was cut into 1 mm<sup>3</sup> cubes and placed in a 1.5 mL tube. Gel pieces were rinsed with 300 µL of water. Coomassie dye was extracted by drying the gel with 300 µL acetonitrile, followed by rehydration with 300 µL of freshly prepared 100 mM ammonium bicarbonate, pH 8.0. The gel was dried with 100 µL acetonitrile, the supernatant was discarded. 50 µL of 10 mM DTT was added to the gel for 1 hr at 60°C, the supernatant was discarded. The gel was washed with 300 µL of 100 mM ammonium bicarbonate for 5 min, then 50 µL 50 mM iodoacetamide was added and incubated in the dark for 30 minutes. The gel was washed twice with 300 µL 100 mM ammonium bicarbonate and dried with 100 µL acetonitrile. 40 µL of sequencing grade modified trypsin (Promega V511A) was added with enough 50 mM ammonium bicarbonate to cover the gel. Samples were trypsinized overnight at 37°C. 140 µL of water was added to the gel and vortexed and the supernatant was collected. Peptides were twice extracted from

the gel with 50% acetonitrile and 1% formic acid. All three supernatants were pooled and dried in a speed vac. Dried peptides were resuspended in 10% acetonitrile and 1% formic acid.

### **2.21.3 Mass Spectrometry**

Mass spectrometry protein identification was conducted as in section **2.14.3** using LC-MS/MS with an LTQ Orbitrap XL mass spectrometer (Thermo Fisher Scientific) that allows more sensitive detection of low abundant peptides. Proteome Discoverer v1.2 software (Thermo Fisher Scientific) was used to search complete proteome databases using Mascot Search Engine (Matrix Science) and SEQUEST search engine (ThermoFisher Scientific).

### **2.22 GST-BAD transient transfections**

MDA-MB-231 cells were transfected with pEBG, BAD/pEBG, BAD-S118A/pEBG and BAD S118D/pEBG using *TransIT*<sup>®</sup>-LT1 (Mirus, cat. MIR 2300) according to the manufacturer's protocol. GST pull-downs from transfected cells were used to assess interactions with 14-3-3 proteins and BCL-XL.

### **2.23 Miscellaneous Procedures**

#### **2.23.1 Antibody cross-linking**

BAD, Vimentin, Myc and V5 antibodies were cross-linked to Protein A Sepharose<sup>™</sup> beads (GE Healthcare) and protein antigen complexes were eluted with glycine to reduce contamination of immunoprecipitated complexes with

antibody heavy chain and improve detection of vimentin. 0.2 g of Protein A Sepharose<sup>™</sup> beads (GE Healthcare) were rinsed three times with ddH<sub>2</sub>O then rinsed twice with PBS. 100  $\mu$ L of packed beads were diluted in 1 mL of PBS and incubated with 10  $\mu$ L of antibody overnight with gentle mixing. The following day, beads were rinsed 3x with 1 mL of PBS to remove unbound antibody. Cross-linking reactions were performed with freshly prepared dimethyl pimelimidate (DMP) (Sigma-Aldrich, cat. D8388) at 5.2 mg/mL in 0.1 M sodium borate pH 9.0 for 30 minutes at room temperature. Beads were subsequently washed with 1 mL of 0.1 M sodium borate pH 9.0, and the cross-linking and wash steps were repeated. Cross-linking was quenched twice with 50 mM ethanolamine/PBS for 5 minutes followed by 2 washes with PBS. Finally, excess antibody was removed by rinsing twice with 1 mL of 50 mM glycine pH 2.5 for 5 minutes. Beads were rinsed 3 times with PBS and stored at 4°C in PBS.

## **Chapter 3: Results**

### **3.1 BAD mediates paclitaxel cytotoxicity through a nonapoptotic pathway**

Our laboratory previously demonstrated an important role for BAD in paclitaxel induced death of breast cancer cell lines (67). The BAD-dependent death pathway was demonstrated in MCF-7 cells, where siRNA-mediated BAD depletion largely attenuated paclitaxel-induced cell death. Given the well characterized role for BAD as an indirect activator of mitochondrial apoptosis, we hypothesized that paclitaxel would stimulate pro-apoptotic BAD function to induce cell death. With our knowledge of the dynamics of typical pro-apoptotic BAD function, we hypothesized that paclitaxel treatment would: i) stimulate BAD interactions with anti-apoptotic BCL-2 family members, and ii) stimulate translocation of BAD from the cytosol to the mitochondria. We decided to assess these two facets of BAD activity under conditions of paclitaxel treatment and compare results with staurosporine treatment, a known apoptotic inducer (91) of MCF-7 cells (79,97).

#### **3.1.1 BAD:BCL-XL interactions are diminished in paclitaxel-treated MCF-7 cells**

First, we assessed BAD interactions with anti-apoptotic BCL-2 family member binding partners, BCL-XL, BCL-2 and BCL-W with paclitaxel treatment (**Figure 3.1 A**). MCF-7 cells were treated with 25 nM paclitaxel for 48 hours in this assay to induce apoptotic cell death as previously determined (67). Studies have shown that treatment of monolayer cultured cells with clinically relevant concentrations of paclitaxel, 10-1000 nM, results in metaphase arrest and

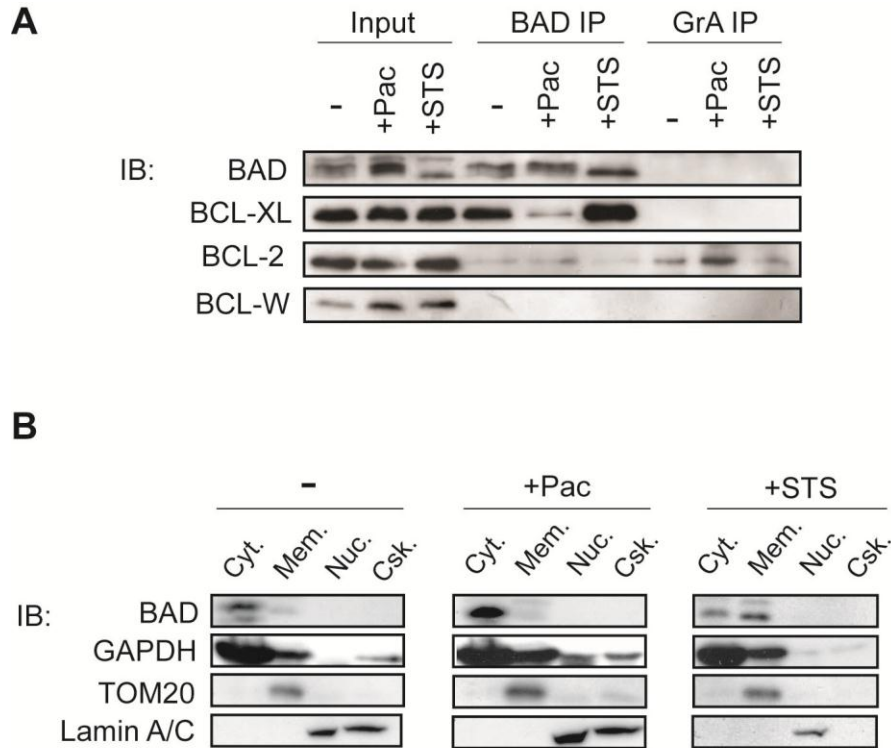


**Figure 3.1 Paclitaxel does not induce typical pro-apoptotic BAD activity.** (A) Paclitaxel does not induce association of BAD with anti-apoptotic BCL-2 family members. MCF-7 cells were untreated (-), treated with 25 nM paclitaxel for 48 hours (+Pac) or treated with 2.5  $\mu$ M staurosporine for 4 hours (+STS). The cells were then lysed in 1% CHAPS buffer and immunoprecipitated with anti-BAD antibody (BAD IP) or negative control antibody for Granzyme A (GrA IP). Western blots were probed for BAD, BCL-XL, BCL-2 and BCL-W. (B) Paclitaxel does not induce translocation of BAD from the cytosol to the mitochondria. MCF-7 cells were treated as in (A) and subcellular fractions were isolated using the Qproteome<sup>®</sup> kit (Qiagen). Cytosolic (Cyt.), membrane (Mem.), nuclear (Nuc.) and cytoskeletal (Csk.) fractions were probed by western blot for cytosolic marker GAPDH, mitochondrial membrane marker Tom20, nuclear marker Lamin A/C and for the presence of BAD. Image from (67).

apoptotic cell death (62). MCF-7 cells were also treated with 2.5  $\mu$ M staurosporine for 4 hours as a positive control for apoptosis induction. We performed BAD coimmunoprecipitation with treated and untreated cells followed by western blot analysis with anti-BAD and anti-BCL-XL antibodies. In untreated cells (-), basal BAD:BCL-XL interactions were revealed. Treatment with staurosporine (+STS) maintained and possibly enhanced BAD:BCL-XL interactions. Additionally, we observed a downward shift in the BAD immunoblotted band with staurosporine treatment, consistent with dephosphorylation of BAD. Treatment with paclitaxel (+Pac), however yielded a surprising result as BAD:BCL-XL interactions were greatly diminished in these cells. This replicate of the experiment was reproducible in MCF-7 cells in work demonstrated by other laboratory members (67). Furthermore, western blot analysis for additional anti-apoptotic proteins, BCL-2 and BCL-W, revealed no detectable interaction with BAD under any treatment condition. These results demonstrate that:

- i) BCL-XL is the predominant anti-apoptotic BAD-binding partner in MCF-7 cells, and
- ii) paclitaxel treatment does not stimulate BAD interactions with anti-apoptotic BCL-2 family members.

### **3.1.2 BAD remains localized to the cytosol in paclitaxel-treated MCF-7 cells**

We decided to assess the second facet of BAD function: BAD subcellular localization in MCF-7 cells in untreated, paclitaxel and staurosporine-treated cells

**(Figure 3.1 B).** Drug treatments were performed consistently with the previous assay; Paclitaxel was applied to MCF-7 cells at a concentration of 25 nM for 48 hours and staurosporine was applied at a concentration of 2.5  $\mu$ M for 4 hours. MCF-7 cells were fractionated using the Qproteome<sup>®</sup> Cell Compartment Kit (Qiagen) into four subcellular fractions, including a cytosolic, membrane, nuclear and cytoskeletal fraction. Antibodies against GAPDH, Tom20 and Lamin A/C were used as markers of the cytosolic, membrane and nuclear fractions respectively. Finally, anti-BAD western blots revealed the anticipated cytosolic localization of BAD in untreated cells. Staurosporine treatment induced partial translocation of BAD from the cytosolic fraction to the membrane fraction which includes the mitochondrial membrane. This result is consistent with the mitochondrial translocation of BAD reported in other cell lines (SKBR-3 and MDA-MB-468 cells) (67) and supports a proapoptotic role for BAD in response to staurosporine, consistent with results of **Figure 3.1 A**. Interestingly, we observed that BAD remained localized to the cytosolic fraction with paclitaxel treatment, with no evidence of mitochondrial translocation. This single experiment in MCF-7 cells was reproducible by other laboratory members. These results demonstrated that:

- i) BAD is localized to the cytosol of MCF-7 cells under basal conditions, and
- ii) Paclitaxel does not stimulate mitochondrial translocation of BAD as we would expect with induction of a BAD-mediated pro-apoptotic pathway.

Taken together, we reasoned that BAD pro-apoptotic activity is not stimulated with paclitaxel treatment. Instead, BAD is required for paclitaxel-induced breast cancer cell death through a novel, nonapoptotic pathway.

### **3.1.3 Investigating BAD pro-proliferative function**

Ongoing studies in our laboratory demonstrated a pro-proliferative role for BAD in MDA-MB-231 cells (113). Specifically, we observed that a BAD-stably expressing cell line (231.BAD), reached higher cell numbers in a proliferation assay compared with 231.vector control cells and the MDA-MB-231 parental cell line (113). We then queried whether BAD also stimulated cell proliferation in other breast cancer cell lines, MCF-7 and SKBR-3 cells. These cell lines express relatively high levels of endogenous BAD compared with the MDA-MB-231 cell line (67), so we investigated the role of BAD in proliferation of these cell lines through depletion studies. siRNA-mediated BAD knock-down decreased cell numbers in a proliferation assay of MCF-7 and SKBR-3 cells, consistent with the notion of a pro-proliferative or anti-apoptotic role for BAD in breast cancer cell lines (67).

Given that paclitaxel leads to metaphase arrest of mitotically dividing cells, we hypothesized that BAD may contribute to taxane sensitivity through stimulation of cell proliferation, thus increasing the population of taxane-affected cells. We decided to investigate BAD-conferred sensitivity to paclitaxel in relation to its putative cell cycle effects in MCF-7 cells with two specific aims in mind:

- i) to investigate how BAD modulates the cell cycle of MCF-7 cells, and
- ii) to determine whether BAD depletion reduces MCF-7 cell apoptotic cell death in cycling vs mitotically arrested cells treated with paclitaxel.

### **3.1.4 BAD stimulates cell cycle progression in MCF-7 cells**

To address the first aim, we performed cell cycle analysis over a time course with BAD siRNA or non-specific siRNA-treated MCF-7 cells (**Figure 3.2**). Paclitaxel was used to stall cells at G2/M phase. Cells were harvested at 6, 12 and 24 hour time-points and fixed in 70% ethanol overnight. Cellular DNA was subsequently stained with propidium iodide and analyzed by flow cytometry. We observed a consistently higher proportion of BAD siRNA-treated cells in G1 phase of the cell cycle compared with N.S. siRNA-treated cells. This difference is most pronounced by 24 hours of paclitaxel treatment, where 80% of N.S. siRNA treated cells were arrested at G2/M phase compared with only 56% of BAD siRNA treated cells. This experiment was also conducted at 12, 24 and 36 hour time points and a similar pattern was observed where the BAD siRNA treated cells demonstrated an increased proportion of cells in G1 relative to the negative control cells (data not shown), indicating delayed G2/M phase progression. Overall, the data suggests an important role for BAD in mediating cell cycle progression in MCF-7 cells. Specifically, BAD may be important for mediating the G1/S phase transition of the cell cycle.

### 3.1.5 The proliferative role of BAD confers paclitaxel sensitivity

We previously determined that BAD pro-apoptotic function was not activated in response to paclitaxel treatment (**Figure 3.1**), and that BAD therefore mediates paclitaxel cytotoxicity through a novel, nonapoptotic pathway. We also determined that BAD plays a role in promoting cell cycle progression (**Figure 3.2**). We therefore hypothesized that the proliferative role of BAD, and not the apoptotic role of BAD, is responsible for conferring paclitaxel sensitivity. To investigate this idea we employed a mitotic shake-off assay to investigate the effects of BAD-depletion on the apoptotic rates of paclitaxel-treated mitotically arrested cells or cycling cells (**Figure 3.3**). We reasoned that if the apoptotic activity of BAD was uninvolved in paclitaxel cytotoxicity, mitotically arrested cells exposed to paclitaxel would exhibit similar amounts of cell death with or without BAD depletion. In the mitotic shake-off experiment, MCF-7 cells were treated with either BAD specific or non-specific siRNA then treated with paclitaxel to induce apoptosis. At 39 hours of paclitaxel treatment, cells were subjected to mitotic shake-off. Lifted mitotic cells (+shake off) were replated and paclitaxel treatment was reapplied to the remaining adherent cells (-shake off). At 48 hours of paclitaxel treatment, all cells were harvested and stained with TMRE for flow cytometry analysis. As we had previously shown (67), BAD-depleted MCF-7 cells not enriched for M-phase were significantly protected from paclitaxel induced cell death (**Figure 3.3B**, left panel –shake off, and **Figure 3.3C**). Interestingly, however, we observed that the mitotically enriched fraction displayed similar loss of  $\Delta\psi$  with or without BAD depletion (**Figure 3.3B**, right

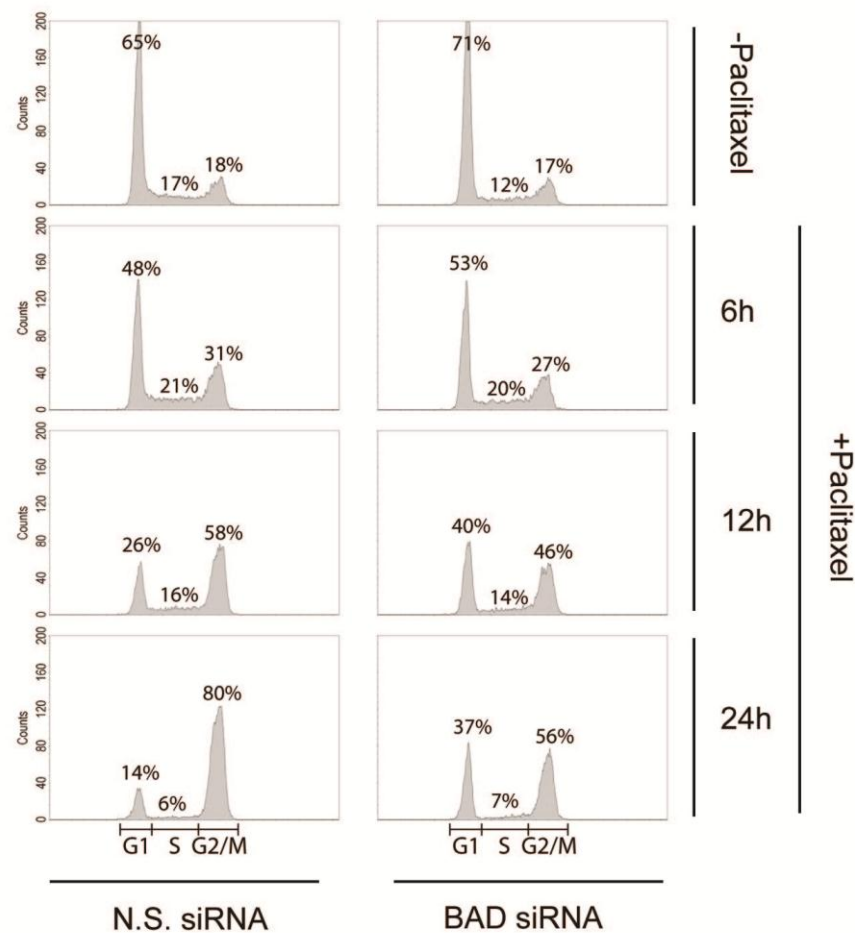


**Figure 3.2 BAD stimulates cell cycle progression.**

MCF-7 cells were treated with non-specific (N.S.) or BAD siRNA then treated with 25 nM paclitaxel (+Paclitaxel) for 6, 12 or 24 hours. Subsequently, the cells were fixed and stained with propidium iodide. DNA content was assessed by flow cytometry. Cells treated with BAD siRNA showed delayed accumulation at G2/M phase with paclitaxel treatment, compared with the N.S. siRNA. A greater proportion of BAD siRNA treated cells were present in G1, indicating a putative role for BAD in cell cycle progression, likely at the G1/S transition. Image from (67).

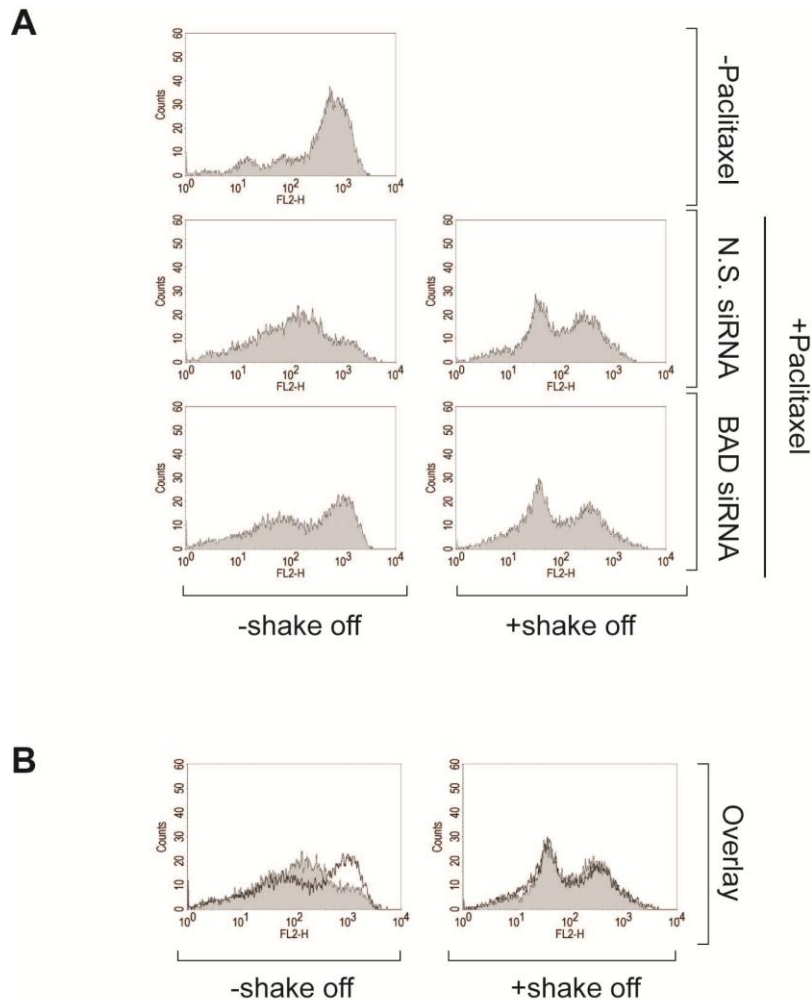


**Figure 3.3 BAD sensitizes MCF-7 cells to paclitaxel induced cell death via its proliferative role, and is not essential for death of M phase arrested cells.**

(A) MCF-7 cells were transfected with non-specific (N.S.) siRNA or BAD siRNA and treated with 25 nM paclitaxel. After 39 hours of treatment, cells were subjected to mitotic shake-off. Cells lifted during shake off (+shake off) were replated. At 48 hours of paclitaxel treatment, both + and -shakeoff cells were stained with TMRE and analyzed by flow cytometry. Representative images are shown. (B) Histogram overlay of BAD siRNA treated cells (black line) with N.S. siRNA treated cells (grey line) for results shown in (A). Image from (67).

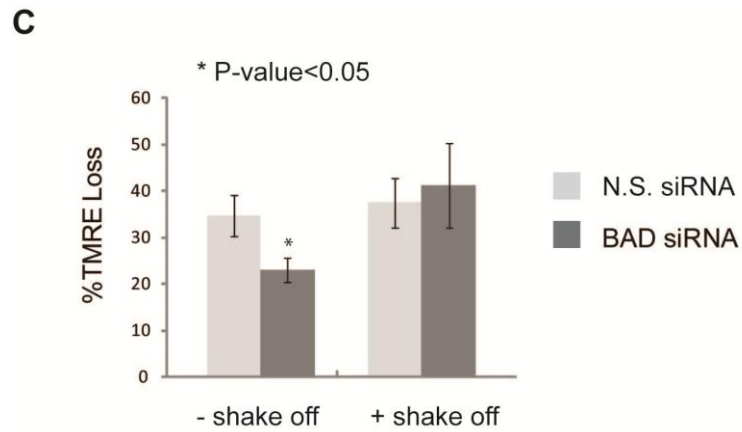


**Figure 3.3 BAD sensitizes MCF-7 cells to paclitaxel induced cell death via its proliferative role, and is not essential for death of M phase arrested cells.**

(C) Bar graph for results shown in Fig 3. (A) and (B), with n=3. Error bars represent mean +/- s.d. \* indicates P<0.05 compared with N.S. siRNA -shakeoff cells. Image from (67).

panel, +shake off, and **Figure 3.3C**). We concluded that while BAD depletion confers some protection to cycling MCF-7 cells against paclitaxel cytotoxicity, cells that have already entered mitotic arrest do not benefit from BAD depletion. This data supports our hypothesis that the BAD-proliferative role, not the BAD-apoptotic role, is important for paclitaxel induced cell death.

### **3.2 Defining BAD interacting proteins**

Studies in our laboratory determined a novel pro-proliferative role for BAD in breast cancer cell lines through BAD overexpression studies in MDA-MB-231 cells and BAD knock-down studies in MCF-7 and SKBR-3 cells. Human BAD has been previously shown to promote cellular proliferation of prostate cancer cells (123), but this pro-proliferative function for BAD has not been previously demonstrated in breast cancer cells. Furthermore, the mechanisms for BAD-mediated proliferation in human cancer cells have not been investigated.

However, murine BAD has been shown to have a pro-proliferative capacity in nontransformed fibroblasts (121) and in thymocytes (106). Both these studies implicated BAD-stimulated S phase progression from G0/G1 phase. In thymocytes, S phase progression was likely the result of enhanced IL-2 production by *BAD* transgenic thymocytes. However, in fibroblasts, BAD was found to inappropriately stimulate S phase entry in the context of anti-growth signals in a manner dependent on BCL-XL. In the context of anti-growth signals led by serum deprivation, BAD:BCL-XL heterodimerization led to bypass G0/G1 phase.

Our laboratory initially hypothesized a similar pro-proliferative mechanism for BAD in MDA-MB-231 breast cancer cells. Paradoxically, these studies found that BAD pro-growth activity actually correlated with decreased BAD:BCL-XL binding (113).

The mechanism of BAD-mediated proliferation in breast cancer cells remains enigmatic. Given the clinical relevance of BAD in taxane-treated breast cancer and our elucidation of a novel pro-growth BAD pathway, we wanted to define precisely the mechanisms of the pro-survival, BAD proliferative pathway in the MDA-MB-231 cells. We hypothesized that BAD mediates its pro-growth activity through a novel pathway that requires protein-protein interaction with novel protein binding partners. To more fully define the molecular dynamics of BAD activity in MDA-MB-231 cells, we undertook protein interaction studies with three prominent aims:

- i) to investigate a putative interaction of BAD with hexokinase isoforms I and II
- ii) to perform unbiased screens to identify any novel BAD-interacting proteins, and
- iii) to characterize BAD interactions with known binding partners, BCL-XL and 14-3-3 protein isoforms.

### **3.2.1 BAD:Hexokinase putative interaction study**

BAD was reported to associate with Glucokinase (also known as hexokinase IV) in a mitochondrial complex that includes PP1c, PKAc, WAVE-1

and AKAP-1 in mouse hepatocytes (180) and pancreatic beta cells (181). In both cell types, the mitochondrial BAD-nucleated complex was essential for stimulation of glucokinase activity and mitochondrial-driven respiration and for glucose homeostasis. Much of the initial characterization of the BAD/GK core complex through techniques such as 3-dimensional native complex isolation, BAD and GK coimmunoprecipitations and microcystin sepharose affinity pull-downs did not demonstrate a direct interaction between the two proteins. However, in 2008 Danial et al used a BAD SAHB phospho-serine peptide containing a photoactivatable benzophenone moiety to covalently capture BAD SAHB peptide targets upon UV light exposure (181). The BAD SAHB peptide captured glucokinase in vitro, indicating a likely direct physiological interaction between BAD and glucokinase in vivo.

Published work presents evidence of a BAD metabolic role in specific cell types (180,181). Glucokinase expression, however, is restricted to hepatocytes, pancreatic beta cells, and hypothalamic neurons (104). It is unknown whether BAD maintains a metabolic role in other cell types where glucokinase expression is lacking, and other hexokinase isoforms are expressed.

We hypothesized that the enhancement of proliferation in BAD-overexpressing MDA-MB-231 cells was the result of a BAD-stimulated metabolic pathway that required BAD interaction with hexokinase isoforms expressed in breast cancer cells. Hexokinase I and II have been reportedly upregulated in human breast cancers (235), with one report also documenting upregulation of hexokinase III activity (218). Hexokinase I is a ubiquitously

expressed isoform in human tissues (198), while most tissues express low levels of hexokinase II (196). During cancer progression, there is an upregulation of mitochondrial bound hexokinase activity (189,236,237) that contributes to the Warburg effect. In human cancers this Warburg activity has been attributed to upregulated mitochondrial-bound hexokinase II, consistent with earlier studies widely reporting hexokinase II upregulation in human cancers (193,235,238). Given the prevalence of hexokinase I and II activity in human cancers, we decided to test whether BAD could interact with either of these hexokinase isoforms.

First, we tested for a putative BAD:Hexokinase I/II interaction by BAD coimmunoprecipitation experiments in MDA-MB-231 cells and 231.BAD cells. Since the 231.BAD cells reach higher cell numbers in a proliferation assay than the parental MDA-MB-231 cell line (113), we postulated that the 231.BAD cells would therefore have a higher level of BAD stimulated metabolism than MDA-MB-231 cells. However, BAD coimmunoprecipitation analysis from confluent cells did not reveal any detectable interaction of BAD with hexokinase I or hexokinase II (**Figure 3.4**).

We also performed coimmunoprecipitation experiments on Myc-BAD and HKI-V5 cotransfected HEK293T/17 cells (**Figure 3.5**) or Myc-BAD and HKII-V5 cotransfected cells (**Figure 3.6**) to determine whether an interaction could be revealed with robust protein expression levels. Coimmunoprecipitation analysis and western blotting revealed that the Myc IP in either case did not coimmunoprecipitate with the V5 epitope. Similarly, the V5 IP did not

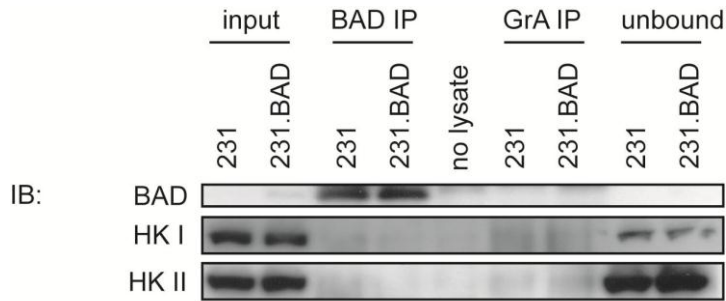


**Figure 3.4 BAD does not detectably coimmunoprecipitate with HK I or HK II.**

MDA-MB-231 cells or 231.BAD cells were harvested in 1% CHAPS lysis buffer and immunoprecipitated with anti-BAD antibody (BAD IP) or negative control Granzyme A antibody (GrA IP). Western blot analysis shows 6% IP input and equivalent amounts of unbound fraction.

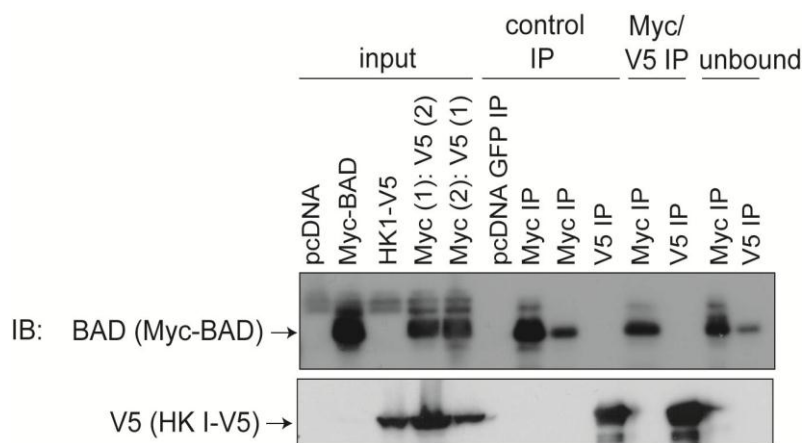


**Figure 3.5 Myc-BAD does not detectably coimmunoprecipitate with HK I-V5.**

HEK293T/17 cells were cotransfected with Myc-BAD/pcDNA3.2 V5-DEST and Hexokinase I-V5/pcDNA3.2 V5-DEST plasmid constructs at 1:2 molar ratios. Cells were lysed in 1% CHAPS lysis buffer 24 hours posttransfection. Immunoprecipitations were performed with either anti-Myc or anti-V5 antibody cross-linked beads for the construct transfected in lowest molar amount.

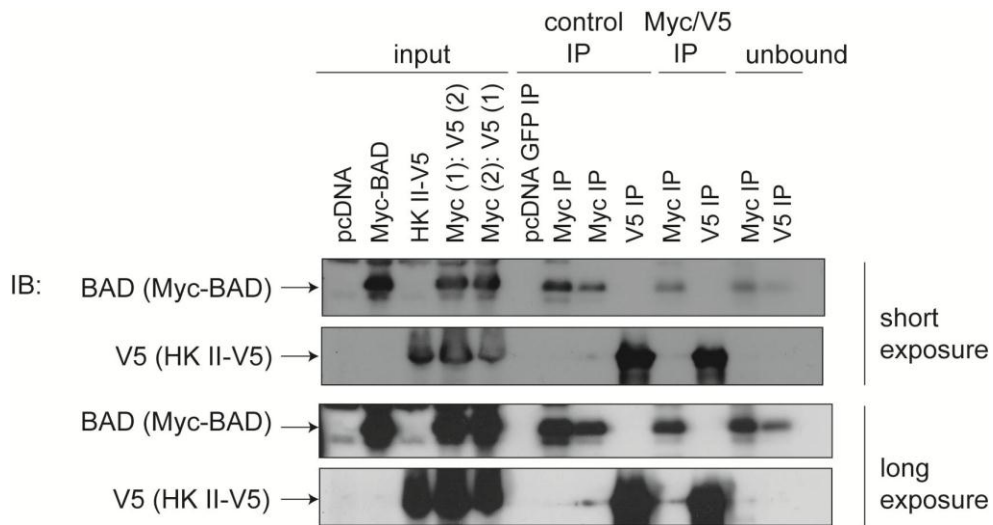


**Figure 3.6 Myc-BAD does not detectably coimmunoprecipitate with HK II-V5.**

HEK293T/17 cells were cotransfected with Myc-BAD/pcDNA3.2 V5-DEST and Hexokinase II-V5/pcDNA3.2 V5-DEST plasmid constructs at 1:2 molar ratios. Cells were lysed in 1% CHAPS lysis buffer 24 hours post-transfection. Immunoprecipitations were performed with either anti-Myc or anti-V5 antibody cross-linked beads for the epitope-tagged construct transfected in lowest molar amounts.

coimmunoprecipitate with the Myc epitope. Thus, no interaction between hexokinases I or II and BAD was detectable with this method.

In their characterization of the specificity of the BAD:glucokinase interaction, Danial et al were able to reconstitute the interaction in vitro (181). BAD and glucokinase proteins were synthesized using an in vitro transcription-translation (IVTT) system, and glucokinase antibody was used to coimmunoprecipitate BAD from the mixture. We hypothesized that the BAD:Hexokinase interaction was analogous to the BAD:Glucokinase interaction. We therefore decided to use an in vitro system similar to that employed by Danial et al. to alternatively assess the purported interaction where high levels of protein expression could be achieved. Equal quantities of each IVTT reaction (BAD, Hexokinase I-V5 or Hexokinase II-V5) were mixed and incubated for one hour prior to coimmunoprecipitation with either anti-BAD antibody or anti-V5 antibody. There was no detectable interaction between BAD and HK I-V5 (**Figure 3.7 A**) or BAD and HK II-V5 (**Figure 3.7 B**) with this method.

Studies by Danial et al further defined a direct interaction between phosphorylated BAD BH3 peptide and gluokinase in vitro (181). Crosslinking to glucokinase was performed using a UV-photoactivatable benzophenone moiety incorporated in a synthetic BAD BH3 peptide with a 3.1 Å reactive radius. We tested whether a short bifunctional crosslinking reagent, formaldehyde, would enable detection of a BAD:Hexokinase interaction. Formaldehyde is reactive towards primary amino groups spanning distances of 2.3-2.7 Å (239), and therefore closely mimics the reactive length of the intrinsic benzophenone

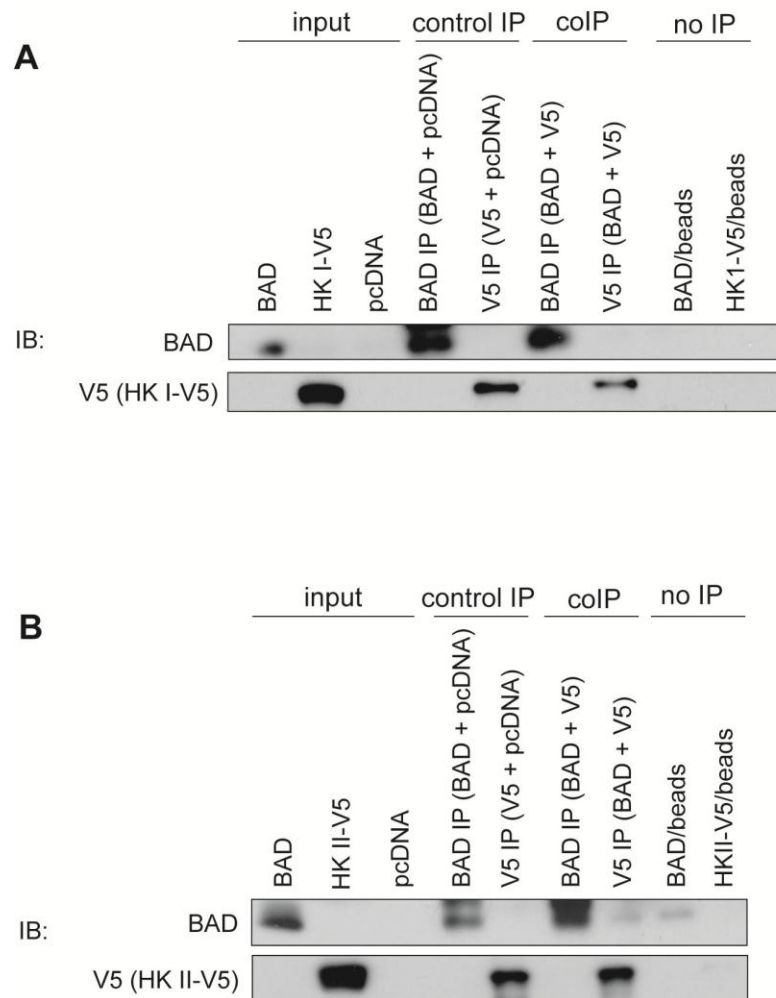


**Figure 3.7 BAD does not detectably coimmunoprecipitate with HK I-V5 or HK II-V5 in vitro.**

BAD, Hexokinase I-V5, Hexokinase II-V5 and pcDNA3.2 V5-DEST (empty vector) were transcribed and translated in vitro using the TNT<sup>®</sup> T7 Coupled Reticulocyte Lysate System (Promega). 10 uL of each IVTT reaction were coincubated with 50 uL of detergent-free IVTT buffer for 1 hour at room temperature. Control immunoprecipitations were performed by coincubating BAD or hexokinase I or II with pcDNA<sup>™</sup> empty vector. Coimmunoprecipitations (coIP) were performed with anti-BAD or anti-V5 antibody.

crosslinker used by Danial et al. We performed IVTT protein synthesis as previously indicated, and incubated BAD IVTT protein with either Hexokinase I-V5 or Hexokinase II-V5 IVTT synthesized protein. After incubation, crosslinking was performed with 1% formaldehyde and quenched with 0.25 M glycine. The effectiveness of formaldehyde crosslinking was assessed with anti-BAD western blotting (**Figure 3.8 B**). Higher molecular weight BAD species were revealed in formaldehyde cross-linked samples (-boil), that collapsed to a single band with cross-link reversal by boiling (+boil). Cross-linking of BAD alone in the absence of HK was not performed (**Figure 3.8 B**). Western blotting indicated that BAD did not detectably coimmunoprecipitate with either HK I-V5 or HK II-V5 (**Figure 3.8 A**) under these conditions. We did observe a background level of BAD immunoreactive bands by western blot in antibody-free (no IP) control lanes and in negative control (GrA IP) lanes, indicating an affinity of the protein A sepharose beads for BAD. However, BAD immunoprecipitated protein (BAD IP) lanes were clearly above these background levels (**Figure 3.8 A**). There was no coimmunoprecipitation of HK I above background levels in the GrA IP lane, and no observed coimmunoprecipitation with HK II. This experiment demonstrated that an interaction between BAD and Hexokinases isoforms I or II could not be captured in vitro despite the use of an effective concentration of cross-linker. There are two repetitions of this experiment.

Similarly, 1% formaldehyde cross-linking was employed on 231.BAD cells and 231.BAD S118D cells harvested for coimmunoprecipitation (**Figure 3.9**). Cross-linking was again observed by anti-BAD western blot as higher

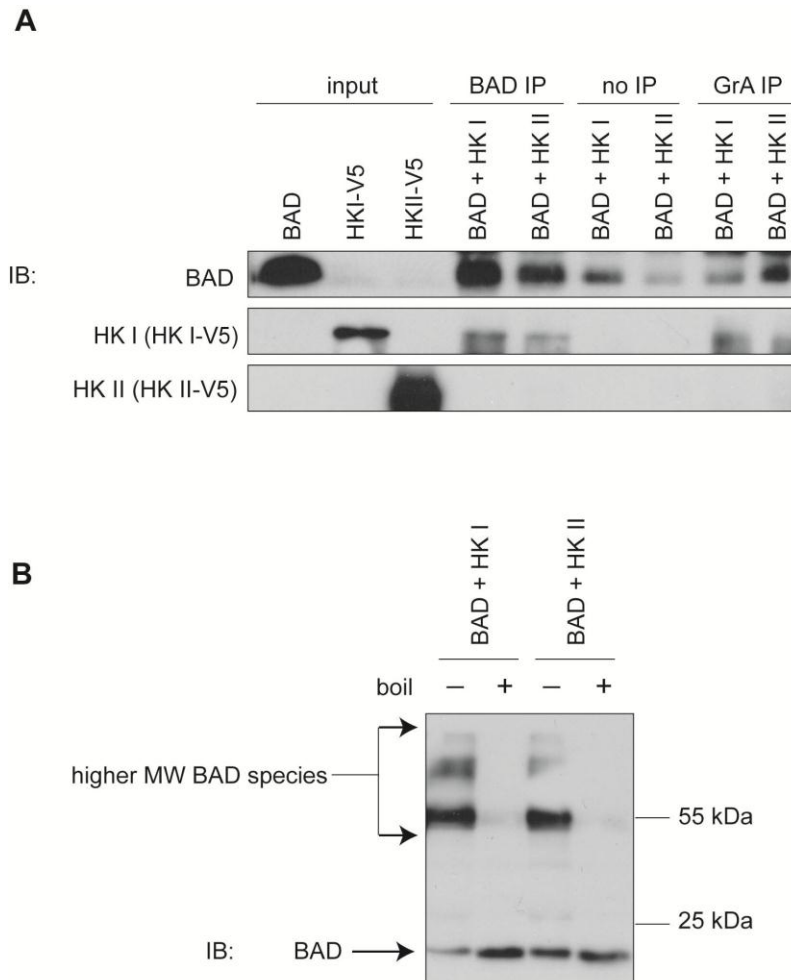


**Figure 3.8 Formaldehyde cross-linking does not reveal an interaction between BAD and HK I-V5 or HK II-V5 in vitro.**

(A) BAD, Hexokinase I-V5, Hexokinase II-V5 and pcDNA3.2 V5-DEST (empty vector) were transcribed and translated in vitro using the TNT<sup>®</sup> T7 Coupled Reticulocyte Lysate System (Promega). 10 uL of each IVTT reaction were coincubated with 50 uL of detergent-free IVTT buffer for 1 hour at room temperature. Samples were cross-linked with 1% formaldehyde for 10 minutes at room temperature. Coimmunoprecipitations were then performed with anti-BAD antibody and all samples were boiled to reverse cross-links prior to SDS-PAGE. (B) Demonstration of formaldehyde cross-linking. Anti-BAD western blot reveals higher order BAD complexes formed by cross-linking that are effectively reversed by boiling for 20 minutes.

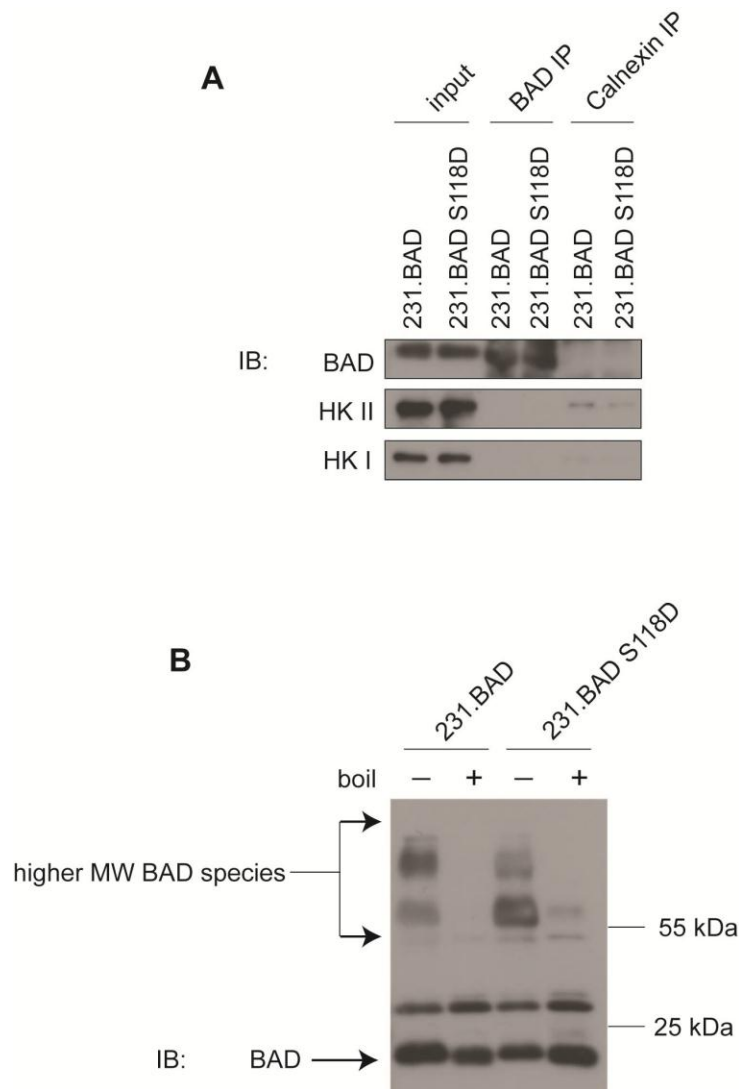


**Figure 3.9 Formaldehyde cross-linking does not reveal an interaction between BAD and HK I-V5 or HK II-V5 in cells.**

(A) 231.BAD and 231.BAD S118D cells were cross-linked with 1% formaldehyde for 10 minutes. Cells were subsequently lysed in 1% CHAPS lysis buffer and coimmunoprecipitated with anti-BAD antibody (BAD IP). Calnexin antibody was used as a negative control (Calnexin IP). Western blotting was performed with anti-BAD, anti-HK I and anti-HK II antibodies. 10% input was loaded. (B) Formaldehyde cross-links were reversed by boiling in laemmli buffer for 20 minutes. Anti-BAD western blot reveals higher order BAD complexes formed by cross-linking that are eliminated by boiling.

molecular weight BAD species (-boil) that largely collapsed with cross-link reversal by boiling (**Figure 3.9 B**). BAD coimmunoprecipitation did not reveal an interaction with endogenous HK I or HK II in cells (**Figure 3.9 A**). Altogether, these results do not demonstrate a positive interaction between BAD and Hexokinases I and II isoforms with these methods.

### **3.2.2 GST-BAD pull-down assay as a screen for BAD- interacting proteins**

Our results demonstrate that the hypothesized BAD:Hexokinase interaction was not detectable using coimmunoprecipitation methods. On the basis of our original hypothesis, that BAD directs a pro-survival pathway by binding novel protein partners, we decided to pursue unbiased protein interaction screens to define the BAD binding partners in MDA-MB-231 cells. First, MDA-MB-231 cell lines stably expressing GST-BAD (231.GST-BAD) or GST control (231.GST) were generated (**Figure 3.10 A**). Preliminary GST pull-down assays revealed effective elution of GST from 231.GST cells and GST-BAD from 231.GST-BAD cells (**Figure 3.10 B**). Furthermore, GST-BAD co-eluted with a known interacting protein, BCL-XL (**Figure 3.10 B**). Since this approach could be used to detect known BAD binding partners like BCL-XL, we decided it would be appropriate to pursue GST-BAD pull-down assays as an unbiased screening method for interacting proteins.

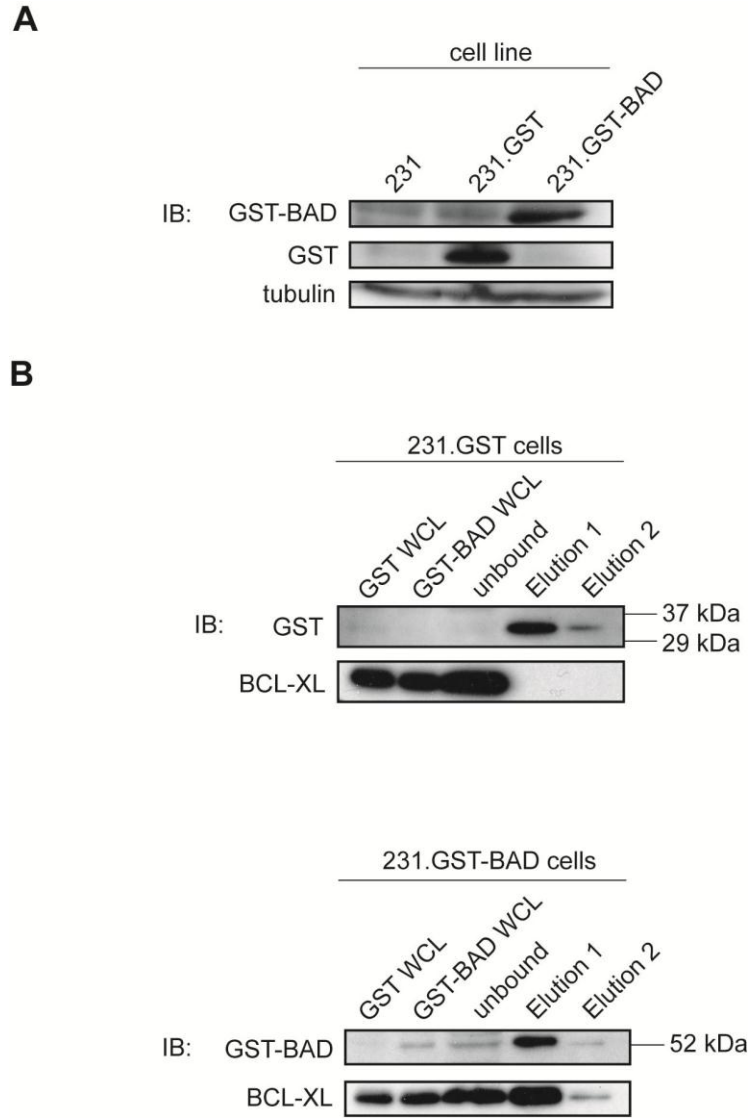


**Figure 3.10 Validating GST-BAD pull-down assay in MDA-MB-231 cells.** (A) Western blot panel showing the expression levels of GST- and GST-BAD in stably expressing MDA-MB-231 cell lines. (B) Small-scale GST-BAD pull-down assays. Approximately  $10 \times 10^6$  cells from stable cell lines were harvested for glutathione sepharose pull-down. Beads were eluted twice with glutathione buffer (Elution 1 & 2). Western blots indicate elution of GST-BAD and known BAD interacting partner BCL-XL (lower panel).

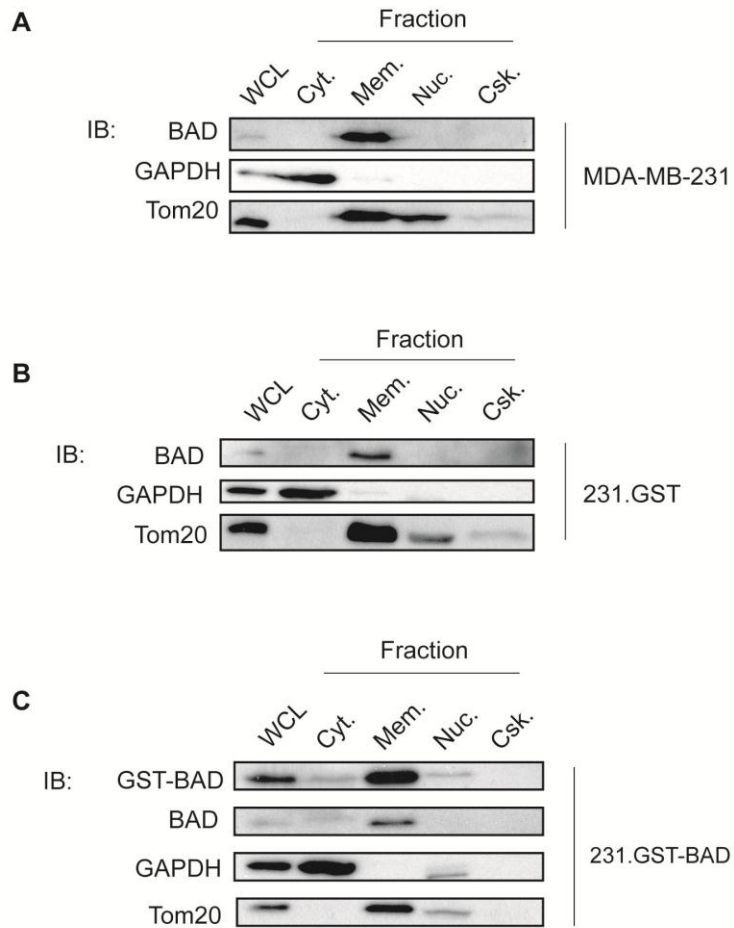
### **3.2.3 GST-BAD localizes to membrane subfractions with endogenous BAD**

Before using GST-BAD pull-downs as a screen, we wanted to determine whether GST-tagged BAD has similar properties to endogenous BAD in terms of its subcellular localization. Subcellular fractionation revealed membrane localization for endogenous BAD in MDA-MB-231 cells (**Figure 3.11 A**), 231.GST cells (**Figure 3.11 B**) and 231.GST-BAD cells (**Figure 3.11 C**). GST-BAD also localized to the membrane fraction (**Figure 3.11 C**), which includes the mitochondrial membrane as indicated by the mitochondrial marker Tom20. The similar localization of GST-tagged BAD with endogenous BAD supports the use of GST-BAD as bait for physiologically relevant interacting proteins.

### **3.2.4 The GST-BAD interactome in MDA-MB-231 cells**

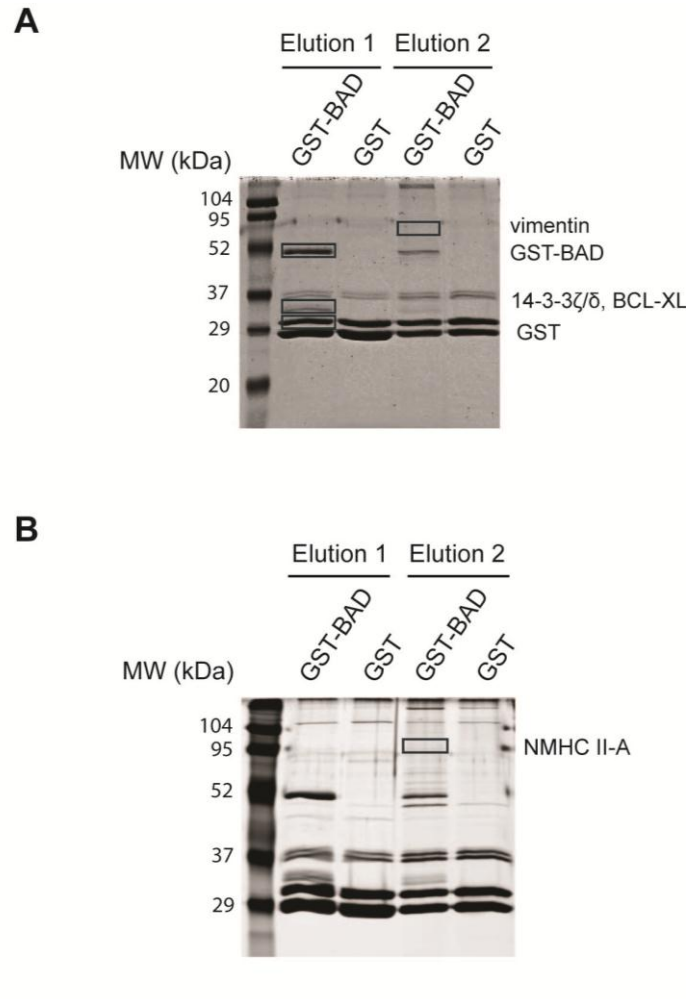
A large-scale GST pull-down assay from 231.GST cells and 231.GST-BAD cells was performed to screen for interacting proteins. SDS-PAGE gels were stained with colloidal coomassie stain (**Figure 3.12 A**) or silver stain (**Figure 3.12 B**) and visible protein bands were excised for protein identification by mass spectrometry. Proteins identified in the GST-BAD eluate included: glutathione S-transferase, BAD, vimentin, BCL-X short, 14-3-3  $\zeta/\delta$  and non-muscle myosin heavy chain 9 (**Figure 3.12 C**).

BCL-XS and BCL-XL are alternatively spliced forms of the BCL-X gene (240) and are translated to protein products of 178 amino acids and 241 amino acids respectively. The peptides identified by mass spectrometry localized to the N-terminus common to the primary sequence of both isoforms. However, on the



**Figure 3.11 GST-BAD and endogenous BAD both localize to membrane fractions.**

MDA-MB-231 cells, 231.GST and 231.GST-BAD cells were fractionated using the Qproteome<sup>®</sup> Cell Compartment Kit (Qiagen). Equal fraction proportions were analyzed by western blot for the presence of BAD, GST-BAD, cytosolic marker GAPDH and mitochondrial membrane marker Tom20.

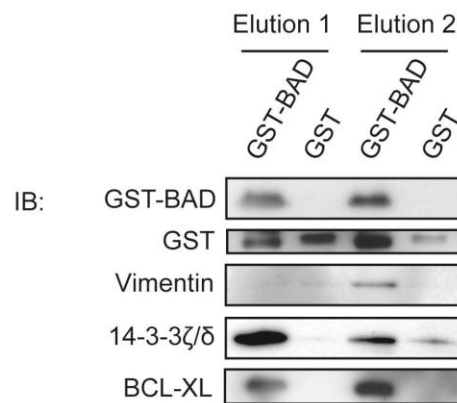


**Figure 3.12 GST-BAD pull-down assay to isolate interacting proteins in MDA-MB-231 cells.**

Eluate from a  $1.6 \times 10^9$  cell pull-down from 231.GST and 231.GST-BAD cells was run on SDS-PAGE. The gel was stained with colloidal coomassie G-250 (**A**) or silver stained (**B**) to visualize protein. Indicated protein bands were excised from the gel and identified by LC-MS/MS.

**C**

Protein identified	Mr (kDa)	# peptides	% sequence coverage
Glutathione S-transferase mu 3	27	13	51
bcl2 antagonist of cell death	18.4	6	40
vimentin	53.7	8	22
bcl-x short	18.9	2	14
cellular myosin heavy chain	155.3	6	6
14-3-3 protein zeta/delta	28	2	8

**D**

**Figure 3.12 GST-BAD pull down assay to isolate interacting proteins in MDA-MB-231 cells.**

(C) Proteins excised in (A) and (B) identified by mass spectrometry using the Mascot search engine (Matrix Science). Number of peptides and % sequence coverage are indicated. (D) Western blot analysis validates the presence of identified proteins in pull-downs, including vimentin, 14-3-3 $\zeta/\delta$  and BCL-XL.

basis of molecular weight, we reasoned that the BCL-XL was actually detected in the GST-BAD pull-down. We further verified the presence of vimentin, 14-3-3 $\zeta/\delta$  and BCL-XL in the GST-BAD pull-down by western blot (**Figure 3.12 D**).

Given the interaction of these proteins with GST-tagged BAD, we wanted to verify whether these protein interactions could also be detected with untagged BAD. BAD coimmunoprecipitation analysis from MDA-MB-231 cells and 231.BAD cells revealed an interaction with BCL-XL (**Figure 3.13 A**) and 14-3-3 $\zeta$  (**Figure 3.13 B**). BAD coimmunoprecipitation from 231.BAD cells did not reveal an interaction with MYH9 (**Figure 3.13 C**). Vimentin interaction was not detected in 1% CHAPS buffer, but a suspected vimentin band was detected in BAD coimmunoprecipitation from 231.BAD cells in 1% NP-40 buffer (**Figure 3.13 D**). This result was observed three times. It was later found that the vimentin band was not consistent in further coimmunoprecipitations, particularly when antibody-crosslinked beads were used (**Figure 3.20**). Given that vimentin appeared to be the only novel interacting partner for BAD identified in this screen, we decided to further investigate a putative BAD:vimentin interaction.

### **3.2.5 Pursuing vimentin as a putative BAD interacting partner**

We decided to further assess a putative BAD:vimentin interaction through: i) characterizing protein (co)localization through subcellular fractionation and immunofluorescence techniques and ii) coimmunoprecipitation studies. Towards the first aim, we began by exploring vimentin expression levels in breast cancer cell lines by western blotting (**Figure 3.14**). We found that vimentin was

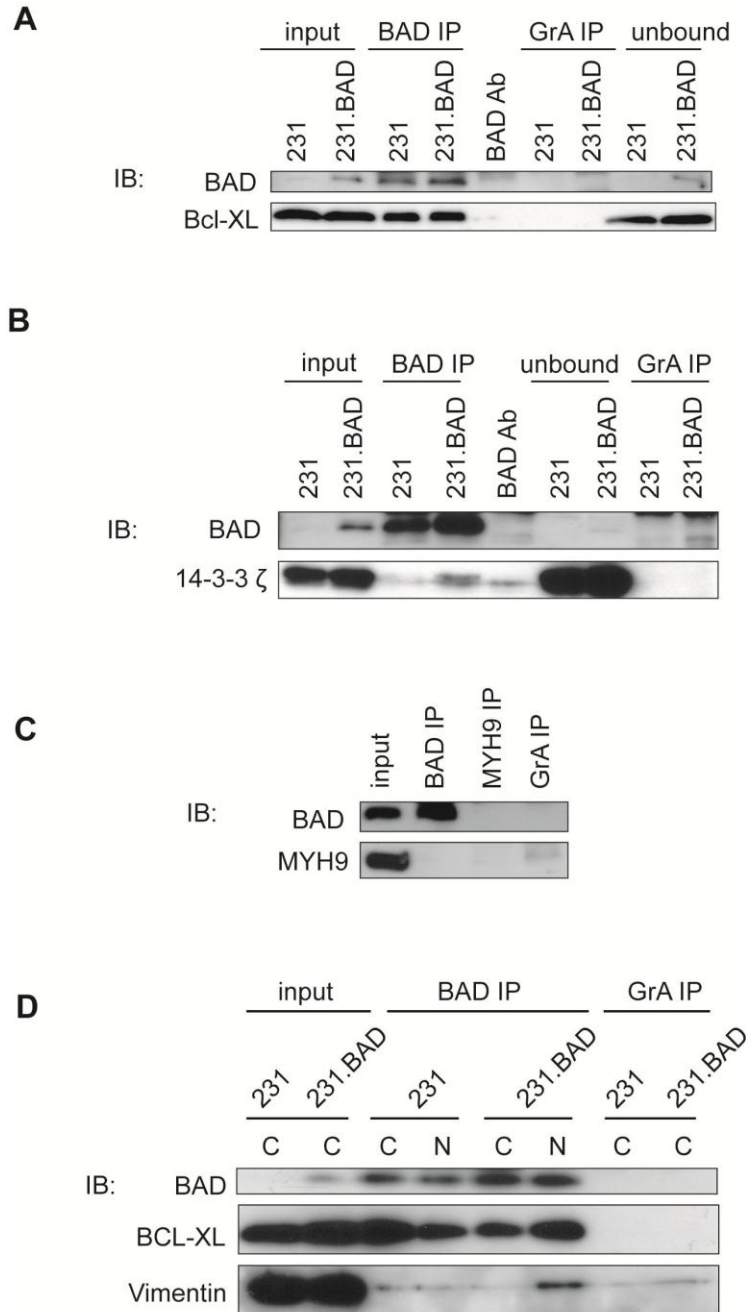


**Figure 3.13 BAD interacting targets verified by coimmunoprecipitation in MDA-MB-231 cells and 231.BAD cells.** Cells were harvested in 1% NP-40 buffer and BAD coimmunoprecipitations were performed. Western blots detected coimmunoprecipitation of BCL-XL (A) and 14-3-3 $\zeta$  (B), but not MYH9 (C). For vimentin detection cells were harvested in 1% CHAPS (C) or 1% NP-40 (N) buffer (D).

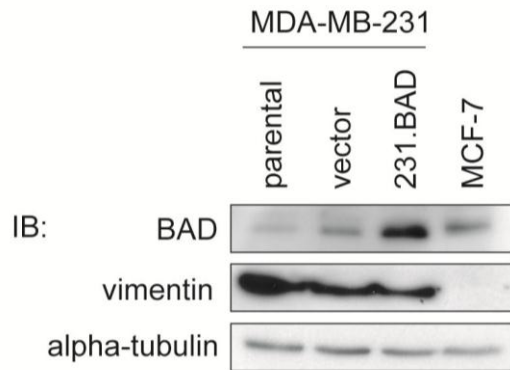


**Figure 3.14 Vimentin expression in breast cancer cell lines.**  
MDA-MB-231 and MCF-7 cell lysate was analyzed by western blot for vimentin expression.

expressed in the MDA-MB-231 cells, and not in the MCF-7 cells, in accordance with previous reports (241). Subcellular fractionation of MDA-MB-231 cells (**Figure 3.15 A**) and 231.BAD (**Figure 3.15 B**) cells demonstrated predominant localization of BAD to the membrane fraction in these cells. Vimentin was predominantly localized to the cytoskeletal fraction, with only a small proportion of total vimentin localizing to the membrane fraction (**Figure 3.15**). Given that at least a low proportion of vimentin is found in the membrane fraction with BAD, an interaction between these proteins may be permissible.

Next, we verified the protein localization results with immunofluorescence. In MDA-MB-231 cells and 231.BAD cells, BAD staining largely colocalized with cytochrome c staining (**Figure 3.16 A**), indicating a mitochondrial localization for BAD. There was no clear colocalization, however, between the filamentous vimentin staining and mitochondrial BAD staining in MDA-MB-231 cells (**Figure 3.16 B**). Taken together, these experiments attribute major subcellular localization of BAD and vimentin to different subcellular compartments: to mitochondria and cytoskeletal fractions respectively.

Towards the second aim, we wanted to assess whether vimentin was a bona fide BAD interacting partner. We pursued BAD:vimentin coimmunoprecipitation experiments using an alternative in vitro approach. IVTT synthesized BAD and vimentin proteins were mixed and coimmunoprecipitated with anti-BAD antibody. Western blot analysis demonstrated that BAD did not visibly coimmunoprecipitate with vimentin (**Figure 3.17**).

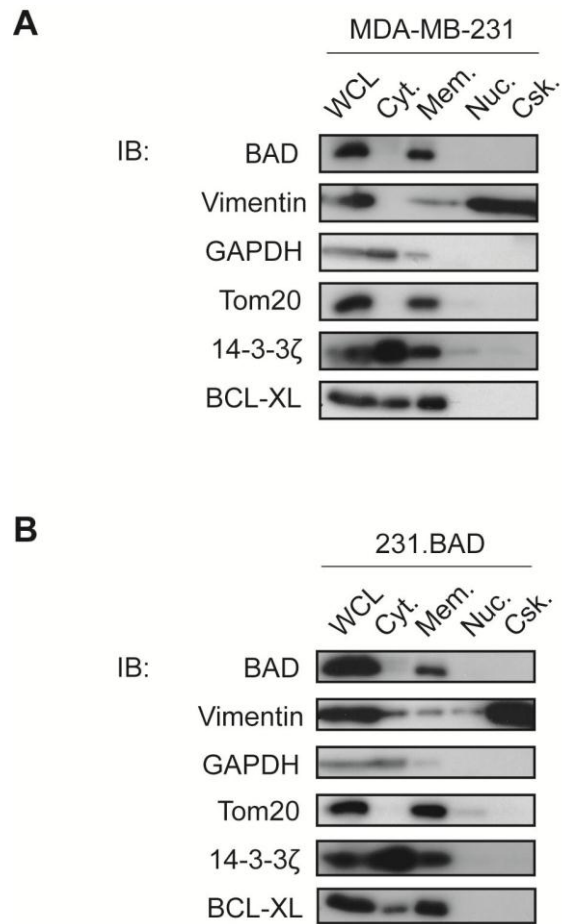


**Figure 3.15 BAD localizes to membrane fractions and may be the site of interaction with multiple proteins.**

MDA-MB-231 cells (**A**) and 231.BAD cells (**B**) were fractionated using the Qproteome<sup>®</sup> Cell Compartment kit (Qiagen) into cytosolic (Cyt.), membrane (Mem.), nuclear (Nuc.) and cytoskeletal (Csk.) fractions. Western blots were probed for cytosolic marker GAPDH and mitochondrial marker Tom20. Distributions of 14-3-3ζ, BCL-XL and vimentin are indicated.

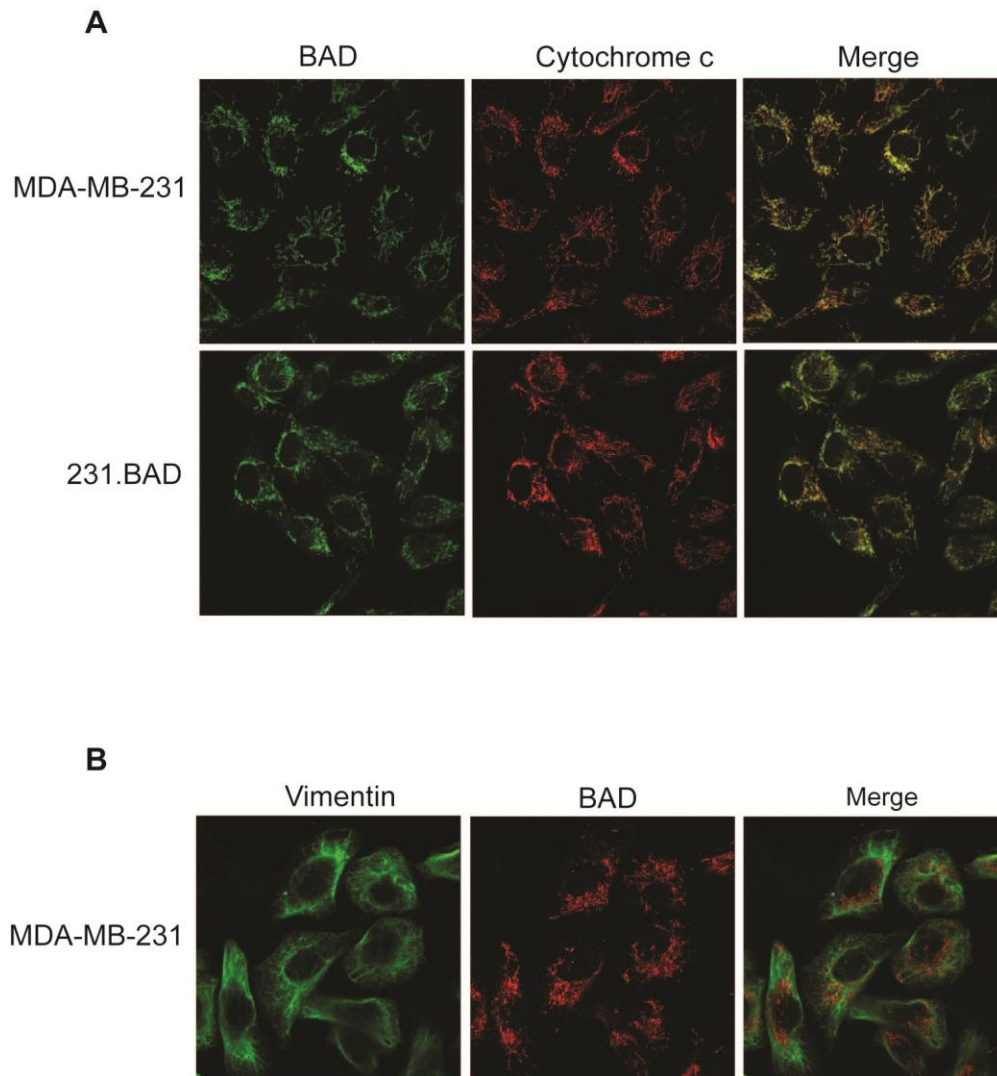


**Figure 3.16 BAD localizes to mitochondria in MDA-MB-231 cells.** (A) Immunofluorescence images of MDA-MB-231 cells and 231.BAD cells probed for BAD and cytochrome c. Merge indicates colocalization. (B) Immunofluorescence images for vimentin and BAD detection in MDA-MB-231 cells showed no significant colocalization of these proteins.

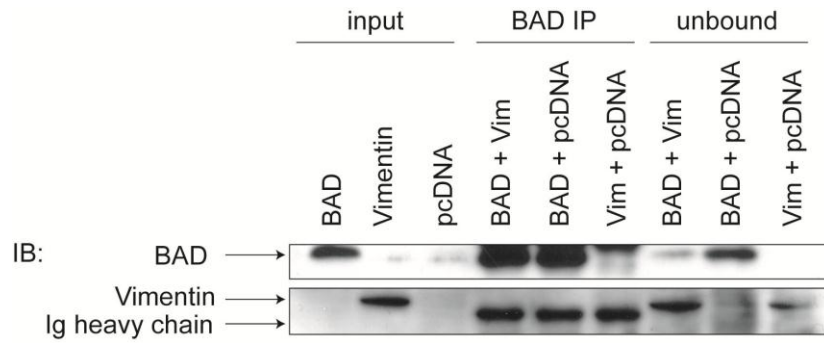


**Figure 3.17 BAD and vimentin do not interact in vitro.**

BAD, vimentin and pcDNA3.2 V5-DEST (empty vector) plasmids were transcribed and translated in vitro using the TNT<sup>®</sup> T7 Coupled Reticulocyte Lysate System (Promega). 10 uL of each IVTT reaction were incubated in 50 uL of 0.2% NP-40 IVTT buffer. Coimmunoprecipitations were performed with anti-BAD antibody (BAD IP). Western blot analysis indicates the detection of vimentin as a higher band than IgG antibody heavy chain.

### 3.2.6 Determination of vimentin solubility in the presence or absence of NaCl

Vimentin is a type III intermediate filament protein which exists in cells as a filamentous polymer in continuous exchange with a small pool of soluble tetrameric subunits (230,242,243). In vitro experiments have demonstrated assembly of vimentin monomers to stable tetrameric subunits at low ionic strength (50 mM salt) which polymerize into filaments at high ionic strength (150 mM salt) (244,245). Previous reports have employed the addition of 150 mM NaCl to vimentin preparations in non-ionic detergents to induce polymerization, or have eliminated NaCl to increase vimentin solubility (246). Given that the 1% NP-40 lysis buffer used in the initial BAD:vimentin coimmunoprecipitation (**Figure 3.13 D**) contained 150 mM NaCl, we decided to determine whether salt depletion would enable increased solubility of vimentin in the lysis buffer, and therefore increase the propensity for BAD:vimentin detection.

MDA-MB-231 cells were harvested and lysed in the presence of 150 mM NaCl (+salt) and 0 mM NaCl (-salt). Fractionation was performed by centrifuging lysate at 500xg, 10,000xg and 16,000xg. Western blot analysis of the 16,000xg fractions revealed that in the presence of salt, vimentin segregated predominantly to the insoluble pellet fraction (16,000xg pellet) with only a low level detectable in the soluble fraction (16,000xg sup) (**Figure 3.18**). However, in the absence of salt, vimentin segregated predominantly to the soluble fraction (16,000xg sup) compared to the insoluble fraction (16,000xg pellet). These results indicate that omitting salt from the lysis buffer increases the soluble pool of vimentin that could subsequently be used for coimmunoprecipitation.

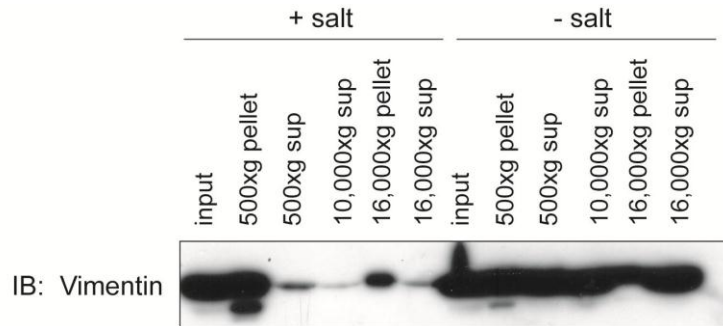


**Figure 3.18 Salt depletion increases solubility of vimentin in lysis buffer.** MDA-MB-231 cells were lysed in 1% NP-40 buffer containing 150 mM NaCl (+salt) or without salt (-salt). The lysate was centrifuged at 500xg, 10,000xg and 16,000xg for 5 minutes. Equal proportions of each fraction were loaded for SDS-PAGE. Western blots were probed with vimentin. Vimentin solubility in the 10,000xg and 16,000xg supernatant is increased in -salt compared to +salt conditions.

### 3.2.7 BAD:vimentin coimmunoprecipitations in the absence of NaCl

We decided to test whether omission of NaCl in the lysis buffer would result in BAD:vimentin coimmunoprecipitation by increasing the soluble pool of vimentin. Epitope-tagged constructs Myc-BAD and Vimentin-V5 were cloned for this purpose. First, we verified whether Myc-BAD would mimic the subcellular localization of endogenous BAD. MDA-MB-231 cells were transfected with Myc-BAD plasmids and stained with MitoTracker<sup>®</sup> Red. Anti-Myc immunofluorescence subsequently revealed colocalization of transfected Myc-BAD with MitoTracker staining, indicating a mitochondrial localization for Myc-BAD (**Figure 3.19 A**). This mimics the mitochondrial localization of endogenous BAD in MDA-MB-231 cells (**Figure 3.16 A**). Next, MDA-MB-231 cells were cotransfected with Myc-BAD and Vimentin-V5 using 1:3 molar ratios. Coimmunoprecipitations were performed for the epitope tagged construct transfected in the lowest molar amount in 1% NP-40 in the absence of NaCl. Western blots revealed that Myc-BAD did not coimmunoprecipitate with Vimentin-V5; similarly, Vimentin-V5 did not coimmunoprecipitate with Myc-BAD (**Figure 3.19 B**).

Coimmunoprecipitations for endogenous BAD and vimentin were repeated in +salt and –salt conditions in MDA-MB-231 cells (**Figure 3.20**). The yield of immunoprecipitated vimentin (Vim IP) was greatly enhanced in –salt compared to +salt conditions, however there was no coimmunoprecipitation with BAD in either case. Similarly, BAD coimmunoprecipitation in +salt and –salt conditions did not reveal any interaction with vimentin. However, BAD:BCL-XL

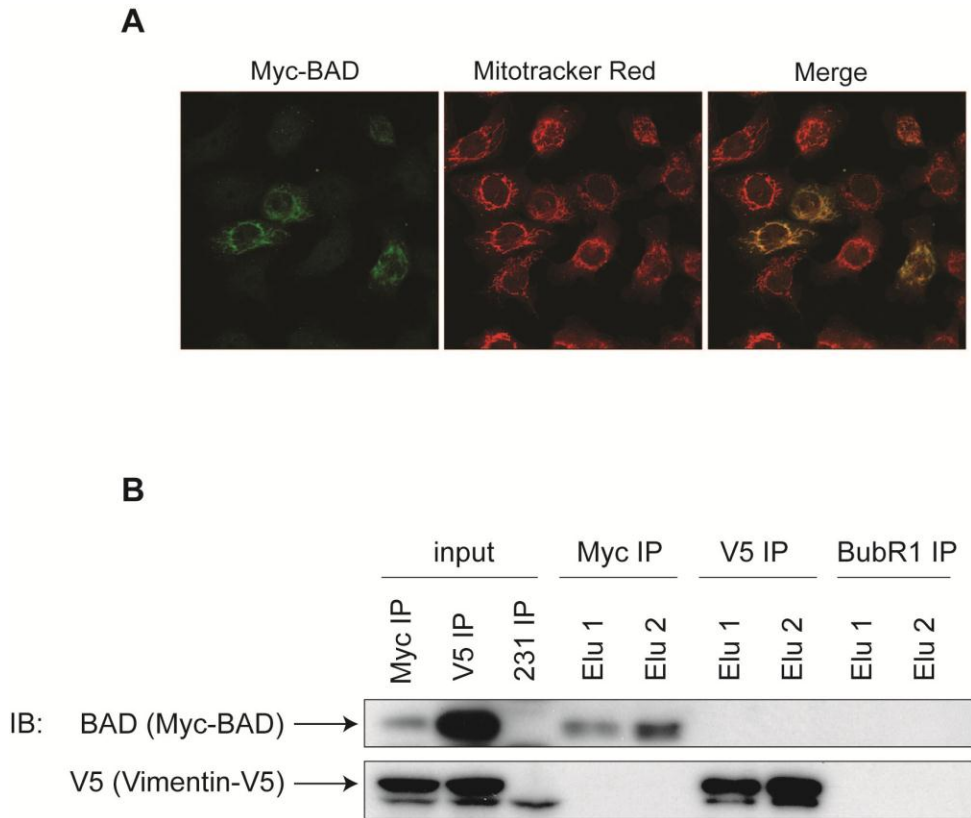


**Figure 3.19 Myc-BAD does not coimmunoprecipitate detectably with Vimentin-V5 in cotransfected cells.**

(A) Myc-BAD localizes to mitochondria. MDA-MB-231 cells were transfected with Myc-BAD/pcDNA3.2 V5-DEST plasmid. 24 hours post-transfection, cells were stained with MitoTracker<sup>®</sup> Red CMXRos. Cells were then fixed, permeabilized and stained with anti-Myc antibody. Merge indicates mitochondrial localization of Myc-BAD. (B) Myc-BAD and Vimentin-V5 were cotransfected in MDA-MB-231 cells at a 1:3 molar ratios. Cells were harvested 24 hours post-transfection and immunoprecipitated with anti-Myc antibody or anti-V5 antibody. Immunoprecipitated proteins were eluted twice (Elu1, Elu2) with 0.1 M glycine pH 2.5. Anti-BubR1 immunoprecipitation was included as a negative control IP.

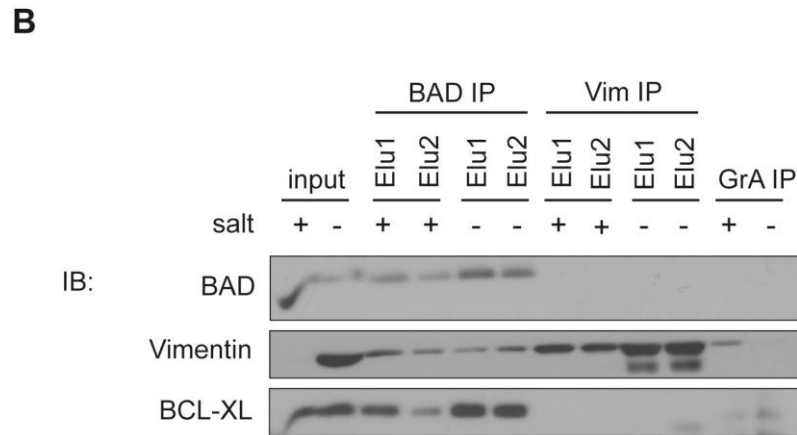
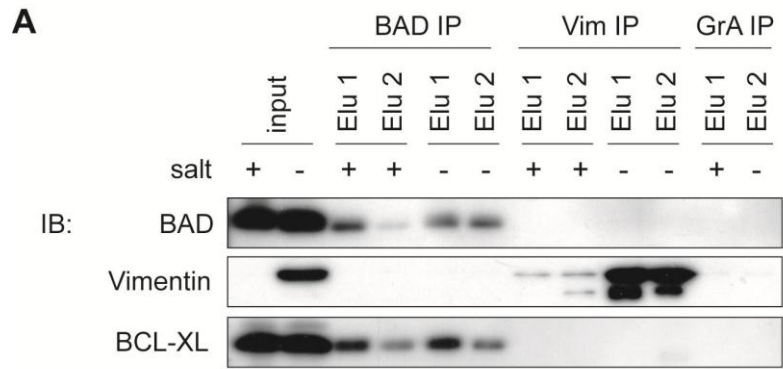


**Figure 3.20 Salt depletion does not enable detection of BAD:vimentin interactions.**

MDA-MB-231 cells (**A**) or 231.BAD cells (**B**) were harvested in 1% NP-40 buffer in the presence (+) or absence (-) of 150 mM NaCl. BAD immunoprecipitation in + and -salt buffers revealed interaction with BCL-XL but not vimentin. Vimentin immunoprecipitation was enhanced in -salt buffer but did not reveal interaction with BAD. Granzyme A immunoprecipitation (GrA IP) was included as a negative control.

interactions were maintained in both conditions, indicating that this experiment was able to detect known BAD binding partners. Taken together, these experiments were unable to replicate the BAD:vimentin interaction initially detected in the GST-BAD pull down screen (**Figure 3.12**).

### **3.2.8 Screening for GST-BAD S118A/D interacting proteins**

Ongoing studies in the laboratory continued to characterize BAD pro-growth activity. Proliferation assays and mouse tumor xenograft studies elucidated a pro-growth role for wild type overexpressed BAD (113). As previously mentioned, we had initially hypothesized that BAD mediated proliferation would correlate with increased BAD:BCL-XL binding. This hypothesis was tested by assessing the proliferation of MDA-MB-231 stable cell lines that express either BAD S118A or BAD S118D. It was verified that BAD:BCL-XL interactions are enhanced in 231.BAD S118A cells and diminished in 231.BAD S118D cells (113). While 231.BAD S118D cells reached higher cell numbers in a proliferation assay than 231.BAD S118A, in vitro studies indicated no differences in cell cycle progression between 231.BAD S118D and 231.BAD S118A cells (113). Instead, these studies suggested that observed enhanced growth of the 231.BAD S118D cells was likely due to decreased cell death compared with enhanced apoptotic phenotype of the 231.BAD S118A cells (113).

Given the unexpected phenotypes of the 231.BAD S118D cells and the vastly different propensities of the 231.BAD S118A and S118D cells for in vitro

and in vivo growth, we queried whether these differences correlated only with a difference in BAD:BCL-XL binding. To determine if other qualitative differences existed amongst protein binding partners for the BAD S118A and BAD S118D mutants, we pursued GST-BAD pull-down studies using these mutants.

HEK293T/17 cells were transfected with GST, GST-BAD wt, GST-BAD S118A or GST-BAD S118D plasmids. GST pull-downs were performed as previously described and isolated proteins were subjected to SDS-PAGE. Proteins were excised as a single band from the gel and extracted as peptide fragments digested with trypsin. Eluted peptides were identified by LC-MS/MS and searched against a human protein database using the SEQUEST search engine. Protein identification results revealed that 14-3-3 isoforms were detected in GST-BAD, GST-BAD S118A and GST-BAD S118D pull-downs in addition to GST and BAD controls (**Figure 3.21**). GST-BAD wt, S118A and S118D all eluted with 14-3-3 isoforms  $\epsilon$ ,  $\gamma$  and  $\zeta/\delta$ . Additionally GST-BAD S118A and S118D interacted with  $\alpha/\beta$  and  $\eta$  isoforms. Carbonyl reductase is known to bind to cytosolic GST (247) and Hsp71 has previously been found to elute in GST control (data not shown), therefore these hits were not further explored.

While there were no qualitative differences in 14-3-3 isoform binding between GST-BAD S118A and GST-BAD S118D, we decided to examine if there were any quantitative differences in the binding of different isoforms. Studies had shown that stably expressed BAD S118D in MDA-MB-231 cells was hyperphosphorylated on multiple sites (113). We predicted that a possible

Transfection	Protein ID	Mr (kDa)	# peptides	Coverage
GST	Glutathione S-transferase P	23.3	6	43.81
	Brain type mu-glutathione S-transferase	24.8	2	14.29
GST-BAD	Glutathione S-transferase P	23.3	6	43.81
	14-3-3 protein epsilon	29.2	9	39.61
	14-3-3 protein gamma	28.3	5	29.15
	14-3-3 protein zeta/delta	27.7	5	26.94
	Bcl2 antagonist of cell death	18.4	3	20.24
GST-BAD S118A	Glutathione S-transferase P	23.3	7	49.05
	Glutathione S-transferase Mu 3	26.5	4	22.22
	Carbonyl reductase [NADPH] 1	30.4	3	13.72
	14-3-3 protein epsilon	29.2	8	38.04
	14-3-3 protein gamma	28.3	4	23.48
	14-3-3 protein zeta/delta	27.7	5	27.35
	Isoform Short of 14-3-3 protein beta/alpha	27.8	4	21.31
	14-3-3 protein eta	28.2	3	14.63
	Bcl2 antagonist of cell death	18.4	3	20.24
GST-BAD S118D	Glutathione S-transferase P	23.3	7	49.05
	Brain type mu-glutathione S-transferase	24.8	4	26.67
	cDNA FLJ60474, highly similar to Carbonyl reductase	18.7	2	15.61
	Heat shock cognate 71 kDa protein	53.5	2	5.48
	14-3-3 protein epsilon	29.2	8	41.18
	14-3-3 protein gamma	28.3	3	17.14
	14-3-3 protein zeta/delta	27.7	6	34.69
	Isoform Short of 14-3-3 protein beta/alpha	27.8	4	21.13
	14-3-3 protein eta	28.2	3	14.63
	Bcl2 antagonist of cell death	18.4	4	33.33

**Figure 3.21 GST-BAD Serine 118 mutants interact with multiple 14-3-3 isoforms.**

HEK293T/17 cells were transfected with GST-BAD, GST-BAD S118A, GST-BAD S118D or GST (pEBG empty vector). Cells were harvested in 1% CHAPS pull-down buffer for glutathione sepharose pull-down. Beads were boiled in 1xlaemmli buffer and run on SDS-PAGE until the dye front reached the separating gel. Proteins were excised in a single band and subjected to tryptic digestion. Peptides were identified by LC-MS/MS and proteins matched using SEQUEST to search complete human proteome databases.

increase in phosphorylation of Serine 75 and 99 on GST-BAD S118D would allow for increased 14-3-3 binding compared to GST-BAD S118A.

To test this hypothesis, we repeated GST-BAD S118A/D pull-down assays in both HEK 293T/17 cells (**Figure 3.22**) and MDA-MB-231 cells (**Figure 3.23**) and assessed interactions with a panel of six 14-3-3 isoforms by western blot. In HEK293T/17 cells, no major differences were observed in the interactions between GST-BAD S118A and GST-BAD S118D with each of the 14-3-3 isoforms tested:  $\alpha/\beta$ ,  $\gamma$ ,  $\epsilon$ ,  $\zeta/\delta$ ,  $\eta$  and  $\tau$  (**Figure 3.22**). However, in MDA-MB-231 cells GST-BAD S118D had enhanced interactions with several 14-3-3 isoforms (including  $\alpha/\beta$ ,  $\gamma$ ,  $\zeta/\delta$  and  $\eta$ ) compared with GST-BAD S118A (**Figure 3.23**), in support of our hypothesis.

### 3.3 Summary

In summary, no novel interacting proteins were identified that could describe the BAD pro-growth phenotype. However, we verified BAD interactions with known binding partners, BCL-XL and 14-3-3 in MDA-MB-231 cells. We also determined that the BAD S118D mutant, which correlates with increased growth in vitro and in vivo relative to vector control, has increased propensity for 14-3-3 isoform interaction in MDA-MB-231 cells.

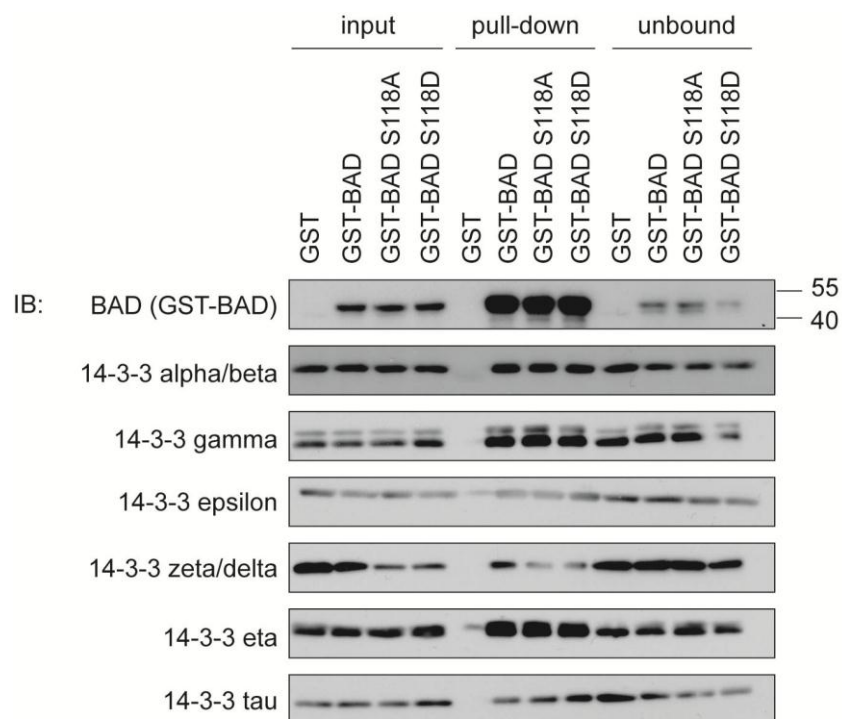


**Figure 3.22 BAD Serine 118 phosphorylation site mutants interact equivalently with 14-3-3 isoforms in HEK293T/17 cells.**

HEK293T/17 cells were transfected with GST control (empty vector) or GST-BAD constructs (wt BAD, BAD S118A or BAD S118D). Glutathione sepharose beads were used to capture GST-tagged bait and interacting proteins. 14-3-3 interacting partners were identified by western blot.

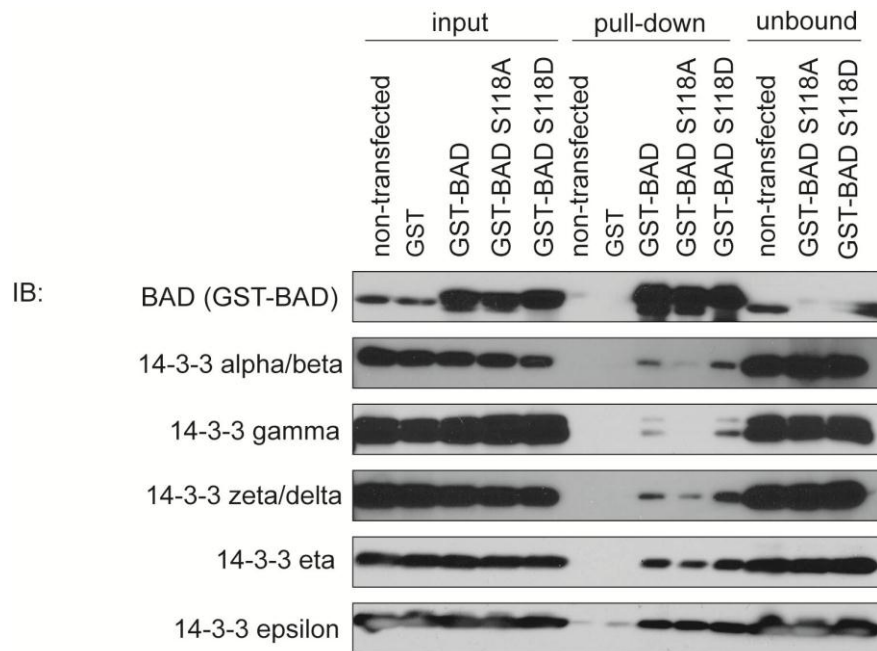


**Figure 3.23 BAD S118D interacts preferentially with 14-3-3 isoforms compared with BAD S118A in MDA-MB-231 cells.**

MDA-MB-231 cells were transfected with GST control (empty vector) or GST-BAD constructs (wt BAD, BAD S118A or BAD S118D). Glutathione sepharose beads were used to capture GST-tagged bait and interacting proteins. 14-3-3 interacting partners were identified by western blot.

## **Chapter 4: Discussion & Future Directions**

## **4.1 Role of BAD in paclitaxel induced cell death**

### **4.1.1 BAD is involved in paclitaxel induced cell death through a novel, non-apoptotic pathway**

Low concentrations of paclitaxel (200 nM or less) induce cellular mitotic arrest by binding to  $\beta$ -tubulin, stabilizing microtubules and activating the spindle assembly checkpoint (reviewed in (42)). Prolonged mitotic arrest ultimately leads to cell death, however the molecular mechanisms that activate the apoptotic program remain unclear. In previous work, our laboratory established a correlation between BAD protein levels in breast cancer cell lines and sensitivity to paclitaxel. Higher BAD levels correlated with enhanced cell death (67), and siRNA BAD depletion reduced cell death in breast cancer cell lines (75). This result is consistent with BAD overexpression and enhanced sensitivity to paclitaxel in ovarian cancer cells (248). We therefore postulated that BAD was a key player in activating the pro-apoptotic pathway in response to paclitaxel treatment.

We assessed the role of BAD in MCF-7 cells by looking for biochemical indications of pro-apoptotic BAD activity, including i) BAD interactions with anti-apoptotic members BCL-XL, BCL-2 and BCL-W, and ii) translocation of BAD from the cytosol to the mitochondria in response to 25 nM paclitaxel. In agreement with previous reports, we found that BCL-XL was the major anti-apoptotic binding partner for BAD (99). Surprisingly, we found that paclitaxel greatly diminished BAD:BCL-XL interactions (**Figure 3.1 A**), in contradiction to studies in ovarian cancer cells where the authors suggested paclitaxel sensitivity

correlates with enhanced BAD:BCL-XL interactions (248). Additionally, BAD stayed in the cytosolic fraction in response to paclitaxel, but translocated to the mitochondria in response to staurosporine (**Figure 3.1 B**). These determinants suggest that paclitaxel does not induce BAD pro-apoptotic activity; rather, BAD pro-apoptotic activity may be inactivated by diminished interaction with BCL-XL. Our research group and others have reported that BCL-XL is phosphorylated (249) and degraded following paclitaxel treatment (250), which may explain why these BAD:BCL-XL interactions are depleted. On the other hand, we cannot rule out a more direct effect of paclitaxel on the modulation of BAD which may actively disrupt BAD:BCL-XL complexes.

Overall, it would be interesting to further test whether paclitaxel treatment induces BAD phosphorylation and correlates with increased BAD:14-3-3 interactions, which would be consistent with inactivation of BAD apoptotic activity previously documented (251). Mabuchi S et al found that chemoresistant ovarian cancer cells treated with paclitaxel activated the Akt and ERK cascades to phosphorylate mBAD at Serine 136 and Serine 112 respectively (251). Furthermore, inhibition of BAD phosphorylation by Serine to Alanine substitutions at these sites sensitized these cells to paclitaxel (251). Therefore it may be possible that similar kinase cascades are activated in MCF-7 cells that lead to BAD phosphorylation, abrogate BAD:BCL-XL binding and inhibit pro-apoptotic BAD function. If BAD:14-3-3 interactions are not increased in paclitaxel treated MCF-7 cells, it may be that phosphorylated BAD binds to a novel protein partner under these conditions. Characterization of BAD binding

partners in paclitaxel treated breast cancer cells may therefore shed light on these possible mechanistic behaviors.

#### **4.1.2 BAD stimulates cell cycle progression**

Previously, our studies have shown that siRNA mediated depletion of BAD reduced cell numbers in proliferation assays of breast cancer cell lines, MCF-7 and SKBR-3 (67). We pursued further study of the role of BAD in cell cycle progression using propidium iodide staining to monitor cellular DNA content and paclitaxel to induce G2/M phase arrest (**Figure 3.2**). We found that BAD-depleted cells were retarded in G1/S phase transition and had delayed accumulation in G2/M phase compared to control cells. Overall, these results support a pro-proliferative role for BAD in MCF-7 cells. To our knowledge, we are the first group to report a pro-proliferative role for BAD in breast cancer cells. However, further studies in the laboratory found that BAD stimulation of cell cycle progression was not consistent in other cell lines, including MDA-MB-231 cells, where no discernible differences in cell cycle profiles between BAD-overexpressing MDA-MB-231 cells and control cells were found (113).

Overall, it is important to investigate the mechanisms of BAD stimulation of proliferation and its cell line specific effects. Specific directions could include:

- i) Documenting the phosphorylation state of BAD at specific sites in both MCF-7 cells and MDA-MB-231 cells to determine whether differential BAD phosphorylation correlates with enhanced cell cycle progression. This may shed

light on whether the pro-growth role of BAD is responsive to activation of specific pro-survival kinase cascades.

ii) Determining the mechanisms for increased cell numbers in 231.BAD cells relative to controls in proliferation assays without changes in cell cycle profiles.

Interestingly, BAD pro-growth activity has also been documented in vitro and in vivo in prostate cancer cells (123). With an emerging pro-growth role for BAD in cancer cells, it is imperative for us to determine how BAD toggles between apoptotic and pro-growth roles. Additionally, we need to precisely define the BAD pro-growth roles in terms of cell cycle changes and acquired transformative characteristics.

#### **4.1.3 BAD is required for paclitaxel induced cell death in cycling cells but not in G2/M phase arrested cells**

Our results demonstrate that BAD plays a critical role in paclitaxel induced cell death prior to G2/M phase arrest (**Figure 3.2**), consistent with a non-apoptotic role for BAD in the paclitaxel mediated cell death pathway. Taken together, our results suggest that BAD confers sensitivity to paclitaxel by promoting cell cycle progression and increasing the target population of mitotic cells susceptible to paclitaxel mediated arrest. If the sole function of BAD in this context is to promote cell cycle progression, we would expect BAD expression levels to also influence the sensitivity of breast cancer cells to other microtubule targeting drugs (eg epothilones, nocodazole) that may also activate the spindle assembly checkpoint during mitotic block and converge with the apoptotic cell

death pathway (252,253). Such future studies would help elucidate the importance of the BAD proliferative role towards chemotherapeutic sensitivity.

Altogether, the clinical implications of BAD mediated proliferation are interesting. We have previously seen that BAD expression correlates with docetaxel sensitivity and tumor regression (**Figure 1.3**) and with overall patient survival (**Figure 1.4**). We found that high BAD protein levels are prognostic of improved therapeutic outcomes for docetaxel treated breast cancer patients. Currently, randomized control trials are underway to determine whether BAD may also serve as a clinically predictive marker of taxane responsiveness in breast cancer patients. These advances are significant in terms of taxane research since there are currently no clinically used predictive markers of taxane responsiveness in patients (254). Predictive markers would allow clinicians to select for patient populations most likely to respond to treatment and spare other patients from the toxic side-effects of docetaxel.

## **4.2 BAD interacting proteins study**

### **4.2.1 Discussion of Hexokinases**

Since BAD plays an important role physiologically in stimulating glucokinase activity in mouse liver and pancreatic  $\beta$  cells (180,181), we hypothesized that cancer cells may be able to hijack BAD metabolic activity to promote growth. Specifically, we wanted to address possible interactions of BAD with HK isoforms I and II which have not been previously explored (104). Coimmunoprecipitation studies with endogenous protein in MDA-MB-231 cells

did not reveal a BAD:HK I or BAD:HK II interaction (**Figure 3.4**). Additionally, we were unable to detect interactions between Myc-BAD and HK I-V5 or HK II-V5 in cotransfected HEK293T/17 cells (**Figure 3.5, Figure 3.6**).

Danial et al were able to demonstrate an interaction between BAD and GK in the presence or absence of cross linker using multiple methods, including BAD and GK coimmunoprecipitation from solubilized mitochondrial fractions, microcystin sepharose affinity pull-down of PP1-interacting proteins from mitochondrial fractions, and coimmunoprecipitation of BAD and GK using IVTT synthesized protein (180,181). Additionally, Danial et al demonstrated a direct interaction between BAD and GK using a photoactivatable crosslinker as part of a BAD SAHB peptide that permeabilizes pancreatic islet cells (181). If the interaction between BAD and HK is transient in nature, a protein cross-linker may be required to detect the interaction by coimmunoprecipitation. We decided to use a comparative IVTT BAD coimmunoprecipitation assay in vitro with the addition of 1% formaldehyde protein cross-linker to determine whether transient interactions could be detected. However, even in the presence of protein cross-linker, there was no detection of BAD:HK I-V5 or BAD:HK II-V5 interactions (**Figure 3.7**).

Phosphorylation of mBAD at Serine 155 is required for stimulation of glucokinase activity in hepatocytes but not required for assembly of BAD:GK mitochondrial complex (180). We wanted to determine whether phosphorylation of the equivalent site, hBAD S118, would affect our ability to detect BAD:HK interactions. In the presence or absence of 1% formaldehyde cross-linker applied

to whole cells, 231.BAD or 231.BAD S118D, endogenous BAD:HK interactions were not detected (**Figure 3.8, Figure 3.9**).

The molecular interaction between BAD and GK that requires the BH3 domain has been modeled using murine BID since there is no 3-dimensional structural information for BAD (255). Since structural information is also available for the 100 kDa HK isoforms HK I and HK II, similar molecular models could be computed to determine whether there are likely to be equivalent interaction sites between BAD and HK as between BAD and GK. Alternatively, GK may be a unique binding partner for BAD that stimulates metabolism only in liver and pancreatic cells, and this metabolic function of BAD may not be relevant in other cell types or in cancer cells.

#### **4.2.2 Discussion of Vimentin**

Vimentin is an abundant cytoskeletal component of MDA-MB-231 cells (**Figure 3.14**), and an important intermediate filament protein of mesenchymal cells (256). Vimentin is also expressed in cells undergoing the epithelial-to-mesenchymal transition during normal development of tissues, eg embryogenesis (257), as well as during cancer progression (258). Vimentin has important implications in cell signaling through modulation of protein kinases (256), and in cell-matrix adhesion and cellular motility through modulation of integrins and their membrane trafficking (259). Furthermore, vimentin provides important structural support to intracellular organelles including the mitochondria (260). Overall, studies support a predominant role for vimentin in the EMT. Notably,

microinjection or transfection of vimentin in MCF-7 cells is sufficient to induce changes in cell shape and enhance motility consistent with EMT (261).

Experiments in this thesis demonstrate a mitochondrial localization for BAD in MDA-MB-231 cells (**Figure 3.15, Figure 3.16**). A putative BAD:vimentin interaction at the mitochondria may therefore implicate an unforeseen structural support role for BAD that bridges mitochondria with the intermediate filament network. However, while vimentin was initially identified in the GST-BAD pull down screen in MDA-MB-231 cells (**Figure 3.12**), we were unable to replicate the interaction in vitro using IVTT synthesized protein (**Figure 3.17**), or in cells cotransfected with Myc-BAD and Vimentin-V5 (**Figure 3.19**). Work on vimentin was therefore discontinued.

An alternative approach to identifying BAD interacting proteins that may increase the yield of relevant positive hits would involve isolating and solubilizing the mitochondrial fraction from MDA-MB-231 cells prior to GST-BAD pull-down, similar to techniques used by Danial et al to isolate the BAD:GK mitochondrial complex (180,181).

#### **4.2.3 Discussion of NMHC II-A**

Non-muscle myosin II is an important component of the actin cytoskeleton with contractile properties that regulates cell adhesion (262), cell migration (263) and cytokinesis (264,265). There are three isoforms of non-muscle myosin: NM II-A, NM II-B and NM II-C. Non-muscle myosin molecules are composed of two heavy chains (230 kDa), two light chains (20 kDa) and two essential light chains

(17 kDa) (262). The heavy chains of NM II-A, II-B and II-C (NMHC II-A, II-B and II-C) are encoded by the *MYH9*, *MYH10* and *MYH14* genes respectively (262). In this study, NMHC II-A was identified in a GST-BAD pull-down screen in MDA-MB-231 cells (**Figure 3.12**). This was an intriguing result initially since NM II-A is an important component of actin stress fibre formation (263) and helps regulate retraction of the trailing edge during cell migration (266,267). NMHC II-A and vimentin as initial hits seemed to provide a previously unforeseen link between BAD and the cytoskeleton. However, we were unable to verify a BAD:NMHC II-A interaction in cells (**Figure 3.13**).

#### **4.3 BAD:BCL-XL interactions**

The mitochondrial localization of BAD in MDA-MB-231 cells (**Figure 3.11, Figure 3.16**) is consistent with an interaction with BCL-XL (**Figure 3.13**). Both the C-terminal transmembrane domain of BCL-XL and BAD LBD2 are required for efficient BAD:BCL-XL translocation to mitochondrial membranes (153). BCL-XL was consistently detected in GST-BAD pull-downs and BAD interaction studies in different breast cancer cell lines, MCF-7 (**Figure 3.1**) and MDA-MB-231 (**Figure 3.13**).

Work in our laboratory demonstrates that MDA-MB-231 cells overexpressing hBAD S118D have significant pro-growth activities (113). First, hBAD S118D-overexpressing cells form larger tumors than hBAD wt-overexpressing cells when injected into mice. Secondly, hBAD and hBAD S118D overexpression both lead to pro-growth effects in cellular proliferation assays in

vitro, although hBAD S118D is slightly less effective than hBAD wt in promoting growth of MDA-MB-231 cells. The S118D point mutation within the BAD BH3 domain also correlates with diminished BCL-XL binding, diminished mitochondrial localization and an increased cytosolic localization when compared with the distinct mitochondrial localization of hBAD wt (113). Future work may involve separating these tenets of BAD activity and individually determining the importance of BCL-XL binding and mitochondrial binding to the BAD pro-growth phenotype. We could employ an hBAD S118A  $\Delta$ LBD2 mutant that retains the BH3 domain and BCL-XL binding capacity while disrupting its ability to bind mitochondrial membranes to test the importance of these distinct BAD properties in proliferation assays in vitro and mouse tumor xenograft studies in vivo. Furthermore, these studies may help determine whether BAD pro-growth activity is a function of BAD localization to either the cytosolic or mitochondrial compartments.

#### **4.4 BAD:14-3-3 interactions**

Our studies demonstrate interactions of BAD with 14-3-3 isoforms:  $\alpha/\beta$ ,  $\gamma$ ,  $\epsilon$ ,  $\zeta/\delta$ ,  $\eta$  and  $\tau$  (**Figure 3.22**), as has previously been reported (179). Interestingly, we determined that hBAD S118A had diminished interactions with multiple 14-3-3 isoforms ( $\alpha/\beta$ ,  $\gamma$ ,  $\zeta/\delta$ ,  $\eta$ ) in MDA-MB-231 cells (**Figure 3.23**) but not in HEK293T/17 cells (**Figure 3.22**) when compared with hBAD S118D. These results were surprising because BAD Serine 118 is not a 14-3-3 consensus binding site, yet mutation of this site influences the 14-3-3 binding capacity of

BAD at Serine 75 and 99. Further work demonstrated that BAD S118D is hyperphosphorylated on multiple sites compared with BAD wt in MDA-MB-231 cells (113). Collectively these results suggest that Serine 118 may act as an apical site than can influence the overall phosphorylation status of BAD and accommodate changes in 14-3-3 binding. Alternatively, the S118D mutant may specifically induce conformational changes that enhance accessibility of Serine 75 and 99 sites to kinases that are otherwise occluded by the S118A mutant.

While these studies identify multiple 14-3-3 isoforms as important BAD interacting partners, the contribution of 14-3-3 proteins towards cellular proliferation has not yet been determined. BAD S99A site mutants could be used to abrogate 14-3-3 binding and assess the effect on BAD mediated proliferation in vitro and in vivo. Alternatively, BAD:14-3-3 binding may not directly promote proliferation per se, but may correlate with enhanced sensitivity to apoptosis at different points during the cell cycle. Studies have shown that mBAD and 14-3-3 $\zeta$  form a complex in G1 phase that dissociates in G2/M phase with concordant phosphorylation of S128 by Cdc2 (268). The cell cycle dependent dissociation of the BAD:14-3-3 $\zeta$  complex is critical for effectively initiating IL-3 deprivation-induced apoptosis in FL5.12 cells (268). Likewise, persistent BAD:14-3-3 $\zeta$  complexes in G2/M phase in BAD S128A expressing cells delayed initiation of apoptosis (268). It would therefore be interesting to study the cell cycle dependent association of BAD:14-3-3 isoform complexes in MCF-7 and MDA-MB-231 breast cancer cells. Perhaps the hyperphosphorylated state of BAD in MDA-MB-231 cells in response to survival kinases precludes BAD:14-3-3 complex

dissociation and promotes cellular resistance to apoptosis in response to growth factor deprivation or nutrient depletion in cellular proliferation assays or tumor growth in mice.

## **4.5 Additional future directions**

### **4.5.1 Paclitaxel-induced cell death**

Our studies focused on the contributions of BAD towards paclitaxel mediated cell death. However, our clinical studies also support investigation of the BH3-only protein, BIK, in paclitaxel mediated cell death. Like BAD, *BIK* gene expression also correlates with docetaxel sensitivity (**Figure 1.3**). Additionally, BIK protein levels in primary breast tumors also correlate with overall survival of docetaxel treated breast cancer patients (data not shown). Unlike BAD, BIK resides in the endoplasmic reticulum and induces mitochondrial apoptosis (269) through calcium release (270). BIK mediated calcium release to the mitochondria is thought to stimulate DRP1 recruitment, which remodels the mitochondrial membrane cristae and mobilizes cytochrome c (271). While the ER is thought to contribute to paclitaxel mediated apoptosis through calcium release (272), a role for BIK in the paclitaxel induced cell death pathway has not been previously defined, and forms the basis for future study.

### **4.5.2 The role of BAD in cancer**

BAD expression has been associated with positive clinical outcomes in multiple human cancers. In primary breast tumors, BAD expression is associated

with estrogen receptor expression and disease-free survival, but also with increased tumor size (273). BAD expression also correlates with improved disease-free survival of tamoxifen-treated breast cancer patients (274). Our study identified BAD as a strong, independent prognostic factor for overall survival and disease-free survival of primary breast cancer patients receiving adjuvant docetaxel chemotherapy (67), while BAD expression also correlated with enhanced cell growth. In non-small cell lung cancer, BAD expression is diminished compared to normal lung tissues, and loss of BAD expression is predictive of poor clinical outcomes in patients (275). These correlations between BAD expression and survival are typically attributed to the BAD apoptotic effect. However, the phosphorylation status of BAD is also important to consider. Studies from our laboratory indicate that BAD S118D phosphomimic ultimately correlates with accelerated cell growth in vitro and in vivo (113). Furthermore, BAD phosphorylation confers resistance of ovarian cancer cells to chemotherapeutic drugs such as paclitaxel (251) and cisplatin (276).

Overall, it is necessary to more precisely define the mechanisms of BAD action in tumor cells. It is imperative to determine whether cancer cells selectively upregulate or downregulate BAD expression, how BAD mediates its pro-growth activities, and how BAD phosphorylation status influences the switch between BAD apoptotic vs pro-growth phenotypes.

## 4.6 Summary

BAD plays a critical role in the paclitaxel induced cell death pathway of breast cancer cells. Our studies found that BAD pro-apoptotic activity was not activated in response to paclitaxel, but that BAD expression was required for cell death through a novel, non-apoptotic pathway. Collectively, data from our laboratory suggests a pro-growth mechanism of BAD action in breast cancer cells. In MCF-7 cells, data suggests a role for BAD in promoting cell cycle progression, particularly at G1/S phase transition. In MDA-MB-231 cells, phosphorylated BAD correlates with enhanced growth in vitro and in vivo without measurable differences in cell cycle profiles (113). Overall, the molecular mechanisms of BAD mediated growth activity remain enigmatic. This study employed unbiased protein interaction screens with the goal of identifying protein factors that may mediate the BAD pro-growth pathway. No novel interacting proteins were identified; however interactions with known BAD binding proteins, BCL-XL and 14-3-3 were validated. Given the increased propensity of BAD S118D for growth activity and its increased interaction with 14-3-3 isoforms, future studies may focus on exploring the relevance of BAD:14-3-3 interactions towards the BAD pro-growth phenotype.

## **Chapter 5: References**

- (1) Kerr JF, Wyllie AH, Currie AR. Apoptosis: a basic biological phenomenon with wide-ranging implications in tissue kinetics. *Br J Cancer* 1972 Aug;26(4):239-257.
- (2) Kroemer G, Galluzzi L, Vandenabeele P, Abrams J, Alnemri ES, Baehrecke EH, et al. Classification of cell death: recommendations of the Nomenclature Committee on Cell Death 2009. *Cell Death Differ* 2009 Jan;16(1):3-11.
- (3) Coucouvanis E, Martin GR. Signals for death and survival: a two-step mechanism for cavitation in the vertebrate embryo. *Cell* 1995 Oct 20;83(2):279-287.
- (4) Brison DR, Schultz RM. Apoptosis during mouse blastocyst formation: evidence for a role for survival factors including transforming growth factor alpha. *Biol Reprod* 1997 May;56(5):1088-1096.
- (5) Saunders JW, Jr. Death in embryonic systems. *Science* 1966 Nov 4;154(3749):604-612.
- (6) Zakeri Z, Quaglino D, Ahuja HS. Apoptotic cell death in the mouse limb and its suppression in the hammertoe mutant. *Dev Biol* 1994 Sep;165(1):294-297.
- (7) Walker NI, Bennett RE, Kerr JF. Cell death by apoptosis during involution of the lactating breast in mice and rats. *Am J Anat* 1989 May;185(1):19-32.
- (8) Hanahan D, Weinberg RA. Hallmarks of cancer: the next generation. *Cell* 2011 Mar 4;144(5):646-674.
- (9) Hanahan D, Weinberg RA. The hallmarks of cancer. *Cell* 2000 Jan 7;100(1):57-70.
- (10) Martinou JC, Youle RJ. Mitochondria in apoptosis: Bcl-2 family members and mitochondrial dynamics. *Dev Cell* 2011 Jul 19;21(1):92-101.
- (11) Giam M, Huang DC, Bouillet P. BH3-only proteins and their roles in programmed cell death. *Oncogene* 2008 Dec;27 Suppl 1:S128-36.
- (12) Strasser A, Cory S, Adams JM. Deciphering the rules of programmed cell death to improve therapy of cancer and other diseases. *EMBO J* 2011 Aug 23;30(18):3667-3683.
- (13) Ola MS, Nawaz M, Ahsan H. Role of Bcl-2 family proteins and caspases in the regulation of apoptosis. *Mol Cell Biochem* 2011 May;351(1-2):41-58.

- (14) Li P, Nijhawan D, Budihardjo I, Srinivasula SM, Ahmad M, Alnemri ES, et al. Cytochrome c and dATP-dependent formation of Apaf-1/caspase-9 complex initiates an apoptotic protease cascade. *Cell* 1997 Nov 14;91(4):479-489.
- (15) Wani MC, Taylor HL, Wall ME, Coggon P, McPhail AT. Plant antitumor agents. VI. The isolation and structure of taxol, a novel antileukemic and antitumor agent from *Taxus brevifolia*. *J Am Chem Soc* 1971 May 5;93(9):2325-2327.
- (16) Labi V, Grespi F, Baumgartner F, Villunger A. Targeting the Bcl-2-regulated apoptosis pathway by BH3 mimetics: a breakthrough in anticancer therapy? *Cell Death Differ* 2008 Jun;15(6):977-987.
- (17) Andersen A, Warren DJ, Brunsvig PF, Aamdal S, Kristensen GB, Olsen H. High sensitivity assays for docetaxel and paclitaxel in plasma using solid-phase extraction and high-performance liquid chromatography with UV detection. *BMC Clin Pharmacol* 2006 Jan 13;6:2.
- (18) Fuchs DA, Johnson RK. Cytologic evidence that taxol, an antineoplastic agent from *Taxus brevifolia*, acts as a mitotic spindle poison. *Cancer Treat Rep* 1978 Aug;62(8):1219-1222.
- (19) Schiff PB, Fant J, Horwitz SB. Promotion of microtubule assembly in vitro by taxol. *Nature* 1979 Feb 22;277(5698):665-667.
- (20) Schiff PB, Horwitz SB. Taxol stabilizes microtubules in mouse fibroblast cells. *Proc Natl Acad Sci U S A* 1980 Mar;77(3):1561-1565.
- (21) Rowinsky EK, Cazenave LA, Donehower RC. Taxol: a novel investigational antimicrotubule agent. *J Natl Cancer Inst* 1990 Aug 1;82(15):1247-1259.
- (22) Riondel J, Jacrot M, Picot F, Beriel H, Mouriquand C, Potier P. Therapeutic response to taxol of six human tumors xenografted into nude mice. *Cancer Chemother Pharmacol* 1986;17(2):137-142.
- (23) Denis JN, Greene AE, Guenard D, Gueritte-Voegelein F, Mangatal L, Potier P. Highly efficient, practical approach to natural taxol. *J Am Chem Soc* 1988 08/01; 2012/04;110(17):5917-5919.
- (24) Mangatal L, Adeline M-, Guénard D, Guéritte-Voegelein F, Potier P. Application of the vicinal oxyamination reaction with asymmetric induction to the hemisynthesis of taxol and analogues. *Tetrahedron* 1989;45(13):4177-4190.
- (25) Ringel I, Horwitz SB. Studies with RP 56976 (taxotere): a semisynthetic analogue of taxol. *J Natl Cancer Inst* 1991 Feb 20;83(4):288-291.

- (26) Olmsted JB, Borisy GG. Microtubules. *Annu Rev Biochem* 1973;42:507-540.
- (27) Luduena RF, Shooter EM, Wilson L. Structure of the tubulin dimer. *J Biol Chem* 1977 Oct 25;252(20):7006-7014.
- (28) Amos L, Klug A. Arrangement of subunits in flagellar microtubules. *J Cell Sci* 1974 May;14(3):523-549.
- (29) Erickson HP. The structure and assembly of microtubules. *Ann N Y Acad Sci* 1975 Jun 30;253:60-77.
- (30) Andreu JM, Bordas J, Diaz JF, Garcia de Ancos J, Gil R, Medrano FJ, et al. Low resolution structure of microtubules in solution. Synchrotron X-ray scattering and electron microscopy of taxol-induced microtubules assembled from purified tubulin in comparison with glycerol and MAP-induced microtubules. *J Mol Biol* 1992 Jul 5;226(1):169-184.
- (31) Pierson GB, Burton PR, Himes RH. Alterations in number of protofilaments in microtubules assembled in vitro. *J Cell Biol* 1978 Jan;76(1):223-228.
- (32) Desai A, Mitchison TJ. Microtubule polymerization dynamics. *Annu Rev Cell Dev Biol* 1997;13:83-117.
- (33) Weisenberg RC, Deery WJ, Dickinson PJ. Tubulin-nucleotide interactions during the polymerization and depolymerization of microtubules. *Biochemistry* 1976 Sep 21;15(19):4248-4254.
- (34) Carlier MF, Pantaloni D. Kinetic analysis of guanosine 5'-triphosphate hydrolysis associated with tubulin polymerization. *Biochemistry* 1981 Mar 31;20(7):1918-1924.
- (35) Pantaloni D, Carlier MF. Involvement of guanosine triphosphate (GTP) hydrolysis in the mechanism of tubulin polymerization: regulation of microtubule dynamics at steady state by a GTP cap. *Ann N Y Acad Sci* 1986;466:496-509.
- (36) Dimitrov A, Quesnoit M, Moutel S, Cantaloube I, Pous C, Perez F. Detection of GTP-tubulin conformation in vivo reveals a role for GTP remnants in microtubule rescues. *Science* 2008 Nov 28;322(5906):1353-1356.
- (37) Sammak PJ, Borisy GG. Direct observation of microtubule dynamics in living cells. *Nature* 1988 Apr 21;332(6166):724-726.
- (38) Davis A, Sage CR, Dougherty CA, Farrell KW. Microtubule dynamics modulated by guanosine triphosphate hydrolysis activity of beta-tubulin. *Science* 1994 May 6;264(5160):839-842.

- (39) Holy TE, Leibler S. Dynamic instability of microtubules as an efficient way to search in space. *Proc Natl Acad Sci U S A* 1994 Jun 7;91(12):5682-5685.
- (40) Musacchio A, Salmon ED. The spindle-assembly checkpoint in space and time. *Nat Rev Mol Cell Biol* 2007 May;8(5):379-393.
- (41) Matson DR, Stukenberg PT. Spindle poisons and cell fate: a tale of two pathways. *Mol Interv* 2011 Apr;11(2):141-150.
- (42) Wang TH, Wang HS, Soong YK. Paclitaxel-induced cell death: where the cell cycle and apoptosis come together. *Cancer* 2000 Jun 1;88(11):2619-2628.
- (43) Schiff PB, Horwitz SB. Taxol assembles tubulin in the absence of exogenous guanosine 5'-triphosphate or microtubule-associated proteins. *Biochemistry* 1981 May 26;20(11):3247-3252.
- (44) Diaz JF, Andreu JM. Assembly of purified GDP-tubulin into microtubules induced by taxol and taxotere: reversibility, ligand stoichiometry, and competition. *Biochemistry* 1993 Mar 23;32(11):2747-2755.
- (45) Amos LA, Lowe J. How Taxol stabilises microtubule structure. *Chem Biol* 1999 Mar;6(3):R65-9.
- (46) Orr GA, Verdier-Pinard P, McDaid H, Horwitz SB. Mechanisms of Taxol resistance related to microtubules. *Oncogene* 2003 Oct 20;22(47):7280-7295.
- (47) Rao S, Horwitz SB, Ringel I. Direct photoaffinity labeling of tubulin with taxol. *J Natl Cancer Inst* 1992 May 20;84(10):785-788.
- (48) Rao S, Krauss NE, Heering JM, Swindell CS, Ringel I, Orr GA, et al. 3'-(p-azidobenzamido)taxol photolabels the N-terminal 31 amino acids of beta-tubulin. *J Biol Chem* 1994 Feb 4;269(5):3132-3134.
- (49) Rao S, Orr GA, Chaudhary AG, Kingston DG, Horwitz SB. Characterization of the taxol binding site on the microtubule. 2-(m-Azidobenzoyl)taxol photolabels a peptide (amino acids 217-231) of beta-tubulin. *J Biol Chem* 1995 Sep 1;270(35):20235-20238.
- (50) Rao S, He L, Chakravarty S, Ojima I, Orr GA, Horwitz SB. Characterization of the Taxol binding site on the microtubule. Identification of Arg(282) in beta-tubulin as the site of photoincorporation of a 7-benzophenone analogue of Taxol. *J Biol Chem* 1999 Dec 31;274(53):37990-37994.
- (51) Nogales E, Wolf SG, Downing KH. Structure of the alpha beta tubulin dimer by electron crystallography. *Nature* 1998 Jan 8;391(6663):199-203.

- (52) Nogales E, Wolf SG, Khan IA, Luduena RF, Downing KH. Structure of tubulin at 6.5 Å and location of the taxol-binding site. *Nature* 1995 Jun 1;375(6530):424-427.
- (53) Diaz JF, Strobe R, Engelborghs Y, Souto AA, Andreu JM. Molecular recognition of taxol by microtubules. Kinetics and thermodynamics of binding of fluorescent taxol derivatives to an exposed site. *J Biol Chem* 2000 Aug 25;275(34):26265-26276.
- (54) Magnani M, Maccari G, Andreu JM, Diaz JF, Botta M. Possible binding site for paclitaxel at microtubule pores. *FEBS J* 2009 May;276(10):2701-2712.
- (55) Diaz JF, Valpuesta JM, Chacon P, Diakun G, Andreu JM. Changes in microtubule protofilament number induced by Taxol binding to an easily accessible site. Internal microtubule dynamics. *J Biol Chem* 1998 Dec 11;273(50):33803-33810.
- (56) Diaz JF, Barasoain I, Andreu JM. Fast kinetics of Taxol binding to microtubules. Effects of solution variables and microtubule-associated proteins. *J Biol Chem* 2003 Mar 7;278(10):8407-8419.
- (57) Snyder JP. The microtubule-pore gatekeeper. *Nat Chem Biol* 2007 Feb;3(2):81-82.
- (58) Calvo E, Barasoain I, Matesanz R, Pera B, Camafeita E, Pineda O, et al. Cyclostreptin derivatives specifically target cellular tubulin and further map the paclitaxel site. *Biochemistry* 2012 Jan 10;51(1):329-341.
- (59) Blagosklonny MV, Fojo T. Molecular effects of paclitaxel: myths and reality (a critical review). *Int J Cancer* 1999 Oct 8;83(2):151-156.
- (60) Yeung TK, Germond C, Chen X, Wang Z. The mode of action of taxol: apoptosis at low concentration and necrosis at high concentration. *Biochem Biophys Res Commun* 1999 Sep 24;263(2):398-404.
- (61) McCloskey DE, Kaufmann SH, Prestigiacomo LJ, Davidson NE. Paclitaxel induces programmed cell death in MDA-MB-468 human breast cancer cells. *Clin Cancer Res* 1996 May;2(5):847-854.
- (62) Jordan MA, Wendell K, Gardiner S, Derry WB, Copp H, Wilson L. Mitotic block induced in HeLa cells by low concentrations of paclitaxel (Taxol) results in abnormal mitotic exit and apoptotic cell death. *Cancer Res* 1996 Feb 15;56(4):816-825.

- (63) Jordan MA, Toso RJ, Thrower D, Wilson L. Mechanism of mitotic block and inhibition of cell proliferation by taxol at low concentrations. *Proc Natl Acad Sci U S A* 1993 Oct 15;90(20):9552-9556.
- (64) Long BH, Fairchild CR. Paclitaxel inhibits progression of mitotic cells to G1 phase by interference with spindle formation without affecting other microtubule functions during anaphase and telephase. *Cancer Res* 1994 Aug 15;54(16):4355-4361.
- (65) Hernandez-Vargas H, Palacios J, Moreno-Bueno G. Telling cells how to die: docetaxel therapy in cancer cell lines. *Cell Cycle* 2007 Apr 1;6(7):780-783.
- (66) Blajeski AL, Kottke TJ, Kaufmann SH. A multistep model for paclitaxel-induced apoptosis in human breast cancer cell lines. *Exp Cell Res* 2001 Nov 1;270(2):277-288.
- (67) Craik AC, Veldhoen RA, Czernick M, Buckland TW, Kyselytzia K, Ghosh S, et al. The BH3-only protein Bad confers breast cancer taxane sensitivity through a nonapoptotic mechanism. *Oncogene* 2010 Sep 30;29(39):5381-5391.
- (68) Kuwana T, Bouchier-Hayes L, Chipuk JE, Bonzon C, Sullivan BA, Green DR, et al. BH3 domains of BH3-only proteins differentially regulate Bax-mediated mitochondrial membrane permeabilization both directly and indirectly. *Mol Cell* 2005 Feb 18;17(4):525-535.
- (69) Letai A, Bassik MC, Walensky LD, Sorcinelli MD, Weiler S, Korsmeyer SJ. Distinct BH3 domains either sensitize or activate mitochondrial apoptosis, serving as prototype cancer therapeutics. *Cancer Cell* 2002 Sep;2(3):183-192.
- (70) O'Connor L, Strasser A, O'Reilly LA, Hausmann G, Adams JM, Cory S, et al. Bim: a novel member of the Bcl-2 family that promotes apoptosis. *EMBO J* 1998 Jan 15;17(2):384-395.
- (71) Hsu SY, Lin P, Hsueh AJ. BOD (Bcl-2-related ovarian death gene) is an ovarian BH3 domain-containing proapoptotic Bcl-2 protein capable of dimerization with diverse antiapoptotic Bcl-2 members. *Mol Endocrinol* 1998 Sep;12(9):1432-1440.
- (72) Li R, Moudgil T, Ross HJ, Hu HM. Apoptosis of non-small-cell lung cancer cell lines after paclitaxel treatment involves the BH3-only proapoptotic protein Bim. *Cell Death Differ* 2005 Mar;12(3):292-303.
- (73) Li Z, Zhang J, Liu Z, Woo CW, Thiele CJ. Downregulation of Bim by brain-derived neurotrophic factor activation of TrkB protects neuroblastoma cells from paclitaxel but not etoposide or cisplatin-induced cell death. *Cell Death Differ* 2007 Feb;14(2):318-326.

- (74) Bouillet P, Metcalf D, Huang DC, Tarlinton DM, Kay TW, Kontgen F, et al. Proapoptotic Bcl-2 relative Bim required for certain apoptotic responses, leukocyte homeostasis, and to preclude autoimmunity. *Science* 1999 Nov 26;286(5445):1735-1738.
- (75) Czernick M, Rieger A, Goping IS. Bim is reversibly phosphorylated but plays a limited role in paclitaxel cytotoxicity of breast cancer cell lines. *Biochem Biophys Res Commun* 2009 Jan 30;379(1):145-150.
- (76) Chang JC, Wooten EC, Tsimelzon A, Hilsenbeck SG, Gutierrez MC, Elledge R, et al. Gene expression profiling for the prediction of therapeutic response to docetaxel in patients with breast cancer. *Lancet* 2003 Aug 2;362(9381):362-369.
- (77) Kutuk O, Letai A. Displacement of Bim by Bmf and Puma rather than increase in Bim level mediates paclitaxel-induced apoptosis in breast cancer cells. *Cell Death Differ* 2010 Oct;17(10):1624-1635.
- (78) Sunters A, Fernandez de Mattos S, Stahl M, Brosens JJ, Zoumpoulidou G, Saunders CA, et al. FoxO3a transcriptional regulation of Bim controls apoptosis in paclitaxel-treated breast cancer cell lines. *J Biol Chem* 2003 Dec 12;278(50):49795-49805.
- (79) Janicke RU, Sprengart ML, Wati MR, Porter AG. Caspase-3 is required for DNA fragmentation and morphological changes associated with apoptosis. *J Biol Chem* 1998 Apr 17;273(16):9357-9360.
- (80) Li F, Srinivasan A, Wang Y, Armstrong RC, Tomaselli KJ, Fritz LC. Cell-specific induction of apoptosis by microinjection of cytochrome c. Bcl-xL has activity independent of cytochrome c release. *J Biol Chem* 1997 Nov 28;272(48):30299-30305.
- (81) Kagawa S, Gu J, Honda T, McDonnell TJ, Swisher SG, Roth JA, et al. Deficiency of caspase-3 in MCF7 cells blocks Bax-mediated nuclear fragmentation but not cell death. *Clin Cancer Res* 2001 May;7(5):1474-1480.
- (82) Graham KA, Trent JM, Osborne CK, McGrath CM, Minden MD, Buick RN. The use of restriction fragment polymorphisms to identify the cell line MCF-7. *Breast Cancer Res Treat* 1986;8(1):29-34.
- (83) Osborne CK, Hobbs K, Trent JM. Biological differences among MCF-7 human breast cancer cell lines from different laboratories. *Breast Cancer Res Treat* 1987;9(2):111-121.
- (84) Bahia H, Ashman JN, Cawkwell L, Lind M, Monson JR, Drew PJ, et al. Karyotypic variation between independently cultured strains of the cell line MCF-

- 7 identified by multicolour fluorescence in situ hybridization. *Int J Oncol* 2002 Mar;20(3):489-494.
- (85) Omura S, Iwai Y, Hirano A, Nakagawa A, Awaya J, Tsuchya H, et al. A new alkaloid AM-2282 OF *Streptomyces* origin. Taxonomy, fermentation, isolation and preliminary characterization. *J Antibiot (Tokyo)* 1977 Apr;30(4):275-282.
- (86) Karaman MW, Herrgard S, Treiber DK, Gallant P, Atteridge CE, Campbell BT, et al. A quantitative analysis of kinase inhibitor selectivity. *Nat Biotechnol* 2008 Jan;26(1):127-132.
- (87) Tamaoki T, Nakano H. Potent and specific inhibitors of protein kinase C of microbial origin. *Biotechnology (N Y)* 1990 Aug;8(8):732-735.
- (88) Nakano H, Kobayashi E, Takahashi I, Tamaoki T, Kuzuu Y, Iba H. Staurosporine inhibits tyrosine-specific protein kinase activity of Rous sarcoma virus transforming protein p60. *J Antibiot (Tokyo)* 1987 May;40(5):706-708.
- (89) Nakadate T, Jeng AY, Blumberg PM. Comparison of protein kinase C functional assays to clarify mechanisms of inhibitor action. *Biochem Pharmacol* 1988 Apr 15;37(8):1541-1545.
- (90) Ruegg UT, Burgess GM. Staurosporine, K-252 and UCN-01: potent but nonspecific inhibitors of protein kinases. *Trends Pharmacol Sci* 1989 Jun;10(6):218-220.
- (91) Bertrand R, Solary E, O'Connor P, Kohn KW, Pommier Y. Induction of a common pathway of apoptosis by staurosporine. *Exp Cell Res* 1994 Apr;211(2):314-321.
- (92) Zhang XD, Gillespie SK, Hersey P. Staurosporine induces apoptosis of melanoma by both caspase-dependent and -independent apoptotic pathways. *Mol Cancer Ther* 2004 Feb;3(2):187-197.
- (93) Belmokhtar CA, Hillion J, Segal-Bendirdjian E. Staurosporine induces apoptosis through both caspase-dependent and caspase-independent mechanisms. *Oncogene* 2001 Jun 7;20(26):3354-3362.
- (94) Tang D, Kidd VJ. Cleavage of DFF-45/ICAD by multiple caspases is essential for its function during apoptosis. *J Biol Chem* 1998 Oct 30;273(44):28549-28552.
- (95) Tang D, Lahti JM, Kidd VJ. Caspase-8 activation and bid cleavage contribute to MCF7 cellular execution in a caspase-3-dependent manner during staurosporine-mediated apoptosis. *J Biol Chem* 2000 Mar 31;275(13):9303-9307.

- (96) Janicke RU, Ng P, Sprengart ML, Porter AG. Caspase-3 is required for alpha-fodrin cleavage but dispensable for cleavage of other death substrates in apoptosis. *J Biol Chem* 1998 Jun 19;273(25):15540-15545.
- (97) Xue LY, Chiu SM, Oleinick NL. Staurosporine-induced death of MCF-7 human breast cancer cells: a distinction between caspase-3-dependent steps of apoptosis and the critical lethal lesions. *Exp Cell Res* 2003 Feb 15;283(2):135-145.
- (98) Tafani M, Minchenko DA, Serroni A, Farber JL. Induction of the mitochondrial permeability transition mediates the killing of HeLa cells by staurosporine. *Cancer Res* 2001 Mar 15;61(6):2459-2466.
- (99) Yang E, Zha J, Jockel J, Boise LH, Thompson CB, Korsmeyer SJ. Bad, a heterodimeric partner for Bcl-XL and Bcl-2, displaces Bax and promotes cell death. *Cell* 1995 Jan 27;80(2):285-291.
- (100) Zha J, Harada H, Osipov K, Jockel J, Waksman G, Korsmeyer SJ. BH3 domain of BAD is required for heterodimerization with BCL-XL and pro-apoptotic activity. *J Biol Chem* 1997 Sep 26;272(39):24101-24104.
- (101) Otilie S, Diaz JL, Horne W, Chang J, Wang Y, Wilson G, et al. Dimerization properties of human BAD. Identification of a BH-3 domain and analysis of its binding to mutant BCL-2 and BCL-XL proteins. *J Biol Chem* 1997 Dec 5;272(49):30866-30872.
- (102) Sattler M, Liang H, Nettlesheim D, Meadows RP, Harlan JE, Eberstadt M, et al. Structure of Bcl-xL-Bak peptide complex: recognition between regulators of apoptosis. *Science* 1997 Feb 14;275(5302):983-986.
- (103) Yao Y, Bobkov AA, Plesniak LA, Marassi FM. Mapping the interaction of pro-apoptotic tBID with pro-survival BCL-XL. *Biochemistry* 2009 Sep 15;48(36):8704-8711.
- (104) Danial NN. BAD: undertaker by night, candyman by day. *Oncogene* 2008 Dec;27 Suppl 1:S53-70.
- (105) Ranger AM, Zha J, Harada H, Datta SR, Danial NN, Gilmore AP, et al. Bad-deficient mice develop diffuse large B cell lymphoma. *Proc Natl Acad Sci U S A* 2003 Aug 5;100(16):9324-9329.
- (106) Mok C, Gil-Gómez G, Williams O, Coles M, Taga S, Tolaini M, et al. Bad Can Act as a Key Regulator of T Cell Apoptosis and T Cell Development. *The Journal of Experimental Medicine* 1999 February 01;189(3):575-586.

- (107) Kitada S, Krajewska M, Zhang X, Scudiero D, Zapata JM, Wang HG, et al. Expression and location of pro-apoptotic Bcl-2 family protein BAD in normal human tissues and tumor cell lines. *Am J Pathol* 1998 Jan;152(1):51-61.
- (108) Schorr K, Li M, Krajewski S, Reed JC, Furth PA. Bcl-2 gene family and related proteins in mammary gland involution and breast cancer. *J Mammary Gland Biol Neoplasia* 1999 Apr;4(2):153-164.
- (109) Metcalfe AD, Gilmore A, Klinowska T, Oliver J, Valentijn AJ, Brown R, et al. Developmental regulation of Bcl-2 family protein expression in the involuting mammary gland. *J Cell Sci* 1999 Jun;112 ( Pt 11)(Pt 11):1771-1783.
- (110) Baxter FO, Neoh K, Tevendale MC. The beginning of the end: death signaling in early involution. *J Mammary Gland Biol Neoplasia* 2007 Mar;12(1):3-13.
- (111) Chittenden T, Flemington C, Houghton AB, Ebb RG, Gallo GJ, Elangovan B, et al. A conserved domain in Bak, distinct from BH1 and BH2, mediates cell death and protein binding functions. *EMBO J* 1995 Nov 15;14(22):5589-5596.
- (112) Kelekar A, Thompson CB. Bcl-2-family proteins: the role of the BH3 domain in apoptosis. *Trends Cell Biol* 1998 Aug;8(8):324-330.
- (113) T. W. Buckland. *The Tumor Promoting Role of BAD in Breast Cancer Cells*. University of Alberta; 2012.
- (114) Fernando R, Foster JS, Bible A, Strom A, Pestell RG, Rao M, et al. Breast cancer cell proliferation is inhibited by BAD: regulation of cyclin D1. *J Biol Chem* 2007 Sep 28;282(39):28864-28873.
- (115) Kato J, Matsushime H, Hiebert SW, Ewen ME, Sherr CJ. Direct binding of cyclin D to the retinoblastoma gene product (pRb) and pRb phosphorylation by the cyclin D-dependent kinase CDK4. *Genes Dev* 1993 Mar;7(3):331-342.
- (116) Brady HJ, Gil-Gomez G, Kirberg J, Berns AJ. Bax alpha perturbs T cell development and affects cell cycle entry of T cells. *EMBO J* 1996 Dec 16;15(24):6991-7001.
- (117) Greider C, Chattopadhyay A, Parkhurst C, Yang E. BCL-x(L) and BCL2 delay Myc-induced cell cycle entry through elevation of p27 and inhibition of G1 cyclin-dependent kinases. *Oncogene* 2002 Nov 7;21(51):7765-7775.
- (118) Vairo G, Soos TJ, Upton TM, Zalvide J, DeCaprio JA, Ewen ME, et al. Bcl-2 retards cell cycle entry through p27(Kip1), pRB relative p130, and altered E2F regulation. *Mol Cell Biol* 2000 Jul;20(13):4745-4753.

- (119) Janumyan Y, Cui Q, Yan L, Sansam CG, Valentin M, Yang E. G0 function of BCL2 and BCL-xL requires BAX, BAK, and p27 phosphorylation by Mirk, revealing a novel role of BAX and BAK in quiescence regulation. *J Biol Chem* 2008 Dec 5;283(49):34108-34120.
- (120) Janumyan YM, Sansam CG, Chattopadhyay A, Cheng N, Soucie EL, Penn LZ, et al. Bcl-xL/Bcl-2 coordinately regulates apoptosis, cell cycle arrest and cell cycle entry. *EMBO J* 2003 Oct 15;22(20):5459-5470.
- (121) Chattopadhyay A, Chiang CW, Yang E. BAD/BCL-[X(L)] heterodimerization leads to bypass of G0/G1 arrest. *Oncogene* 2001 Jul 27;20(33):4507-4518.
- (122) Maslyar DJ, Aoki M, Vogt PK. The growth-promoting activity of the Bad protein in chicken embryo fibroblasts requires binding to protein 14-3-3. *Oncogene* 2001 Aug 23;20(37):5087-5092.
- (123) Smith AJ, Karpova Y, D'Agostino R, Jr, Willingham M, Kulik G. Expression of the Bcl-2 protein BAD promotes prostate cancer growth. *PLoS One* 2009 Jul 13;4(7):e6224.
- (124) Royuela M, Arenas MI, Bethencourt FR, Sanchez-Chapado M, Fraile B, Paniagua R. Immunoexpressions of p21, Rb, mcl-1 and bad gene products in normal, hyperplastic and carcinomatous human prostates. *Eur Cytokine Netw* 2001 Oct-Dec;12(4):654-663.
- (125) Hojabrpour P, Waissbluth I, Ghaffari M, Cox ME, Duronio V. CaMKII-gamma mediates phosphorylation of BAD at Ser170 to regulate cytokine-dependent survival and proliferation. *Biochem J* 2012 Feb 15;442(1):139-149.
- (126) Polzien L, Baljuls A, Albrecht M, Hekman M, Rapp UR. BAD contributes to RAF-mediated proliferation and cooperates with B-RAF-V600E in cancer signaling. *J Biol Chem* 2011 May 20;286(20):17934-17944.
- (127) Datta SR, Katsov A, Hu L, Petros A, Fesik SW, Yaffe MB, et al. 14-3-3 proteins and survival kinases cooperate to inactivate BAD by BH3 domain phosphorylation. *Mol Cell* 2000 Jul;6(1):41-51.
- (128) Polzien L, Baljuls A, Rennefahrt UE, Fischer A, Schmitz W, Zahedi RP, et al. Identification of novel in vivo phosphorylation sites of the human proapoptotic protein BAD: pore-forming activity of BAD is regulated by phosphorylation. *J Biol Chem* 2009 Oct 9;284(41):28004-28020.
- (129) Ye DZ, Jin S, Zhuo Y, Field J. p21-Activated kinase 1 (Pak1) phosphorylates BAD directly at serine 111 in vitro and indirectly through Raf-1 at serine 112. *PLoS One* 2011;6(11):e27637.

- (130) Macdonald A, Campbell DG, Toth R, McLauchlan H, Hastie CJ, Arthur JS. Pim kinases phosphorylate multiple sites on Bad and promote 14-3-3 binding and dissociation from Bcl-XL. *BMC Cell Biol* 2006 Jan 10;7:1.
- (131) Schurmann A, Mooney AF, Sanders LC, Sells MA, Wang HG, Reed JC, et al. P21-Activated Kinase 1 Phosphorylates the Death Agonist Bad and Protects Cells from Apoptosis. *Mol Cell Biol* 2000 Jan;20(2):453-461.
- (132) Cotteret S, Jaffer ZM, Beeser A, Chernoff J. p21-Activated kinase 5 (Pak5) localizes to mitochondria and inhibits apoptosis by phosphorylating BAD. *Mol Cell Biol* 2003 Aug;23(16):5526-5539.
- (133) Harada H, Becknell B, Wilm M, Mann M, Huang LJ, Taylor SS, et al. Phosphorylation and inactivation of BAD by mitochondria-anchored protein kinase A. *Mol Cell* 1999 Apr;3(4):413-422.
- (134) Yan B, Zemskova M, Holder S, Chin V, Kraft A, Koskinen PJ, et al. The PIM-2 kinase phosphorylates BAD on serine 112 and reverses BAD-induced cell death. *J Biol Chem* 2003 Nov 14;278(46):45358-45367.
- (135) Bonni A, Brunet A, West AE, Datta SR, Takasu MA, Greenberg ME. Cell survival promoted by the Ras-MAPK signaling pathway by transcription-dependent and -independent mechanisms. *Science* 1999 Nov 12;286(5443):1358-1362.
- (136) Lizcano JM, Morrice N, Cohen P. Regulation of BAD by cAMP-dependent protein kinase is mediated via phosphorylation of a novel site, Ser155. *Biochem J* 2000 Jul 15;349(Pt 2):547-557.
- (137) Konishi Y, Lehtinen M, Donovan N, Bonni A. Cdc2 phosphorylation of BAD links the cell cycle to the cell death machinery. *Mol Cell* 2002 May;9(5):1005-1016.
- (138) Donovan N, Becker EB, Konishi Y, Bonni A. JNK phosphorylation and activation of BAD couples the stress-activated signaling pathway to the cell death machinery. *J Biol Chem* 2002 Oct 25;277(43):40944-40949.
- (139) Harada H, Andersen JS, Mann M, Terada N, Korsmeyer SJ. p70S6 kinase signals cell survival as well as growth, inactivating the pro-apoptotic molecule BAD. *Proc Natl Acad Sci U S A* 2001 Aug 14;98(17):9666-9670.
- (140) Datta SR, Dudek H, Tao X, Masters S, Fu H, Gotoh Y, et al. Akt phosphorylation of BAD couples survival signals to the cell-intrinsic death machinery. *Cell* 1997 Oct 17;91(2):231-241.

- (141) Han EK, Butler C, Zhang H, Severin JM, Qin W, Holzman TF, et al. Chkl binds and phosphorylates BAD protein. *Anticancer Res* 2004 Nov-Dec;24(6):3907-3910.
- (142) Virdee K, Parone PA, Tolkovsky AM. Phosphorylation of the pro-apoptotic protein BAD on serine 155, a novel site, contributes to cell survival. *Curr Biol* 2000 Sep 21;10(18):1151-1154.
- (143) Zhou XM, Liu Y, Payne G, Lutz RJ, Chittenden T. Growth factors inactivate the cell death promoter BAD by phosphorylation of its BH3 domain on Ser155. *J Biol Chem* 2000 Aug 11;275(32):25046-25051.
- (144) Dramsi S, Scheid MP, Maiti A, Hojabrpour P, Chen X, Schubert K, et al. Identification of a novel phosphorylation site, Ser-170, as a regulator of bad proapoptotic activity. *J Biol Chem* 2002 Feb 22;277(8):6399-6405.
- (145) Klumpp S, Maurer A, Zhu Y, Aichele D, Pinna LA, Krieglstein J. Protein kinase CK2 phosphorylates BAD at threonine-117. *Neurochem Int* 2004 Oct;45(5):747-752.
- (146) Yu C, Minemoto Y, Zhang J, Liu J, Tang F, Bui TN, et al. JNK suppresses apoptosis via phosphorylation of the proapoptotic Bcl-2 family protein BAD. *Mol Cell* 2004 Feb 13;13(3):329-340.
- (147) Deng H, Yu F, Chen J, Zhao Y, Xiang J, Lin A. Phosphorylation of Bad at Thr-201 by JNK1 promotes glycolysis through activation of phosphofructokinase-1. *J Biol Chem* 2008 Jul 25;283(30):20754-20760.
- (148) Ayllon V, Martinez-A C, Garcia A, Cayla X, Rebollo A. Protein phosphatase 1alpha is a Ras-activated Bad phosphatase that regulates interleukin-2 deprivation-induced apoptosis. *EMBO J* 2000 May 15;19(10):2237-2246.
- (149) Chiang CW, Harris G, Ellig C, Masters SC, Subramanian R, Shenolikar S, et al. Protein phosphatase 2A activates the proapoptotic function of BAD in interleukin-3-dependent lymphoid cells by a mechanism requiring 14-3-3 dissociation. *Blood* 2001 Mar 1;97(5):1289-1297.
- (150) Chiang CW, Kanies C, Kim KW, Fang WB, Parkhurst C, Xie M, et al. Protein phosphatase 2A dephosphorylation of phosphoserine 112 plays the gatekeeper role for BAD-mediated apoptosis. *Mol Cell Biol* 2003 Sep;23(18):6350-6362.
- (151) Wang HG, Pathan N, Ethell IM, Krajewski S, Yamaguchi Y, Shibasaki F, et al. Ca<sup>2+</sup>-induced apoptosis through calcineurin dephosphorylation of BAD. *Science* 1999 Apr 9;284(5412):339-343.

- (152) Zha J, Harada H, Yang E, Jockel J, Korsmeyer SJ. Serine phosphorylation of death agonist BAD in response to survival factor results in binding to 14-3-3 not BCL-X(L). *Cell* 1996 Nov 15;87(4):619-628.
- (153) Hekman M, Albert S, Galmiche A, Rennefahrt UE, Fueller J, Fischer A, et al. Reversible membrane interaction of BAD requires two C-terminal lipid binding domains in conjunction with 14-3-3 protein binding. *J Biol Chem* 2006 Jun 23;281(25):17321-17336.
- (154) Holmgren SP, Huang DC, Adams JM, Cory S. Survival activity of Bcl-2 homologs Bcl-w and A1 only partially correlates with their ability to bind pro-apoptotic family members. *Cell Death Differ* 1999 Jun;6(6):525-532.
- (155) Youle RJ, Strasser A. The BCL-2 protein family: opposing activities that mediate cell death. *Nat Rev Mol Cell Biol* 2008 Jan;9(1):47-59.
- (156) Muchmore SW, Sattler M, Liang H, Meadows RP, Harlan JE, Yoon HS, et al. X-ray and NMR structure of human Bcl-xL, an inhibitor of programmed cell death. *Nature* 1996 May 23;381(6580):335-341.
- (157) Walensky LD. BCL-2 in the crosshairs: tipping the balance of life and death. *Cell Death Differ* 2006 Aug;13(8):1339-1350.
- (158) Jeong SY, Gaume B, Lee YJ, Hsu YT, Ryu SW, Yoon SH, et al. Bcl-x(L) sequesters its C-terminal membrane anchor in soluble, cytosolic homodimers. *EMBO J* 2004 May 19;23(10):2146-2155.
- (159) Aitken A. Post-translational modification of 14-3-3 isoforms and regulation of cellular function. *Semin Cell Dev Biol* 2011 Sep;22(7):673-680.
- (160) van Hemert MJ, Steensma HY, van Heusden GP. 14-3-3 Proteins: Key Regulators of Cell Division, Signalling and Apoptosis. *Bioessays* 2001 Oct;23(10):936-946.
- (161) Aitken A. Functional specificity in 14-3-3 isoform interactions through dimer formation and phosphorylation. Chromosome location of mammalian isoforms and variants. *Plant Mol Biol* 2002 Dec;50(6):993-1010.
- (162) Ichimura T, Isobe T, Okuyama T, Takahashi N, Araki K, Kuwano R, et al. Molecular cloning of cDNA coding for brain-specific 14-3-3 protein, a protein kinase-dependent activator of tyrosine and tryptophan hydroxylases. *Proc Natl Acad Sci U S A* 1988 Oct;85(19):7084-7088.
- (163) Jones DH, Ley S, Aitken A. Isoforms of 14-3-3 protein can form homo- and heterodimers in vivo and in vitro: implications for function as adapter proteins. *FEBS Lett* 1995 Jul 10;368(1):55-58.

- (164) Jones DH, Martin H, Madrazo J, Robinson KA, Nielsen P, Roseboom PH, et al. Expression and structural analysis of 14-3-3 proteins. *J Mol Biol* 1995 Jan 27;245(4):375-384.
- (165) Wilker EW, Grant RA, Artim SC, Yaffe MB. A structural basis for 14-3-3sigma functional specificity. *J Biol Chem* 2005 May 13;280(19):18891-18898.
- (166) Chaudhri M, Scarabel M, Aitken A. Mammalian and yeast 14-3-3 isoforms form distinct patterns of dimers in vivo. *Biochem Biophys Res Commun* 2003 Jan 17;300(3):679-685.
- (167) Freeman AK, Morrison DK. 14-3-3 Proteins: diverse functions in cell proliferation and cancer progression. *Semin Cell Dev Biol* 2011 Sep;22(7):681-687.
- (168) Gardino AK, Smerdon SJ, Yaffe MB. Structural determinants of 14-3-3 binding specificities and regulation of subcellular localization of 14-3-3-ligand complexes: a comparison of the X-ray crystal structures of all human 14-3-3 isoforms. *Semin Cancer Biol* 2006 Jun;16(3):173-182.
- (169) Bridges D, Moorhead GB. 14-3-3 Proteins: a Number of Functions for a Numbered Protein. *Sci STKE* 2005 Aug 9;2005(296):re10.
- (170) Morrison DK. The 14-3-3 proteins: integrators of diverse signaling cues that impact cell fate and cancer development. *Trends Cell Biol* 2009 Jan;19(1):16-23.
- (171) Yaffe MB, Rittinger K, Volinia S, Caron PR, Aitken A, Leffers H, et al. The structural basis for 14-3-3:phosphopeptide binding specificity. *Cell* 1997 Dec 26;91(7):961-971.
- (172) Rittinger K, Budman J, Xu J, Volinia S, Cantley LC, Smerdon SJ, et al. Structural analysis of 14-3-3 phosphopeptide complexes identifies a dual role for the nuclear export signal of 14-3-3 in ligand binding. *Mol Cell* 1999 Aug;4(2):153-166.
- (173) Seimiya H, Sawada H, Muramatsu Y, Shimizu M, Ohko K, Yamane K, et al. Involvement of 14-3-3 proteins in nuclear localization of telomerase. *EMBO J* 2000 Jun 1;19(11):2652-2661.
- (174) Sumioka A, Nagaishi S, Yoshida T, Lin A, Miura M, Suzuki T. Role of 14-3-3gamma in FE65-dependent gene transactivation mediated by the amyloid beta-protein precursor cytoplasmic fragment. *J Biol Chem* 2005 Dec 23;280(51):42364-42374.

- (175) Ottmann C, Yasmin L, Weyand M, Veessenmeyer JL, Diaz MH, Palmer RH, et al. Phosphorylation-independent interaction between 14-3-3 and exoenzyme S: from structure to pathogenesis. *EMBO J* 2007 Feb 7;26(3):902-913.
- (176) Aitken A. 14-3-3 Proteins: a Historic Overview. *Semin Cancer Biol* 2006 Jun;16(3):162-172.
- (177) Masters SC, Yang H, Datta SR, Greenberg ME, Fu H. 14-3-3 inhibits Bad-induced cell death through interaction with serine-136. *Mol Pharmacol* 2001 Dec;60(6):1325-1331.
- (178) Chen XQ, Fung YW, Yu AC. Association of 14-3-3gamma and phosphorylated bad attenuates injury in ischemic astrocytes. *J Cereb Blood Flow Metab* 2005 Mar;25(3):338-347.
- (179) Subramanian RR, Masters SC, Zhang H, Fu H. Functional conservation of 14-3-3 isoforms in inhibiting bad-induced apoptosis. *Exp Cell Res* 2001 Nov 15;271(1):142-151.
- (180) Danial NN, Gramm CF, Scorrano L, Zhang CY, Krauss S, Ranger AM, et al. BAD and glucokinase reside in a mitochondrial complex that integrates glycolysis and apoptosis. *Nature* 2003 Aug 21;424(6951):952-956.
- (181) Danial NN, Walensky LD, Zhang CY, Choi CS, Fisher JK, Molina AJ, et al. Dual role of proapoptotic BAD in insulin secretion and beta cell survival. *Nat Med* 2008 Feb;14(2):144-153.
- (182) Yu C, Minemoto Y, Zhang J, Liu J, Tang F, Bui TN, et al. JNK suppresses apoptosis via phosphorylation of the proapoptotic Bcl-2 family protein BAD. *Mol Cell* 2004 Feb 13;13(3):329-340.
- (183) Koppenol WH, Bounds PL, Dang CV. Otto Warburg's contributions to current concepts of cancer metabolism. *Nat Rev Cancer* 2011 May;11(5):325-337.
- (184) WARBURG O. On the origin of cancer cells. *Science* 1956 Feb 24;123(3191):309-314.
- (185) Racker E. Bioenergetics and the problem of tumor growth. *Am Sci* 1972 Jan-Feb;60(1):56-63.
- (186) Parry DM, Pedersen PL. Intracellular localization and properties of particulate hexokinase in the Novikoff ascites tumor. Evidence for an outer mitochondrial membrane location. *J Biol Chem* 1983 Sep 25;258(18):10904-10912.

- (187) Arora KK, Pedersen PL. Functional significance of mitochondrial bound hexokinase in tumor cell metabolism. Evidence for preferential phosphorylation of glucose by intramitochondrially generated ATP. *J Biol Chem* 1988 Nov 25;263(33):17422-17428.
- (188) Vander Heiden MG, Cantley LC, Thompson CB. Understanding the Warburg effect: the metabolic requirements of cell proliferation. *Science* 2009 May 22;324(5930):1029-1033.
- (189) Pedersen PL. Warburg, me and Hexokinase 2: Multiple discoveries of key molecular events underlying one of cancers' most common phenotypes, the "Warburg Effect", i.e., elevated glycolysis in the presence of oxygen. *J Bioenerg Biomembr* 2007 Jun;39(3):211-222.
- (190) Arora KK, Fanciulli M, Pedersen PL. Glucose phosphorylation in tumor cells. Cloning, sequencing, and overexpression in active form of a full-length cDNA encoding a mitochondrial bindable form of hexokinase. *J Biol Chem* 1990 Apr 15;265(11):6481-6488.
- (191) Nakashima RA, Paggi MG, Scott LJ, Pedersen PL. Purification and characterization of a bindable form of mitochondrial bound hexokinase from the highly glycolytic AS-30D rat hepatoma cell line. *Cancer Res* 1988 Feb 15;48(4):913-919.
- (192) Smith TA. Mammalian hexokinases and their abnormal expression in cancer. *Br J Biomed Sci* 2000;57(2):170-178.
- (193) Kikuchi Y, Sato S, Sugimura T. Hexokinase isozyme patterns of human uterine tumors. *Cancer* 1972 Aug;30(2):444-447.
- (194) Pastorino JG, Hoek JB. Regulation of hexokinase binding to VDAC. *J Bioenerg Biomembr* 2008 Jun;40(3):171-182.
- (195) Pastorino JG, Shulga N, Hoek JB. Mitochondrial binding of hexokinase II inhibits Bax-induced cytochrome c release and apoptosis. *J Biol Chem* 2002 Mar 1;277(9):7610-7618.
- (196) Mathupala SP, Ko YH, Pedersen PL. Hexokinase II: cancer's double-edged sword acting as both facilitator and gatekeeper of malignancy when bound to mitochondria. *Oncogene* 2006 Aug 7;25(34):4777-4786.
- (197) Azoulay-Zohar H, Israelson A, Abu-Hamad S, Shoshan-Barmatz V. In self-defence: hexokinase promotes voltage-dependent anion channel closure and prevents mitochondria-mediated apoptotic cell death. *Biochem J* 2004 Jan 15;377(Pt 2):347-355.

- (198) Wilson JE. Isozymes of mammalian hexokinase: structure, subcellular localization and metabolic function. *J Exp Biol* 2003 Jun;206(Pt 12):2049-2057.
- (199) Wilson JE. Hexokinases. *Rev Physiol Biochem Pharmacol* 1995;126:65-198.
- (200) Polakis PG, Wilson JE. An intact hydrophobic N-terminal sequence is critical for binding of rat brain hexokinase to mitochondria. *Arch Biochem Biophys* 1985 Jan;236(1):328-337.
- (201) Xie GC, Wilson JE. Rat brain hexokinase: the hydrophobic N-terminus of the mitochondrially bound enzyme is inserted in the lipid bilayer. *Arch Biochem Biophys* 1988 Dec;267(2):803-810.
- (202) Katzen HM, Schimke RT. Multiple forms of hexokinase in the rat: tissue distribution, age dependency, and properties. *Proc Natl Acad Sci U S A* 1965 Oct;54(4):1218-1225.
- (203) Grossbard L, Schimke RT. Multiple hexokinases of rat tissues. Purification and comparison of soluble forms. *J Biol Chem* 1966 Aug 10;241(15):3546-3560.
- (204) Nakashima RA, Mangan PS, Colombini M, Pedersen PL. Hexokinase receptor complex in hepatoma mitochondria: evidence from N,N'-dicyclohexylcarbodiimide-labeling studies for the involvement of the pore-forming protein VDAC. *Biochemistry* 1986 Mar 11;25(5):1015-1021.
- (205) Kurokawa M, Oda S, Tsubotani E, Fujiwara H, Yokoyama K, Ishibashi S. Characterization of hexokinase isoenzyme types I and II in ascites tumor cells by an interaction with mitochondrial membrane. *Mol Cell Biochem* 1982 Jun 25;45(3):151-157.
- (206) Imai N, Akimoto H, Oda M, Okazaki H, Ishibashi S, Kurokawa M. Interactions between cations in modifying the binding of hexokinases I and II to mitochondria. *Mol Cell Biochem* 1988 May;81(1):37-41.
- (207) John S, Weiss JN, Ribalet B. Subcellular localization of hexokinases I and II directs the metabolic fate of glucose. *PLoS One* 2011 Mar 9;6(3):e17674.
- (208) Wyatt E, Wu R, Rabeh W, Park HW, Ghanefar M, Ardehali H. Regulation and cytoprotective role of hexokinase III. *PLoS One* 2010 Nov 3;5(11):e13823.
- (209) Preller A, Wilson JE. Localization of the type III isozyme of hexokinase at the nuclear periphery. *Arch Biochem Biophys* 1992 May 1;294(2):482-492.

- (210) Sun L, Shukair S, Naik TJ, Moazed F, Ardehali H. Glucose phosphorylation and mitochondrial binding are required for the protective effects of hexokinases I and II. *Mol Cell Biol* 2008 Feb;28(3):1007-1017.
- (211) Iynedjian PB, Mobius G, Seitz HJ, Wollheim CB, Renold AE. Tissue-specific expression of glucokinase: identification of the gene product in liver and pancreatic islets. *Proc Natl Acad Sci U S A* 1986 Apr;83(7):1998-2001.
- (212) Lynch RM, Tompkins LS, Brooks HL, Dunn-Meynell AA, Levin BE. Localization of glucokinase gene expression in the rat brain. *Diabetes* 2000 May;49(5):693-700.
- (213) Farrelly D, Brown KS, Tieman A, Ren J, Lira SA, Hagan D, et al. Mice mutant for glucokinase regulatory protein exhibit decreased liver glucokinase: a sequestration mechanism in metabolic regulation. *Proc Natl Acad Sci U S A* 1999 Dec 7;96(25):14511-14516.
- (214) Arden C, Baltrusch S, Agius L. Glucokinase regulatory protein is associated with mitochondria in hepatocytes. *FEBS Lett* 2006 Apr 3;580(8):2065-2070.
- (215) Arden C, Harbottle A, Baltrusch S, Tiedge M, Agius L. Glucokinase is an integral component of the insulin granules in glucose-responsive insulin secretory cells and does not translocate during glucose stimulation. *Diabetes* 2004 Sep;53(9):2346-2352.
- (216) Hennipman A, Smits J, van Oirschot B, van Houwelingen JC, Rijkssen G, Neyt JP, et al. Glycolytic enzymes in breast cancer, benign breast disease and normal breast tissue. *Tumour Biol* 1987;8(5):251-263.
- (217) Hennipman A, van Oirschot BA, Smits J, Rijkssen G, Staal GE. Heterogeneity of glycolytic enzyme activity and isozyme composition of pyruvate kinase in breast cancer. *Tumour Biol* 1988;9(4):178-189.
- (218) Gudnason V, Ingvarsson S, Jonasdottir A, Andresdottir V, Egilsson V. Isoenzyme pattern and subcellular localization of hexokinases in human breast cancer and nonpathological breast tissue. *Int J Cancer* 1984 Jul 15;34(1):63-66.
- (219) Brown RS, Goodman TM, Zasadny KR, Greenson JK, Wahl RL. Expression of hexokinase II and Glut-1 in untreated human breast cancer. *Nucl Med Biol* 2002 May;29(4):443-453.
- (220) Hsu SY, Kaipia A, Zhu L, Hsueh AJ. Interference of BAD (Bcl-xL/Bcl-2-associated death promoter)-induced apoptosis in mammalian cells by 14-3-3 isoforms and P11. *Mol Endocrinol* 1997 Nov;11(12):1858-1867.

- (221) Bae J, Hsu SY, Leo CP, Zell K, Hsueh AJ. Underphosphorylated BAD interacts with diverse antiapoptotic Bcl-2 family proteins to regulate apoptosis. *Apoptosis* 2001 Oct;6(5):319-330.
- (222) Laemmli UK. Cleavage of structural proteins during the assembly of the head of bacteriophage T4. *Nature* 1970 Aug 15;227(5259):680-685.
- (223) Shapiro AL, Vinuela E, Maizel JV, Jr. Molecular weight estimation of polypeptide chains by electrophoresis in SDS-polyacrylamide gels. *Biochem Biophys Res Commun* 1967 Sep 7;28(5):815-820.
- (224) Towbin H, Staehelin T, Gordon J. Electrophoretic transfer of proteins from polyacrylamide gels to nitrocellulose sheets: procedure and some applications. *Proc Natl Acad Sci U S A* 1979 Sep;76(9):4350-4354.
- (225) Burnette WN. "Western blotting": electrophoretic transfer of proteins from sodium dodecyl sulfate--polyacrylamide gels to unmodified nitrocellulose and radiographic detection with antibody and radioiodinated protein A. *Anal Biochem* 1981 Apr;112(2):195-203.
- (226) Elbashir SM, Harborth J, Lendeckel W, Yalcin A, Weber K, Tuschl T. Duplexes of 21-nucleotide RNAs mediate RNA interference in cultured mammalian cells. *Nature* 2001 May 24;411(6836):494-498.
- (227) Crissman HA, Steinkamp JA. Rapid, simultaneous measurement of DNA, protein, and cell volume in single cells from large mammalian cell populations. *J Cell Biol* 1973 Dec;59(3):766-771.
- (228) Ehrenberg B, Montana V, Wei MD, Wuskell JP, Loew LM. Membrane potential can be determined in individual cells from the nernstian distribution of cationic dyes. *Biophys J* 1988 May;53(5):785-794.
- (229) Scaduto RC, Jr, Grotyohann LW. Measurement of mitochondrial membrane potential using fluorescent rhodamine derivatives. *Biophys J* 1999 Jan;76(1 Pt 1):469-477.
- (230) Ngai J, Coleman TR, Lazarides E. Localization of newly synthesized vimentin subunits reveals a novel mechanism of intermediate filament assembly. *Cell* 1990 2/9;60(3):415-427.
- (231) Candiano G, Bruschi M, Musante L, Santucci L, Ghiggeri GM, Carnemolla B, et al. Blue silver: A very sensitive colloidal Coomassie G-250 staining for proteome analysis. *Electrophoresis* 2004;25(9):1327-1333.
- (232) Chevallet M, Luche S, Rabilloud T. Silver staining of proteins in polyacrylamide gels. *Nat Protoc* 2006;1(4):1852-1858.

- (233) Kim H, Rafiuddin-Shah M, Tu HC, Jeffers JR, Zambetti GP, Hsieh JJ, et al. Hierarchical regulation of mitochondrion-dependent apoptosis by BCL-2 subfamilies. *Nat Cell Biol* 2006 Dec;8(12):1348-1358.
- (234) Graham FL, van der Eb AJ. A new technique for the assay of infectivity of human adenovirus 5 DNA. *Virology* 1973 Apr;52(2):456-467.
- (235) Balinsky D, Platz CE, Lewis JW. Isozyme patterns of normal, benign, and malignant human breast tissues. *Cancer Res* 1983 Dec;43(12 Pt 1):5895-5901.
- (236) Bustamante E, Morris HP, Pedersen PL. Energy metabolism of tumor cells. Requirement for a form of hexokinase with a propensity for mitochondrial binding. *J Biol Chem* 1981 Aug 25;256(16):8699-8704.
- (237) Bustamante E, Pedersen PL. Mitochondrial hexokinase of rat hepatoma cells in culture: solubilization and kinetic properties. *Biochemistry* 1980 Oct 28;19(22):4972-4977.
- (238) Kamel R, Schwarzfischer F. Hexokinase isozymes in human neoplastic and fetal tissues: the existence of hexokinase II in malignant tumors and in placenta. *Humangenetik* 1975 Nov 6;30(2):181-185.
- (239) Sutherland BW, Toews J, Kast J. Utility of formaldehyde cross-linking and mass spectrometry in the study of protein-protein interactions. *J Mass Spectrom* 2008 Jun;43(6):699-715.
- (240) Boise LH, González-García M, Postema CE, Ding L, Lindsten T, Turka LA, et al. bcl-x, a bcl-2-related gene that functions as a dominant regulator of apoptotic cell death. *Cell* 1993 8/27;74(4):597-608.
- (241) Sommers CL, Walker-Jones D, Heckford SE, Worland P, Valverius E, Clark R, et al. Vimentin rather than keratin expression in some hormone-independent breast cancer cell lines and in oncogene-transformed mammary epithelial cells. *Cancer Res* 1989 Aug 1;49(15):4258-4263.
- (242) Vikstrom KL, Borisy GG, Goldman RD. Dynamic aspects of intermediate filament networks in BHK-21 cells. *Proc Natl Acad Sci U S A* 1989 Jan;86(2):549-553.
- (243) Soellner P, Quinlan RA, Franke WW. Identification of a distinct soluble subunit of an intermediate filament protein: tetrameric vimentin from living cells. *Proc Natl Acad Sci U S A* 1985 Dec;82(23):7929-7933.
- (244) Kouklis PD, Hatzfeld M, Brunkener M, Weber K, Georgatos SD. In vitro assembly properties of vimentin mutagenized at the beta-site tail motif. *J Cell Sci* 1993 Nov;106 ( Pt 3)(Pt 3):919-928.

- (245) Herrmann H, Haner M, Brettel M, Ku NO, Aebi U. Characterization of distinct early assembly units of different intermediate filament proteins. *J Mol Biol* 1999 Mar 12;286(5):1403-1420.
- (246) Janosch P, Kieser A, Eulitz M, Lovric J, Sauer G, Reichert M, et al. The Raf-1 kinase associates with vimentin kinases and regulates the structure of vimentin filaments. *FASEB J* 2000 Oct;14(13):2008-2021.
- (247) Rouimi P, Anglade P, Debrauwer L, Tulliez J. Characterization of pig liver glutathione S-transferases using HPLC-electrospray-ionization mass spectrometry. *Biochem J* 1996 Aug 1;317 ( Pt 3)(Pt 3):879-884.
- (248) Strobel T, Tai YT, Korsmeyer S, Cannistra SA. BAD partly reverses paclitaxel resistance in human ovarian cancer cells. *Oncogene* 1998 Nov 12;17(19):2419-2427.
- (249) Poruchynsky MS, Wang EE, Rudin CM, Blagosklonny MV, Fojo T. Bcl-xL is phosphorylated in malignant cells following microtubule disruption. *Cancer Res* 1998 Aug 1;58(15):3331-3338.
- (250) Liu QY, Stein CA. Taxol and estramustine-induced modulation of human prostate cancer cell apoptosis via alteration in bcl-xL and bak expression. *Clin Cancer Res* 1997 Nov;3(11):2039-2046.
- (251) Mabuchi S, Ohmichi M, Kimura A, Hisamoto K, Hayakawa J, Nishio Y, et al. Inhibition of phosphorylation of BAD and Raf-1 by Akt sensitizes human ovarian cancer cells to paclitaxel. *J Biol Chem* 2002 Sep 6;277(36):33490-33500.
- (252) Bekier ME, Fischbach R, Lee J, Taylor WR. Length of mitotic arrest induced by microtubule-stabilizing drugs determines cell death after mitotic exit. *Mol Cancer Ther* 2009 Jun;8(6):1646-1654.
- (253) Endo K, Mizuguchi M, Harata A, Itoh G, Tanaka K. Nocodazole induces mitotic cell death with apoptotic-like features in *Saccharomyces cerevisiae*. *FEBS Lett* 2010 Jun 3;584(11):2387-2392.
- (254) Noguchi S. Predictive factors for response to docetaxel in human breast cancers. *Cancer Sci* 2006 Sep;97(9):813-820.
- (255) Yang J, Li JH, Wang J, Zhang CY. Molecular modeling of BAD complex resided in a mitochondrion integrating glycolysis and apoptosis. *J Theor Biol* 2010 Sep 21;266(2):231-241.
- (256) Ivaska J, Pallari HM, Nevo J, Eriksson JE. Novel functions of vimentin in cell adhesion, migration, and signaling. *Exp Cell Res* 2007 Jun 10;313(10):2050-2062.

- (257) Franke WW, Grund C, Kuhn C, Jackson BW, Illmensee K. Formation of cytoskeletal elements during mouse embryogenesis. III. Primary mesenchymal cells and the first appearance of vimentin filaments. *Differentiation* 1982;23(1):43-59.
- (258) Guarino M, Rubino B, Ballabio G. The role of epithelial-mesenchymal transition in cancer pathology. *Pathology* 2007 Jun;39(3):305-318.
- (259) Ivaska J, Vuoriluoto K, Huovinen T, Izawa I, Inagaki M, Parker PJ. PKCepsilon-mediated phosphorylation of vimentin controls integrin recycling and motility. *EMBO J* 2005 Nov 16;24(22):3834-3845.
- (260) Tang HL, Lung HL, Wu KC, Le AH, Tang HM, Fung MC. Vimentin supports mitochondrial morphology and organization. *Biochem J* 2008 Feb 15;410(1):141-146.
- (261) Mendez MG, Kojima S, Goldman RD. Vimentin induces changes in cell shape, motility, and adhesion during the epithelial to mesenchymal transition. *FASEB J* 2010 Jun;24(6):1838-1851.
- (262) Vicente-Manzanares M, Ma X, Adelstein RS, Horwitz AR. Non-muscle myosin II takes centre stage in cell adhesion and migration. *Nat Rev Mol Cell Biol* 2009 Nov;10(11):778-790.
- (263) Vicente-Manzanares M, Zareno J, Whitmore L, Choi CK, Horwitz AF. Regulation of protrusion, adhesion dynamics, and polarity by myosins IIA and IIB in migrating cells. *J Cell Biol* 2007 Feb 26;176(5):573-580.
- (264) Guha M, Zhou M, Wang YL. Cortical actin turnover during cytokinesis requires myosin II. *Curr Biol* 2005 Apr 26;15(8):732-736.
- (265) Murthy K, Wadsworth P. Myosin-II-dependent localization and dynamics of F-actin during cytokinesis. *Curr Biol* 2005 Apr 26;15(8):724-731.
- (266) Chrzanowska-Wodnicka M, Burridge K. Rho-stimulated contractility drives the formation of stress fibers and focal adhesions. *J Cell Biol* 1996 Jun;133(6):1403-1415.
- (267) Cai Y, Biais N, Giannone G, Tanase M, Jiang G, Hofman JM, et al. Nonmuscle myosin IIA-dependent force inhibits cell spreading and drives F-actin flow. *Biophys J* 2006 Nov 15;91(10):3907-3920.
- (268) Hashimoto A, Hirose K, Iino M. BAD detects coincidence of G2/M phase and growth factor deprivation to regulate apoptosis. *J Biol Chem* 2005 Jul 15;280(28):26225-26232.

- (269) Germain M, Mathai JP, Shore GC. BH-3-only BIK functions at the endoplasmic reticulum to stimulate cytochrome c release from mitochondria. *J Biol Chem* 2002 May 17;277(20):18053-18060.
- (270) Mathai JP, Germain M, Shore GC. BH3-only BIK regulates BAX,BAK-dependent release of Ca<sup>2+</sup> from endoplasmic reticulum stores and mitochondrial apoptosis during stress-induced cell death. *J Biol Chem* 2005 Jun 24;280(25):23829-23836.
- (271) Germain M, Mathai JP, McBride HM, Shore GC. Endoplasmic reticulum BIK initiates DRP1-regulated remodelling of mitochondrial cristae during apoptosis. *EMBO J* 2005 Apr 20;24(8):1546-1556.
- (272) Liao PC, Tan SK, Lieu CH, Jung HK. Involvement of endoplasmic reticulum in paclitaxel-induced apoptosis. *J Cell Biochem* 2008 Jul 1;104(4):1509-1523.
- (273) Al-Bazz YO, Underwood JC, Brown BL, Dobson PR. Prognostic significance of Akt, phospho-Akt and BAD expression in primary breast cancer. *Eur J Cancer* 2009 Mar;45(4):694-704.
- (274) Cannings E, Kirkegaard T, Tovey SM, Dunne B, Cooke TG, Bartlett JM. Bad expression predicts outcome in patients treated with tamoxifen. *Breast Cancer Res Treat* 2007 Apr;102(2):173-179.
- (275) Huang Y, Liu D, Chen B, Zeng J, Wang L, Zhang S, et al. Loss of Bad expression confers poor prognosis in non-small cell lung cancer. *Med Oncol* 2011 Sep 15.
- (276) Marchion DC, Cottrill HM, Xiong Y, Chen N, Bicaku E, Fulp WJ, et al. BAD phosphorylation determines ovarian cancer chemosensitivity and patient survival. *Clin Cancer Res* 2011 Oct 1;17(19):6356-6366.